2020

ANALYSIS OF A CIRCULAR RESONANT PLATE FOR SHOCK TESTING

Jon Markl
Michigan Technological University, jbmarkl@mtu.edu

ANALYSIS OF A CIRCULAR RESONANT PLATE FOR SHOCK TESTING

By

Jonathan B. Markl

A THESIS

Submitted in partial fulfillment of the requirements for the degree of

MASTER OF SCIENCE

In Mechanical Engineering

MICHIGAN TECHNOLOGICAL UNIVERSITY

2020

This thesis has been approved in partial fulfillment of the requirements for the Degree of MASTER OF SCIENCE in Mechanical Engineering.

Department of Mechanical Engineering-Engineering Mechanics

Thesis Co-Advisor:	*Jason R. Blough*
Thesis Co-Advisor:	*Andrew Barnard*
Committee Member:	*James P. DeClerck*
Committee Member:	*Charles D. Van Karsen*
Department Chair:	*William Predebon*

Table of Contents

Acknowledgments

I would like to thank Dr. Jason Blough for his endless insight and for knowing exactly when I did not understand a concept and drawing pictures to explain until I finally understood.

Thanks to Charles Van Karsen for all the modeling help and being available for conference calls whenever I needed you, even though we still haven't gone fishing…

Many thanks to Dr. Andrew Barnard for guidance and for getting me involved in graduate school.

I would also like to thank Dr. James De Clerck for answering all my questions, many of which by asking me a question. Thank you for making me laugh and keeping me calm when I would get worked up over not understanding a subject.

Thanks to my sponsor David Soine for asking some tough questions and giving me many areas to explore that I would not have thought to investigate.

I would like to give many thanks and much appreciation to Jessica for so much that I could write a small book. I can just say that she knows me more than anyone and knows exactly how to motivate, calm, and inspire me.

Lastly, I would like to thank my parents. Without them, I would not have had this opportunity and I would like to say thank you for always keeping me curious and inspiring me to explore.

Preface

The research conducted was a continuation of a project done by William Larsen at Michigan Technological University. The literature review was presented at SAVE in Dallas, TX in 2018 and many of the methods and results will be presented at IMAC in 2020.

This work was funded by Honeywell Federal Manufacturing & Technologies under Contract No. DE-NA0002839 with the U.S. Department of Energy. The United States Government retains and the publisher, by accepting the article for publication, acknowledges that the United States Government retains a nonexclusive, paid up, irrevocable, world-wide license to publish or reproduce the published form of this manuscript, or allow others to do so, for the United States Government purposes.

Abstract

Designing a resonant plate for shock test specifications involves an understanding of how a system will respond with a given set of input and output locations in all three directions. To investigate how to effectively change the off-axis responses to meet test specifications, a finite element model (FEM) was created and examinations of input location/angle of impact, placement of the test fixture, and placement of the impact pad were conducted. The primary tool used to determine how a structure will respond to a given input at a given output on the test structure was done using the shock response spectra (SRS). An analysis of the modal contribution to the shock response was executed and gives insight to the variations in response at different nodal points on the test fixture.

1 Literature review

This chapter describes mechanical shock and pyroshock and the importance of studying the response of structures from the shock event. A brief introduction on the shock response spectrum describes how it is used to characterize the shock. The topic shifts to testing methods that have been used for shock testing and describes some of the insights gained and what could have been improved. The chapter concludes with the goal of this research and how it can be used to advance the knowledge of resonant plate shock testing.

1.1 Introduction

Mechanical shock can be described as an excitation with a short duration to a physical system that produces a dynamic response. Examples of shock excitations can include impacts, drops, earthquakes, and explosions where the magnitude of the excitation is represented as a function of time or time history. Most often the effects of shock are undesirable and studying the properties of shock on physical systems can provide insight in reducing the severity and help design equipment to endure their effects.

Several experimental methods for shock testing exist depending on the desired response. These include drop tables, air guns or pneumatic projectiles, vibration machines such as electrodynamic shakers, high impact shock machines that can be equipped with a pendulum hammer or pneumatic hammer, Hopkinson bars, and explosives (live ordnance) [11]. Drop tables can be complex and may contain other mechanisms such as elastic shock cords and these can be useful in obtaining velocities higher than that of free fall [11]. They can also be equipped with a programming device to acquire the desired acceleration pulse [11]. Electrodynamic shakers can be useful in supplying a range of various shock pulses and are controllable, however, they have limitations and can lead to over/undertesting [11]. Explosives can be expensive and involve careful safety procedures but are useful in producing realistic high accelerations and high frequencies that are involved in pyrotechnic shock, or pyroshock [11].

Pyroshock is a response of a structure from an explosive event that contains high frequency and high-stress waves and unlike other forms of mechanical shock, there is low rigid-body motion. The range of frequencies and acceleration divide the term pyroshock into categories that are referred to as far-field, mid-field, and near-field pyroshock. The NASA STD 7003 and MIL-STD 810 Method 517 ranges for shock spectrum are contained in Table 1 [NASA,MIL].

Table 1.1: Pyroshock definitions from standards STD 7003 and MIL-STD 810 Method 517 [17, 18]

Standard	Region	Acceleration Amplitude in G	Frequency Range in Hz
NASA STD 7003	Far-field	<1,000	<10,000
	Mid-field	1,000 – 5,000	10,000 – 100,000
	Near-field	>5,000	>100,000
MILSTD 810 Method 517	Far-field	<1,000	<10,000
	Mid-field	1,000 – 10,000	3 – 10,000
	Near-field	>10,000	>3,000

Structures are not typically damaged from pyroshock events, but smaller components can be affected by the high-frequency energy and can cause failures including relay chatter and short circuits. One of the earliest mentions of the adverse consequence of high-frequency shock from ignition firing came from the U.S. Army in 1966 [5]. Shock tests were performed to discover areas in which design changes may be necessary to ensure missile performance [5]. In the aerospace industry, extensive research has been completed to determine the effects of pyroshock and in most cases, the Shock Response Spectra (SRS) is used to quantitatively describe the pyroshock data.

1.1.1 Shock Response Spectrum

History of SRS can be linked to Maurice Biot and his 1932 Ph.D. thesis, Transient Oscillations in Elastic Systems, where he derives the equations to study the transient response of Earthquakes [1]. Later in 1942, Dr. Bernard Miller developed the multifrequency reed gage to measure the shock response spectrum (SRS), also known as the “mechanical shock spectrum analyzer” which was primarily used to analyze the shock motion on naval vessels [2]. The gages consisted of reeds attached to cantilever beams which were attached to a structure that was subjected to motion. Masses were connected to the reeds and styli connected to the ends of the masses to record the motion on waxed paper [2].

The calculation of the SRS is made based on the acceleration time trace of a structure undergoing motion by modeling how an array of single degree of freedom (SDOF) systems react to a given shock input [3].

Several different shock spectra can be represented from one single response event depending on what part of the transient response is selected. The primary region contains only information from the time history during the shock event and the residual is the region of the response after the excitation has ended. SRS calculations are performed on the positive and negative spectrums. Ideally, these curves will be identical. In the case that they are not, "maximax" option is used to take the maximum of the peak hold response of positive or negative spectra [3]. The maximum absolute response (maximax) spectrum contains both the primary and residual and is defined in terms of the peak responses as a function of the systems natural frequency [4]. Figure 1.1 shows an acceleration time trace from a point on a resonant plate with the input from an impact hammer and the corresponding SRS. The SRS from Figure 1.1 shows the rigid body controlled region in the lower frequencies and the slope of the line up to the knee frequency is called the constant velocity line if it is equivalent to 6 – 18 dB per octave [3]. The knee frequency is the point on the SRS where the first bending mode occurs and the slope of the constant velocity line changes.

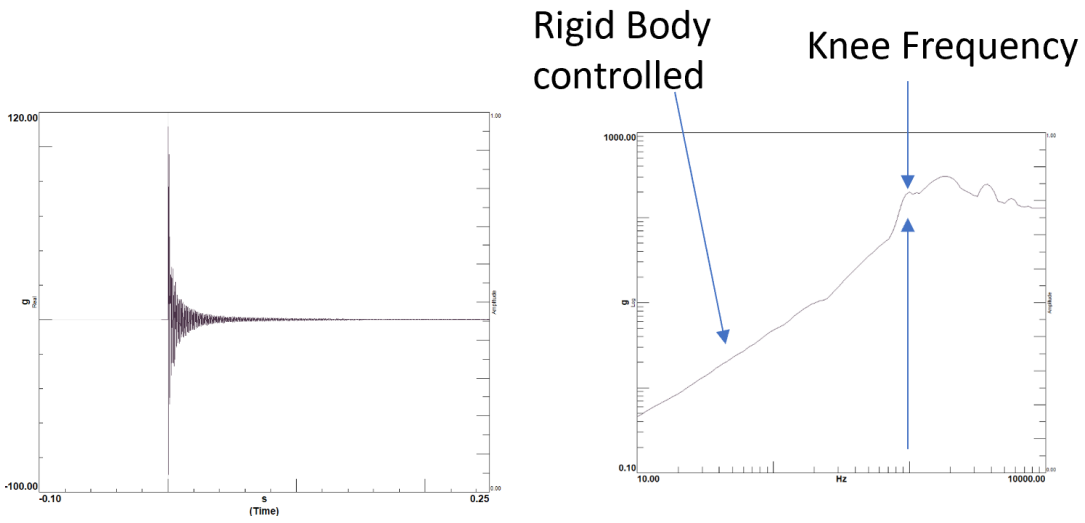

Figure 1.1: Acceleration time history output from shock input and corresponding SRS

1.2 Excitation Techniques and Development

1.2.1 Brooks Shock Testing Methods

In 1962, when mechanical shock testing was just beginning to be explored, R.O. Brooks discussed some key problems that shock testing posed which included nomenclature, test

specifications, shock machine requirements, shock pulse shaping, fixture design, instrumentation, and interpretation [5]. For testing specifications, Brooks outline 13 points the test engineer must know in order to perform a properly designed shock test e.g. what type of acceleration (maximum/peak), duration of the test, pulse shape, directions of applied shock, and the number of shocks applied in each direction [5]. Other points include test item mounting requirements such that it accurately depicts how it is mounted in its normal application.

At the time Brooks referred to Sandia's test machines being classified under "impulse" and "impact" shock where the "impulse" machines increase the velocity of the test article as a result from the input and the "impact" test machines either decrease or change the direction of the velocity of the test article during the impact excitation [5]. Understanding the kinematic relationships between the time traces of acceleration, velocity, and displacement of the shock pulse and the test machine must be explored in order to select the appropriate machine to use for testing. [5].

The fixture's primary function is to position and secure the test item in a specific way so that the desired direction of the shock is obtained and must be rigid as possible so it may be considered part of the carriage [5]. The types of fixtures described by Brooks are plates (rectangular and round), beams, axial and column springs and warns that the fixture can induce complications if the fixtures mass is a "significant percent" of the carriage mass [5]. He classifies the fixtures as an adapter, box, upright, block, and standoff and describes how they are secured to the carriage (e.g bolts) is important due to changing the dynamic effect of the test article.

Brooks emphasized that instrumentation is the most important aspect of shock testing and they must be calibrated in such a way that it limits the amount of error. The shock instrumentation circuits used at Sandia at the time were detailed in SCTM 216-62 and SCTM 217-62 and they described the pickup selection, circuitry, calibration and test restrictions [5].

Interpretation of the shock pulse data can be done with differing opinions from both people and companies, so Brooks described the standard, SC-4452A (M), used by Sandia at the time.

Brooks concludes that four major areas that needed to be improved upon in shock testing are specifications for shock testing being obtained, generating an appropriate shock pulse to reach the desired response of the test article, calibration of the equipment such that it represents an accurate portrayal of the generated pulse, and accurately interpreting the input shock and output response of the test article.

1.2.2 MIPS Testing at GE Astro

Testing at the GE Astro Space Division was conducted in the mid-1980s using a Mechanical Impulse Pyro Shock (MIPS) simulator. Twelve different component designs

were created by changing boundary conditions on the simulator as well as modifying the force input. Components were mounted on an aluminum plate which rested upon a 3-inch foam pad and the input of a moveable pneumatic actuator creates the shock event [6].

Several devices that were tested include "printed wire boards (PWBs), gyroscopes, relays, and passive dampers" [6]. Variations of the testing include adding paper under the striker which resulted in damping out higher frequencies, however replacing the paper with a steel plate under the striker lead to an increase in the frequencies [6]. Other variations in the testing consist of clamping the edges of the plate to the table, reducing the ram pressure, lowering the striker height and supporting the table on wood blocks [6]. All changes to the testing are done so to better understand the nature of the shock response and the effects that boundary conditions contribute.

Data obtained from the tests were consistent from one test to another with variability being under 10 percent, and the pretest objective of understanding the MIPS facility as well as attaining the anticipated shock response spectrum for the 12 tests was accomplished. Those goals would help reduce setup and testing time in addition to reducing the cost [6].

1.2.3 NASA Pyrotechnically Induced Shock

In June of 1982, two solid rocket boosters were lost due to a large level of vibration which prematurely operated a water impact switch, used to separate the parachutes from the boosters, and was prematurely operated from "spurious shock signal" brought on by the separation assembly [7]. The resulting investigation provoked three full-scale ground tests of the separation assembly [7]. The results varied from test to test with the first test showing the switch remained open, test two showed chatter, but remained open, and test three the switch closed [7]. According to James Smith, instrumentation was the largest problem in shock testing where the mounts of accelerometers act as “mechanical filters,” as well as the accelerometers being prone to produce errors [7].

Smith described the testing techniques used at the time for evaluating pyroshock and claimed that hammer tests produced an SRS that was desirable, but the time history pulses were too simplistic in comparison to Linear Shaped Charge (LSC) pulses [7]. Shakers could be used to demonstrate LSC pulses, and despite having the SRS match flight levels the test levels were unrealistic and the time pulse histories were also too simplistic [7]. Drop testing machines do not adequately depict LSC pulses due to imparting a velocity change instead of an acceleration change, but limited success was obtained with a “bounded impact” technique despite not reaching the appropriate levels [7]. Hopkinson's Bars have also shown some limited success, but once again the time histories did not accurately depict the time histories of pyroshock [7]. Explosive testing is the only way to produce the complex time histories but can be expensive of testing on the actual flight equipment, so the use of explosives and plate testing were the optimal choice for pyroshock testing [7].

Piezoelectric and piezoresistive accelerometers are used for studying shock but can be very susceptible to errors which can include accelerometer resonance, signal noise, cable failure, test input error, etc [7]. Similar to Brooks, Smith stresses the importance of proper calibration for the accelerometers.

The main test plate consisted of aluminum and measured 4 ft x 1 ft x 0.25 ft which was modeled after the rocket booster frustum and the separation assembly [7]. The test plate assembly was mounted on a wood and steel table which suspended the plate with bungee cords that had a spring stiffness of 2.793 lb/in [7]. The short ends were free, and during the LSC firing the plate is in a free/free state [7]. The test program was divided into three areas which were "precision and accuracy, basic shock response, and variability [7]." The precision and accuracy portion consisted of a ball drop calibration test for the accelerometers which was performed on all 29 tests, and the results showed that the Endevco 7270 accelerometer showed the best survivability and performance [7]. The basic shock response spectra came from ten test plates used as the control group with the only variations among those plates being the thickness of the plate and the type of aluminum alloy. The conclusions were made that the alloy type did not affect the spectra, and the thickness also did not affect the spectra as long as "complete plate severance occurs [7]." The variability portion was conducted on 26 of the plates with variations in "core-load, standoff, coupling, LSC apex angle, and gross variation of core-load" where the variations were applied one at a time for each test [7].

Conclusions from the NASA tests:

- Spectra was repeatable when the appropriate instrumentation was properly used
- Manufacturing tolerances had little to no effect on the response spectra
- Shock response spectra in all three directions were the same when using linear shaped charges
- No relationship between the distance from the source and shock levels, but noted that with the free-free conditions the total energy was not "dissipated very rapidly as a function of distance" and if the sides perpendicular to the charge were clamped then the energy levels would have "dissipated rapidly with distance."

Recommendations from the NASA tests:

- Mounting blocks should be avoided when doing pyroshock testing
- Tests should be performed on real space structures to determine energy changes of those structures

1.2.4 Sandia Labs Tunable Resonant Fixture

The testing apparatus used at Sandia National Laboratories in the early 1990s consisted of a resonant beam clamped down to a concrete base where the excitation was applied via an air gun assembly. The design utilized the predictability of bending modes from equations and the tunability of the beam allowed for a range of spectra to be obtained [8]. Other variations to the testing include different projectiles and using paper/felt lining where the impact occurred which resulted in altering the amplitude and duration of input [8].

One of the major drawbacks of the tunable fixture phase 1 was simulating the pyroshock for satellite components larger than 10 square inches, and some of the results demonstrated an overestimation of the knee frequencies close to 50 percent at frequencies nearing 3000 Hz [8]. However clear knee frequencies were obtained from 500 – 1400 Hz, with maximum G loads reaching 1000 – 4000 G [8]. Although it was unclear how the results were obtained, the report did show higher mode excitation of around 6000 Hz with G levels over 10000, which is a depiction of true near-field pyroshock [8].

1.2.5 NASA Jet Propulsion Laboratory MIPS Simulation

The MIPS apparatus used by NASA's Jet Propulsion Laboratory (JPL) was built in a similar fashion as the one used by GE Astro with an aluminum mounting plate resting on a foam or plywood pad and excited into resonance where the shock is produced by an actuator on a movable bridge [9]. The impactor heads were interchangeable and consisted of different materials including aluminum, steel, and lead which led to alterations in the pulse duration [9].

Attempts to characterize the MIPS simulator proved difficult using a Buckingham Pi solution due to the intricate modal dynamics of the aluminum plate, so an alternative method of creating a database that related the response spectra to the parameters used during testing including the pressure, damping materials, position of the impactor, etc. [9]. The software tool allowed for the desired spectrum to be obtained using the approximate parameters along with trial and error.

1.2.6 Alcatel ETCA Resonant Fixtures

The Alcatel ETCA testing facility in Belgium experimented with several different types of testing methods including drop test machines, electrodynamic shakers, impact devices, and pyrotechnically induced devices. It was discovered that using drop test machines create a large net change in velocity to the test article which generates a low-frequency energy shock that can cause damage and therefore should not be used [10]. Other problems can occur with different devices including electrodynamic shakers not being able to adequately simulate the SRS, impact devices requiring detailed trial-and-error to achieve the anticipated spectra, and ordnance devices can have concerns with safety as well as difficulty in developing a numerical solution [10].

The main goal of the testing facility was to develop a versatile system that would be able to achieve every type of desired spectra in each of the three directions for a variety of electrical units within a reasonable amount of time and abiding by quality standards [10]. One of the devices they have developed consists of an aluminum plate suspended from cords from a framed structure. The design enables for the use of several shock inputs whether it is impacted by a hammer, pneumatic projectile, or live ordnance.

The testing at the facility on the simple plate test fixture has shown for mechanical impacts that the type of excitation (drop mass vs. air gun) produces much different SRSs where the drop mass has more amplitude at lower frequencies than the air gun and vice versa at higher

frequencies [10]. Another observation made at the facility was the advantages of using live ordnance. Despite the difficulties involved in explosive testing, the live ordnance tests showed that one firing gave excitations in all three directions and the shock levels through the fixation points were more undeviating than using mechanical impacts [10].

The Alcatel ETCA testing facility also experimented with a Hopkinson bar resonant test fixture in response to reducing the trial-and-error testing of the previous testing methods. The results can be verified using longitudinal beam equations for frequencies with:

$$f_n = \frac{ncL}{2} \tag{1.1}$$

where n = 1,2,3, …

c = wave speed ($c^2 = E/\rho$)

L = length of the bar

E = Young's modulus of the bar material

ρ = density

The tests revealed that the participation of the different modes can be achieved by altering the clamp location along with the impact duration [11]. For the desired mode, the input duration should be one half of the period and the clamp should be located at the nodal points of that mode [11]. It was noted that the test benefits from added damping material to reduce the resonant ringing from hundreds of milliseconds to fractions of milliseconds.

1.2.7 Medium Weight Heavy Shock Machine

The Navy's mediumweight shock machine (MWSM) was used to characterize naval shock and was able to produce severe shock, but it was not able to fully depict the response to a vessel from an underwater explosion. The MWSM utilized high impact shock to an anvil table by means of a large swinging hammer, and the impact between the anvil and the hammer was highly elastic where the energy was managed by adjusting the height of the hammer before the release [12]. Ship equipment was attached to the anvil table using a "standard mounting fixture" shown in figure 8 and resonated at frequencies between 55 Hz to 72 Hz, which was not characteristic of shipboard excitation hence the need for a replacement mounting system.

MIL-S-901 D requires test articles to be mounted by means consistent with their shipboard orientation [12]. A report by Chalmers and Shaw provides evidence that using the standard mounting fixture resulted in an overtest and showed that equipment experienced more severe resonant vibrations in real life applications versus testing, so they proposed a tunable fixture to more accurately simulate actual shipboard conditions [12].

A 1/4 scale model of the proposed testing fixture design was built to verify mathematical simulation. The input to the fixture was supplied by a drop table which allowed dropping the fixture model onto a load cell from a specified height where the range of the load cell was 0 lbs – 5000 lbs [12]. The model was built to resemble the proposed fixture with an exception of the I-beam material being made from aluminum instead of steel and a reduction in weight of the tiers. The results from the experimental transfer function with peaks at 80 Hz and 160 Hz were similar to the analytical predictions of 77.8 Hz and 148 Hz which determined that the full-scale fixture would be built and tested with promising results expected [12].

1.2.8 Laser Excitation

Laser excitation is not a common method used to simulate pyroshock and can only achieve small accelerations up to a few Gs. However, it can provide a useful visualization tool for wave propagation of pyroshock. Researchers at Korea Advanced Institute of Science and Technology demonstrated that a laser pulse created localized transient heating which generated thermoelastic strains and stresses which acted as a source of the waves. They determined that the laser excitation can be used to regenerate a mechanical shock wave with accelerations reaching 7000 G and a 70 kHz central frequency [13].

1.2.9 Dynamic Characterization for Shock Testing

The motivation behind this study was how the dynamics of a resonant plate used for shock testing can change dramatically based on the mass, geometry, and location of a surrogate fixture mounted on the plate [2]. The goal was to develop an analytical model that would be able to accurately predict the shock response of the resonant plate with various configurations of the fixture which would lead to more efficient shock testing. The study focused on several different aspects of shock testing machine evaluation involving the development of a finite model, experimental modal and shock testing, and development of an analytical modal based shock response model [2].

A FEM was created to extract the mode shapes and the corresponding natural frequencies using Abaqus where the model was represented with a variety of shell elements. The model was divided into three parts: the plate, the slug, and the upper structure and calculations were performed with and without the upper structure in order to determine the inertial loading it would have on the plate [14]. Lanczos numerical eigensolution was used to calculate the modal frequencies within a range of 5-10,000 Hz.

Experimental modal analysis was then performed to validate the FEM using modal assurance criterion (MAC). The experimental modes were extracted using a roving hammer test, which is a common method along with using an electrodynamic shaker. The results did provide a good correlation for the first three fundamental plate modes (first bending, first torsion, and second bending), but did not show good correlation for the higher modes [14].

The next step was to predict the SRS of the plate by using the modes extracted from the FE model by means of modal superposition technique and the Newmark time integration method. Those methods provided ways to analyze how different parameters of the plate affect the SRS without having to run many operational tests [14]. The parameters changed to understand the overall effects of the variables included the number of modes employed in the superposition technique, the influence of the upper structure, variability of the natural frequencies, assumed damping, and nodal locations on the plate. Results of the number of modes employed in the superposition technique showed that the accuracy of the SRS increases when the highest mode shape in the modal matrix is at least 1500 Hz higher than the desired frequency [14]. It was found from the SRSs of the varying modes that the higher frequency residual modes have a significant impact on the SRS and failure to include them will lead to an inaccurate representation of the actual SRS [14].

Though many aspects were presented, and a better understanding of how certain parameters can affect the overall SRS, the study showed that more detailed experiments need to be conducted to fully develop the analytical shock response model. Addressing the structural dynamic modification approaches should be examined further to develop a more suitable SRS test to meet customer specifications.

1.2.10 Shock Loads on Printed Circuit Boards Jayaraman 2016

At the Indian Space Research Organisation (ISRO) researchers examined the effects of shock on printed circuit boards (PCBs) during the launch sequences of spacecraft. Failures of the components in past launches were the motivation behind the study, and the four basic failure modes due to high levels of acceleration, large displacement amplitudes, high levels of stress, and out of tolerance electrical signals were observed [15].

A finite element model (FEM) of the PCB was made and was evaluated using modal analysis to extract the mode shapes, natural frequencies, damping ratio, etc. [15]. The PCB was modeled as a six-layer isotropic plate with quadrilateral shell elements and used NASTRAN as the solver. Normal mode analyses extracted the first three fundamental modes on the FEM for the bare PCB as well as the PCB with the electrical components attached. The first mode of the PCB with and without components are contained in figure 12. The next step of the study was validating the model using the sine sweep test on the physical component. Accelerometers were mounted at various locations to measure the response and the input was driven by an electrodynamic shaker with signal conditioners. The results of the test showed that the natural frequencies of the FEM and the sine sweep test were within acceptable limits.

The next step in the testing process explored the shock response analysis to examine the maximum dynamic response of the PCB to severe shock loads using the FEM and the physical part [15]. The validated FEM model was used to analyze the shock response to a half sine input of 100 G for a duration of 3ms at three locations on the PCB with a damping ratio of 2%. The physical part was once again placed on an electrodynamic shaker where the input matched that of the FEM. The results of the shock test showed that there was

agreement on the predicted peak response of two locations, but the third predicted well below the measured shock response spectra (SRS). The possible reason for this discrepancy was attributed to the holes that were near the location of the accelerometer which gave motivation for future work to include that in the FEM.

1.3 Goals

The goal of this research was to understand the intricacies of multi-axis shock of a circular resonant plate and to explore the advantages of the techniques of multi-axis shock testing and SRS calculation. The focus of this study will be on modeling the system to incorporate changes that include boundary conditions and configurations of both the locations of impact and testing locations on the structure. The analysis includes interpreting the effects of those changes by examining the shock response spectra and exploring the mode shapes of the structure that have the most significant impact on the overall response. These insights will be useful in developing a method to determine the desired impact and testing location on a structure given a desired response.

2 Theory

This chapter covers the basic theory that encompasses shock testing. It starts with the discussion of single degree of freedom systems and multiple degree of freedoms systems and how they are used to derive the equation of motion. The shock response spectrum described in Chapter 1 is explained further and the derivation is shown. Modal analysis is covered and how it is useful to obtain the response of a point for a given input. The chapter ends by discussing how modal decomposition is used to obtain the response for the subset of modes for a given frequency range and how superposition is used to create the overall response of that point for a given input.

2.1 Single Degree of Freedom Systems

The single degree of freedom system (SDOF) is a simple system used for solving vibratory systems and consists of a mass (m) attached to a spring (k) and damper (c) system which is connected to ground (shown in Figure 2.1).

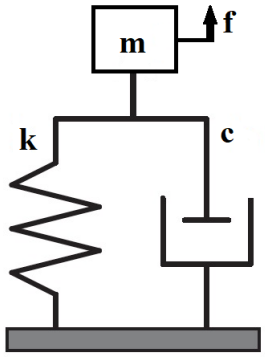

Figure 2.1: Spring-mass-damper model of a SDOF system

The motion of this system is brought on by an external force (f) and creates a vibration which can be expressed by a second-order linear differential equation using Newton's second law of motion:

$$m\ddot{x} + c\dot{x} + kx = f(t)$$

The parameters of mass (m), spring stiffness (k) and damping (c) can be used to find properties of the system including the system's natural frequency (ω_n), damping ratio (ζ) and period(τ):

Natural frequency: $\omega_n = \sqrt{\frac{k}{m}}$

Damping ratio: $\zeta = \frac{c}{c_{critical}} = \frac{c}{2\sqrt{km}}$

Period: $\tau = \frac{2\pi}{\omega_d} = \frac{2\pi}{\sqrt{\frac{k}{m}}}$

Where $\omega_d = \omega_n\sqrt{1-\zeta^2}$

The solution of the equation of motion can be found for less-than-critical (underdamped) damped systems where the system vibrates before coming to rest, critically damped systems with no oscillations, and overdamped systems where there is no oscillatory motion that gradually comes to rest:

Underdamped: $x = e^{-\frac{ct}{2m}}(A\ sin\omega_d t + B\ Cos\omega_d t)$

Critically damped: $x = e^{-\frac{ct}{2m}}(A + Bt)$

Overdamped: $x = e^{-\frac{ct}{2m}}(A\ e^{\omega_n\sqrt{1-\zeta^2}t} + B\ e^{-\omega_n\sqrt{1-\zeta^2}t})$

2.2 Multiple Degree of Freedom Systems

The previously discussed SDOF systems can be useful but are rare in real-world scenarios which often contain more than one degree of freedom. Modeling multiple degree of freedom systems (MDOF) is similar to SDOF, but the parameters are characterized as matrices with *n* number degree of freedoms. Figure 2.2 shows a MDOF system schematic.

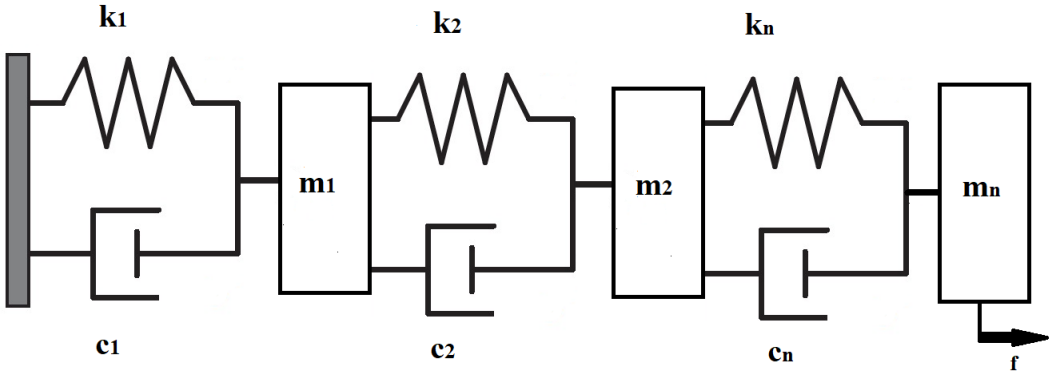

Figure 2.2: Multiple degree of freedom system

The equation of motion for a MDOF system is also similar to a SDOF, and the damping matrix is often proportional to the stiffness matrix in systems where the damping effect is a property of the spring material. The equation of motion for a MDOF is:

$$[M]\ddot{x} + [C]\dot{x} + [K]x = f(t) \tag{2.1}$$

2.3 SRS Calculation

Details of the SRS were shown in section 1.1.1, and this section will cover the calculation of the SRS. Figure 2.3 contains a SDOF model used for simulating shock response spectrum equations where the base response ($\ddot{y}$) is the input acceleration time response for each system and the acceleration responses ($\ddot{x}_i$) are calculated for each frequency.

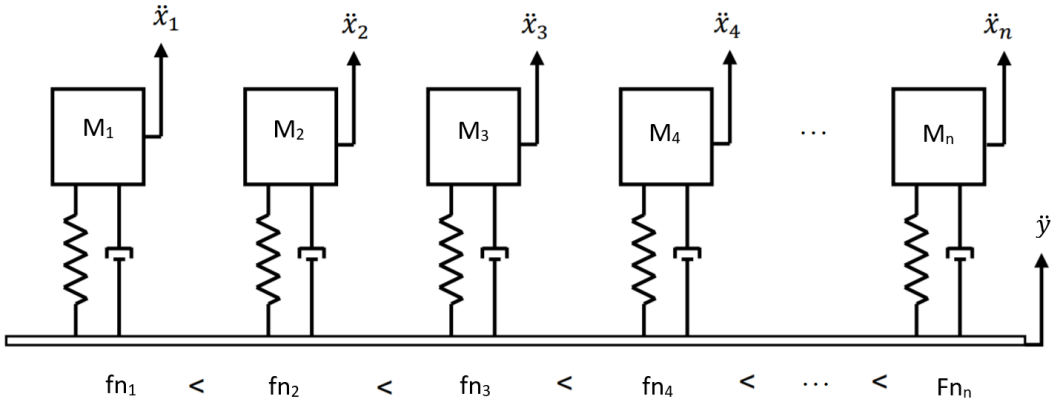

Figure 2.3: SDOF model used for calculating SRS

Using Newton's law on a free body diagram of an individual system, the equation of motion can be found:

$$m\ddot{x} + c(\dot{x} - \dot{y}) + k(x - y) = 0 \tag{2.2}$$

A relative response can be found by using the relative displacement defined as z = x – y

$$m\ddot{z} + c(\dot{z}) + k(z) = -m\ddot{y} \tag{2.3}$$

and using the relationships $\omega_n^2 = \frac{k}{m}$ and $2\zeta\omega_n = \frac{c}{m}$ the response becomes

$$\ddot{z} + 2\zeta\omega_n\dot{z} + \omega_n^2 z = -\ddot{y} \tag{2.4}$$

The above equation is solved using a convolution integral approach which is transformed into a series when $\ddot{y}$ is in the form of digitized data and a solution is produced for each system [3]. The process is expedited after the series is converted into a second-order infinite impulse response filter.

The discrete transfer functions in the z-domain of the digital impulse response filter with the z representing the independent variable in the Z transform from ISO 18431-4 is [19]:

$$H(z) = \frac{\beta_0+\beta_1 z^{-1}+\beta 2}{1+\alpha_1 z^{-1}+\alpha_2 z^{-2}} \quad (2.5)$$

For the estimated SRS calculation, the coefficients of the digital impulse response filter were developed by David Smallwood where it is described as the Ramp Invariant Method which is applied to base excitation to a SDOF system [20]. The SRS calculations have different transfer functions in the LaPlace domain depending on whether it involves displacement, velocity, or acceleration [21]. For the maximax calculation, which is used in the calculations of all SRSs in this thesis, the coefficients of the discrete transfer function are [21,22]:

$$\beta_0 = 1 - exp(-A)sin(B)/B. \quad (2.6)$$

$$\beta_1 = 2\exp(-\mathrm{A})[\sin(\mathrm{B})/\mathrm{B} - \cos(\mathrm{B})] \quad (2.7)$$

$$\mathrm{B}_2 = \exp(-2\mathrm{A}) - \exp(-\mathrm{A})\sin(\mathrm{B})/\mathrm{B} \quad (2.8)$$

$$\alpha_1 = -2exp(-A)cos(B) \quad (2.9)$$

$$\alpha_2 = \exp(-2\mathrm{A}) \quad (2.10)$$

where

$$\mathrm{A} = \frac{\omega_n}{T_s 2Q} \quad (2.11)$$

$$B = \omega_n T_s \sqrt{1 - \frac{1}{4Q^2}} \quad (2.12)$$

and T_s is the sampling time interval which is also $\frac{1}{f_s}$ where f_s is the sampling frequency in Hz [22]. Q is the quality factor which is equivalent to $\frac{1}{2\zeta}$ and ω_n is the natural frequency in rad/s [19].

2.4 Modal Analysis

Experimental modal analysis theory covers both lumped-parameter (discrete) and continuous models that determine the modal parameters (natural frequencies, mode shapes, modal scaling, and damping factors) of an assumed linear system. The theory develops an understanding of the relationship between the structural parameters (mass, stiffness, and damping) and the impulse response function of the time domain, the frequency response function (FRF) in the frequency domain, and the transfer function in the Laplace domain for both SDOF and MDOF systems [4].

The equations of motion for a real structure of infinite degrees of freedom in the time domain and frequency domain by taking the Fourier transform are:

$$[M]\ddot{x} + [C]\dot{x} + [K]x = f(t) \tag{2.13}$$

$$[-m\omega^2 + jc\omega + k]X(\omega) = F(\omega) \tag{2.14}$$

Solutions to the equations of motion for the time domain and the frequency domain respectively are:

$$X(t) = [H(t)] \otimes \{F(t)\} \tag{2.15}$$

$$X(j\omega) = [H(j\omega)]\{F(j\omega)\} \tag{2.16}$$

The frequency response function (FRF) is the quantity $H(j\omega)$ which states the system response is directly related through the forcing function and can also be represented as:

$$H_{pq}(j\omega) = \frac{b_{pq}(j\omega)}{a_{pq}(j\omega)} = \sum_{k=1}^{n}\left(\frac{A_{pq_k}}{j\omega-\lambda_k} + \frac{A_{pq_k}{}^*}{j\omega-\lambda_k{}^*}\right) \tag{2.17}$$

and in the time domain the impulse response function is:

$$h_{pq}(t) = \sum_{k=1}^{n}\frac{e^{-\sigma_k t}}{m_k\omega_{d_k}} sin(\omega_{d_k}t) = \sum_{k=1}^{n}\left(A_{pq_k}e^{\lambda_k t} + A^*_{pq_k}e^{\lambda_k{}^* t}\right) \tag{2.18}$$

where: p = response degree of freedom

q = input degree of freedom

k = mode number

A_{pq_k} = residue

A_{pq_k}= $Q_k\varphi_{p_k}\varphi_{q_k}$

Q_k = modal scaling factor

φ_{p_k} = modal coefficient

λ_k = system pole

n = number of modes

The response at a given location and direction *p* due to an input *q* in the frequency and time domain, respectively, can be rewritten as:

$$x_p(j\omega) = \sum_{k=1}^{n} \left(\frac{A_{pq_k}}{j\omega - \lambda_k} + \frac{A_{pq_k}^*}{j\omega - \lambda_k^*} \right) f_q(j\omega) \quad (2.19)$$

$$x_p(t) = \sum_{k=1}^{n} \left(A_{pq_k} e^{\lambda_k t} + A_{pq_k}^* e^{\lambda_k^* t} \right) \otimes f_q(t) \quad (2.20)$$

where $n = \infty$ in theory, however for practical purposes, the number of modes is condensed based on the significant contribution the modes have on the solution [16]. With these equations the response can be estimated for a given point on the structure with a given input for each mode in either the frequency or time domain. The next section will discuss the superposition principal of modal responses and how it is used in this thesis.

2.5 Modal Decomposition

In the time domain the overall response of a MDOF system is a combination of the subsequent sinusoids that can be examined individually and summed together to create the entire response. The individual responses in the time domain can be analyzed in the frequency domain by performing a Fast Fourier Transform (FFT) and the individual responses can also be summed together in the frequency domain to create the overall response of the system. An SRS can be made from the individual time domain response using the techniques derived in the previous section, but the overall SRS is not simply the summation of the individual SRS responses.

Figure 2.4 shows an example of two individual responses that are obtained from an overall response that contains many individual responses. The figure shows how the time domain response can be used to estimate the FRF and SRS, and how the time domain signals and FRF can be summed to create the overall signal in both the frequency and time domain, but the response of the SRS is not the superposition of responses. In order to obtain the estimated SRS of the overall response the individual signals must be summed in the time domain prior to the process of converting into the SRS due to containing constructive and destructive summations which will have an effect on the calculated SRS. The summations of the SRS functions are only real functions therefore they do not contain any phase information and no destructive summations.

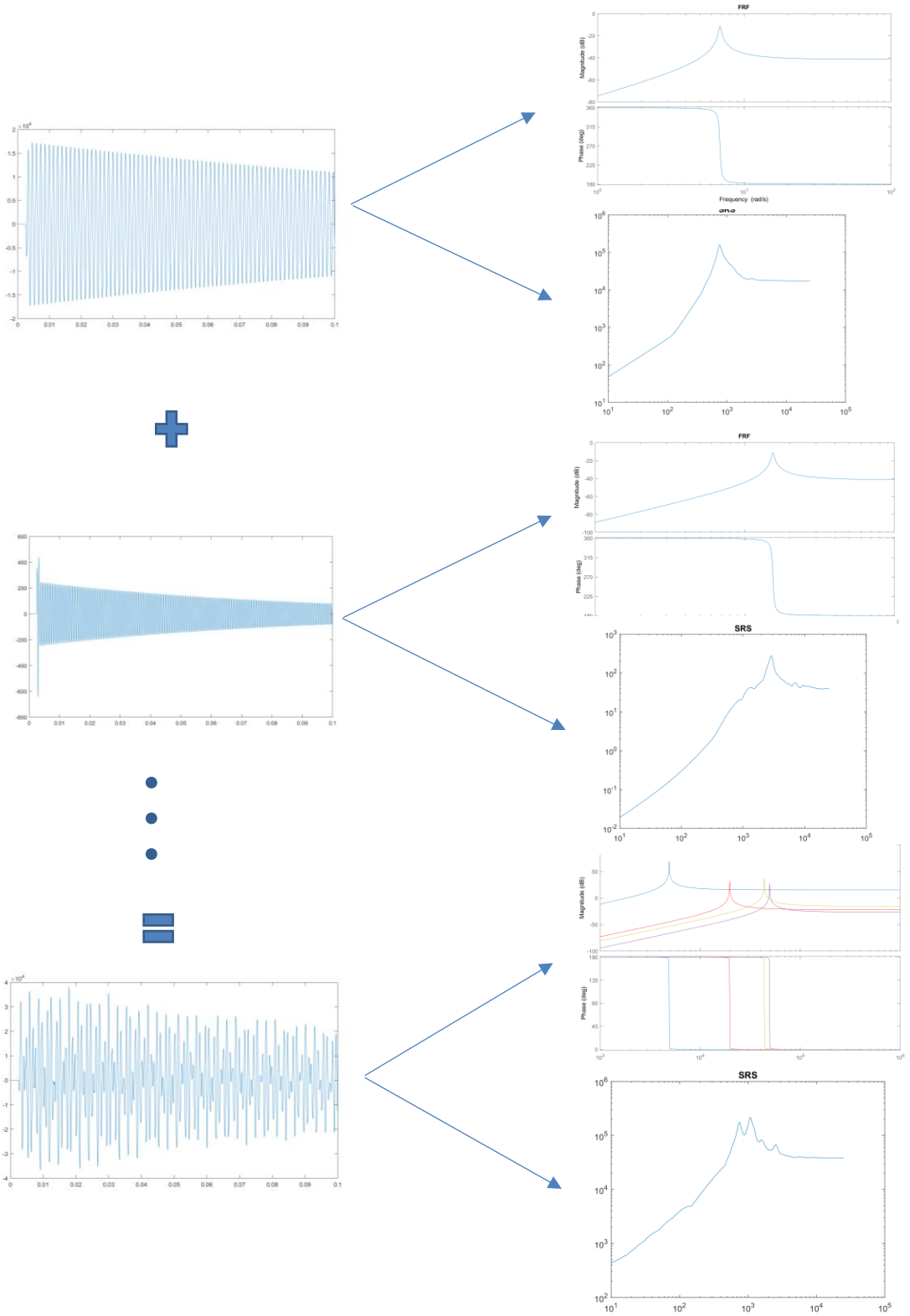

Figure 2.4: Example time history and FRF superposition

3 Solid Circular Plate

This chapter discusses the solid circular resonant plate from the previous research done at Michigan tech performed by William Larsen. The model that was created was used to examine the change in dynamics of the test fixture at two output locations with the inputs at the reverse side of the test fixture in the center, half radius of the plate and the edge of the plate.

3.1 Methods

The Finite Element Analysis (FEA) model was created in Hypermesh using the material properties of the physical aluminum resonant plate used for experimental testing.

Material Properties:

- $\nu = 0.33$ (Poisson's ratio)
- $\rho = 0.000254$ lbf-sec^2/in^4 (density)
- E = 10000000 psi (modulus of elasticity)
- G = 80769 psi (shear modulus)

The model has a diameter of 17 inches and a thickness of 1.125 inches, matching the physical geometry of the experimental test plate (see Figure 3.1). Mesh elements were made using 1st order tetrahedral elements with 0.2-inch size. The boundary conditions of a free-free system with four soft spring attachments (10lbf/in) were created to replicate the conditions under testing. The uniform structural damping coefficient used was the default setting of 0.02.

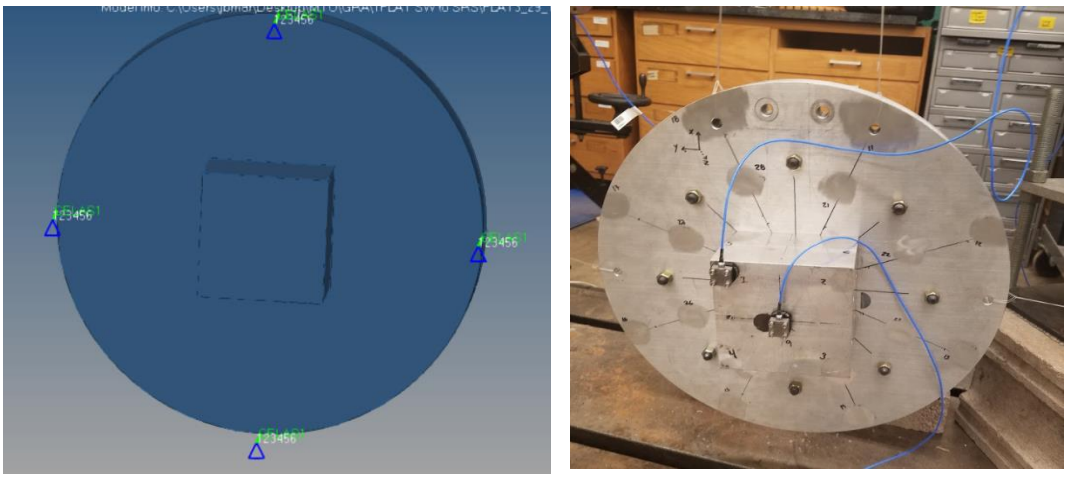

Figure 3.1: Hypermesh FEA model and experimental plate

The model was used to get the acceleration and velocity outputs at particular nodal points of interest. The output nodal points chosen for this part of the study included the points on the fixture in one corner and the center of the fixture (where accelerometers are shown in Figure 3.1). This study examined the effects of input location on the overall SRS, where the inputs are at the center of the plate opposite the fixture, middle of the plate, and on the edge of the plate (far). The input excitation was collected from experimental data using a hammer with metal-to-metal contact. Figures 3.2-3.3 contain the input time history used in the FEA for the center, middle of the plate, and the edge of the plate impacts respectively which were taken from experimental data and imported into Hypermesh with the concept of trying to replicate the exact dynamics the physical plate would have under testing.

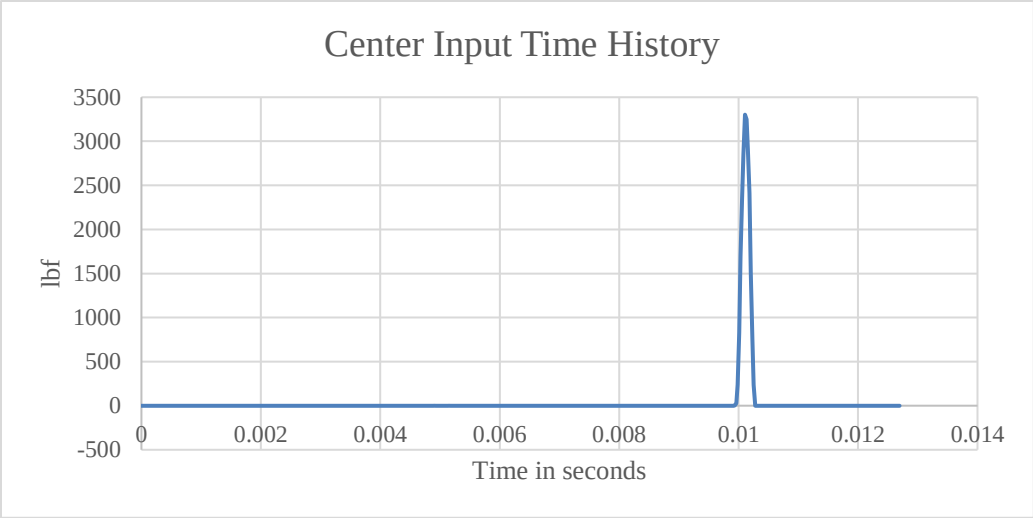

Figure 3.2: Center impact time history used in FEA from experimental data

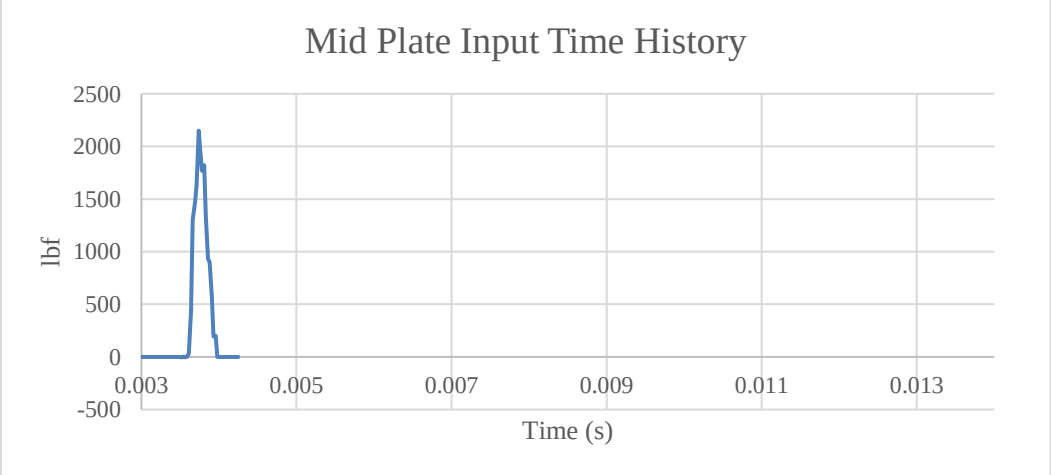

Figure 3.3: Middle of the plate impact time history used in FEA from experimental data

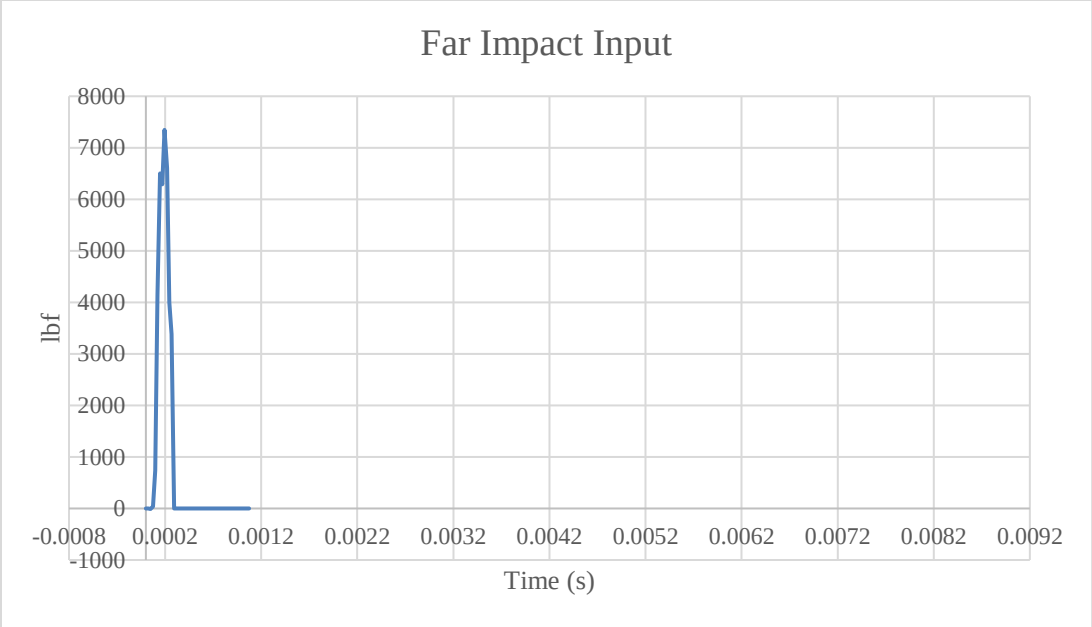

Figure 3.4: Edge of the plate impact time history used in FEA from experimental data

3.2 Results

Experimental testing of resonant plates typically impact the plate in the center and examine the test fixture in the center. In this experiment, the solid resonant plate was impacted in the center, middle of the plate, and the far edge of the plate. The nodal points of interest are the center of the fixture as well as the corner of the fixture.

Using the model made in Hypermesh and at the center of the plate with the output at the center of the fixture yielded results that were to be expected. Figure 4.1 shows the input, velocity and acceleration time histories for all directions and it can be observed that the in axis (Z) direction, shown in pink in velocity time history and green in acceleration time history, has a greater magnitude than the off-axis directions. Examining the corner point on the fixture shows the same trend, which was to be expected, but there is a minor change in the magnitude of the acceleration and velocity time histories which can be explained by the placement on the fixture (shown in Figure 4.2). These differences show that there is different dynamics between the nodal points on the fixture, which will be more evident when viewing the SRS.

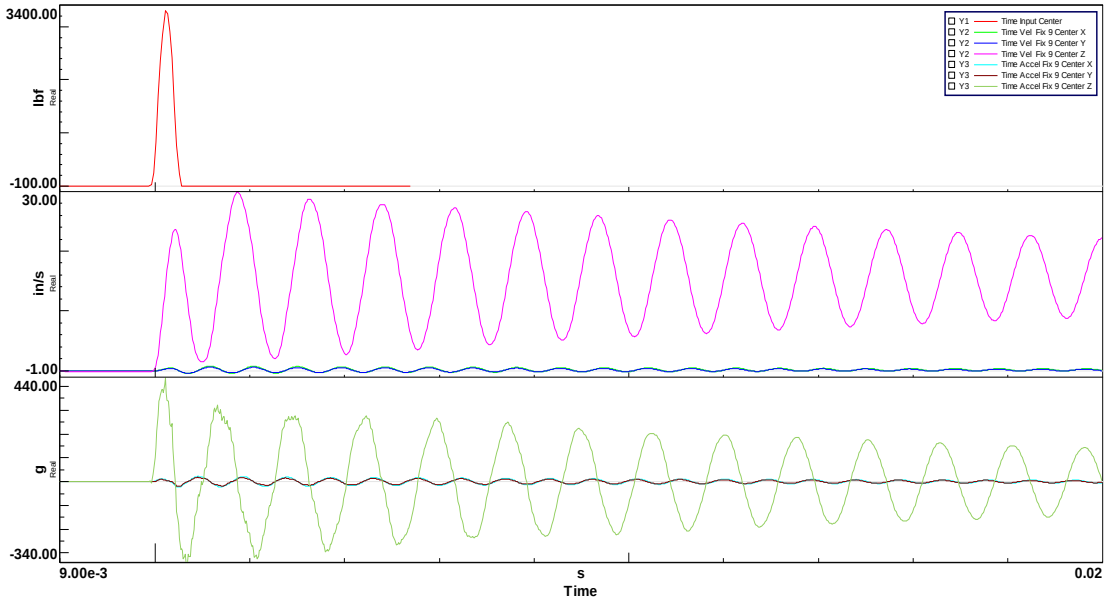

Figure 3.5: Time histories for the input, velocities, and accelerations in all directions with impact in the center and output in the center of the fixture

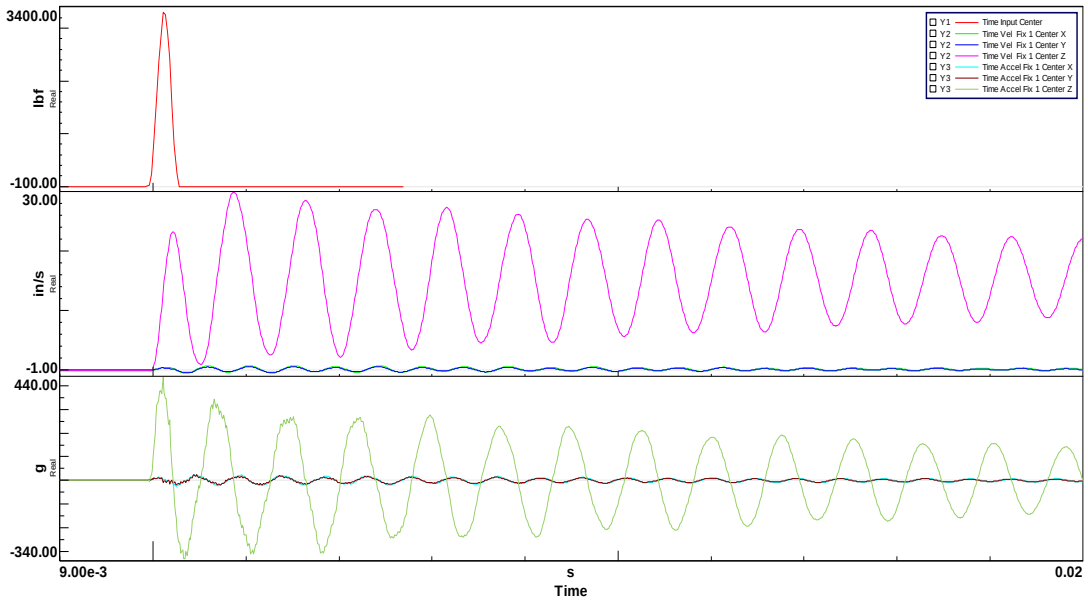

Figure 3.6: Time histories for the input, velocities, and accelerations in all directions with impact in the center and output in the corner of the fixture

The SRS was estimated using LMS Testlab which utilizes Smallwood's Matlab code and was done for both the output locations in the center and corner of the fixture shown in Figures 3.7 and 3.8 respectively. Comparing these it can be noted that the magnitude of the in-axis direction is several orders of magnitude greater than the off-axis directions, which

was expected. The off-axis directions are similar to each other in both scenarios, however, there was some slight difference in the overall shape of the SRS in the regions before and after the knee frequency where it can be noted there are a different number of peaks in the corner node of the impact pad versus the center node due to higher modes affecting the response. There was also a difference in knee frequencies for the in-axis versus the off-axis responses since being out of plane of the impact caused different modal frequencies to be employed.

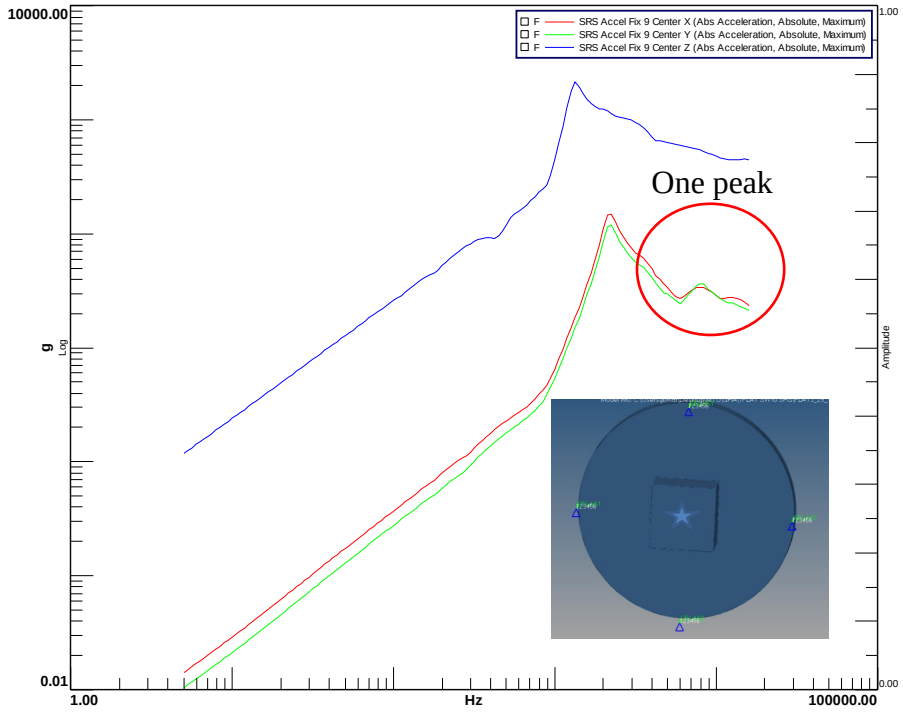

Figure 3.7: SRS of the center node of the fixture in all directions with impact at center

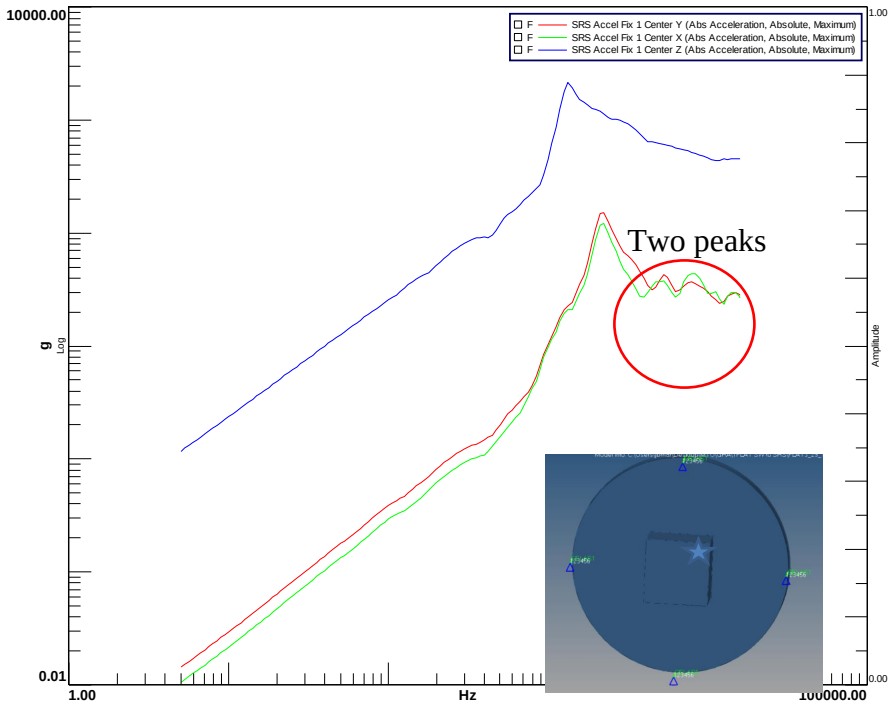

Figure 3.8: SRS of the corner node of the fixture in all directions with impact at center

The next part of the experiment involved changing the input location from the center of the impact pad to an offset position in the middle of the plate shown in Figure 3.9. The input time history from experimental data can be seen in Figure 3.10 and Figure 3.11 along with the time histories of the velocity and acceleration for both the center node and corner node of the fixture respectively. Comparing the velocity and acceleration time histories for the offset input, it can be noted that the off-axis magnitudes have increased. There are also phase changes in the acceleration time histories between the center node and the corner node. These changes show that the off-axis responses can be effectively increased by moving the impact location and the response at different nodal locations will also be affected.

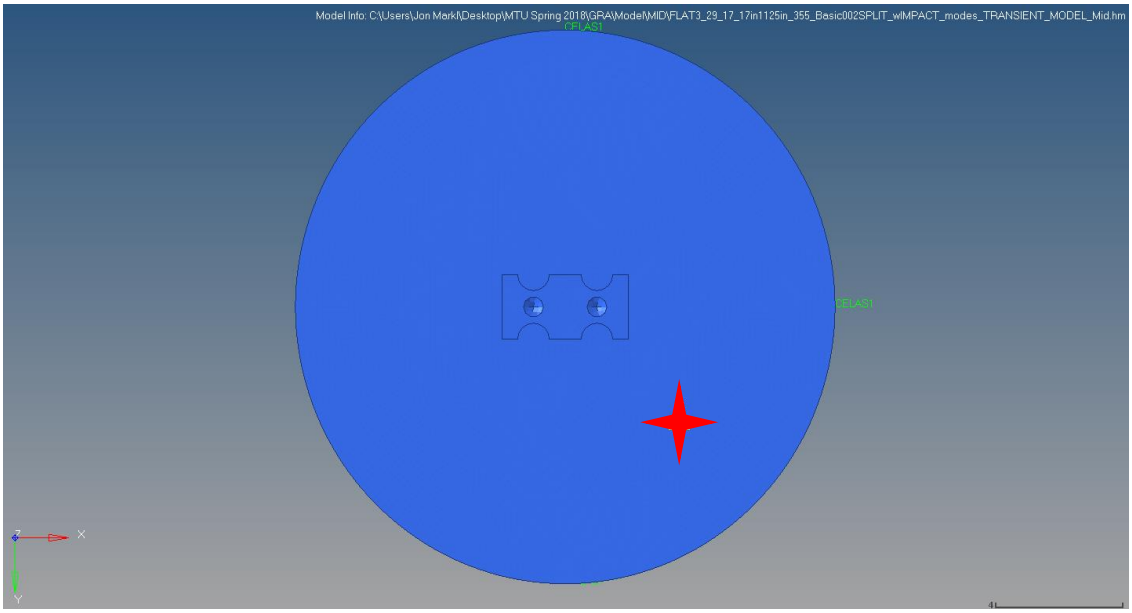

Figure 3.9: Impact location offset in the half-radius of the resonant plate

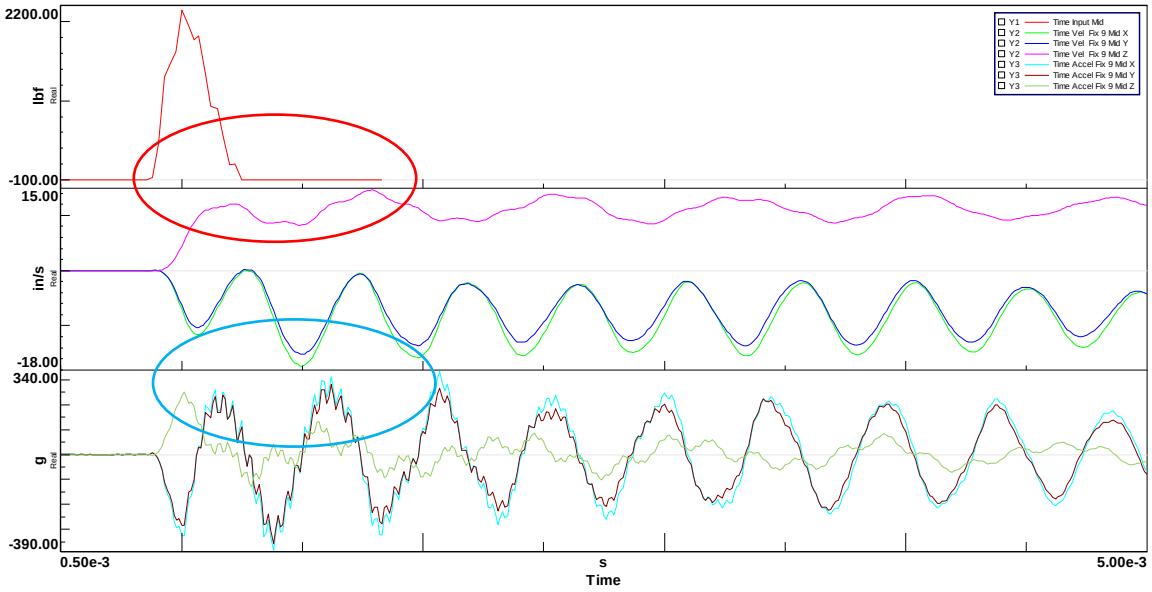

Figure 3.10: Time histories for the input, velocities, and accelerations in all directions with impact offset in the middle of the plate and output in the center of the fixture

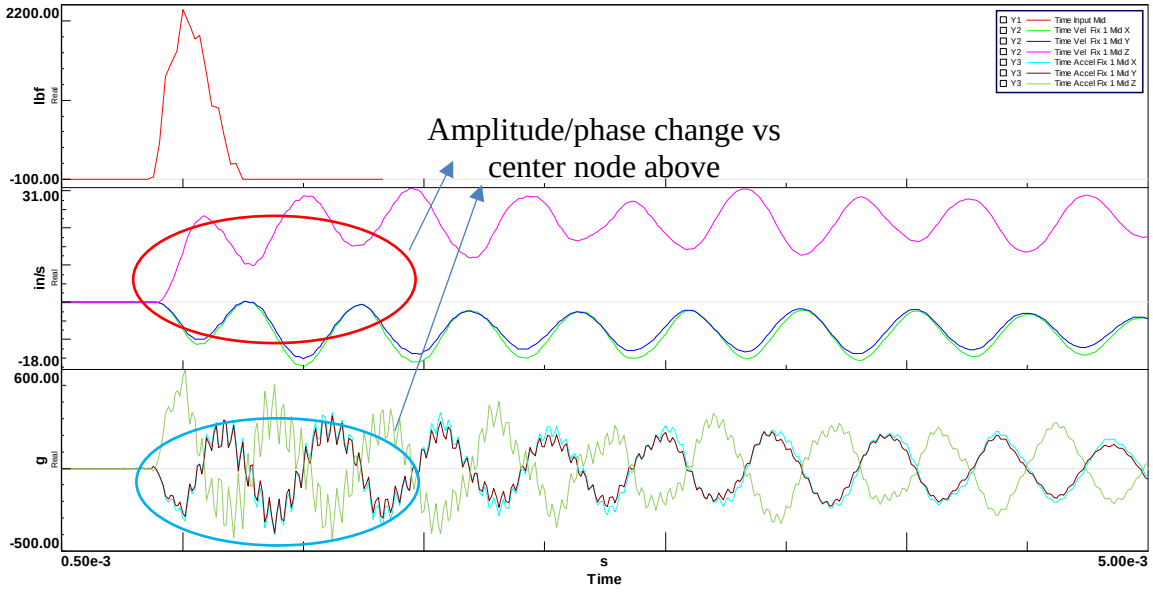

Figure 3.11: Time histories for the input, velocities, and accelerations in all directions with impact offset in the middle of the plate and output in the corner of the fixture

The SRS from the acceleration time histories were again estimated in LMS Testlab and can be found in Figures 3.12 and 3.13 for the output at the center and corner of the fixture respectively. Comparing the SRSs from figures 3.12 and 3.13 to the previous experiment where the impact location was on the center of the impact pad shows the magnitudes of the off-axis directions have increased, and it can be observed in Figure 3.12 that the off-axis responses are greater than the in-axis response at knee frequency and plateau region frequencies. This phenomenon is not true for the corner node shown in Figure 3.13 and it can be observed that the knee frequency of the in-axis response has changed. This shows that the response changes depending on the location on the fixture and can effectively change the knee frequency which can be useful in designing SRS test specifications.

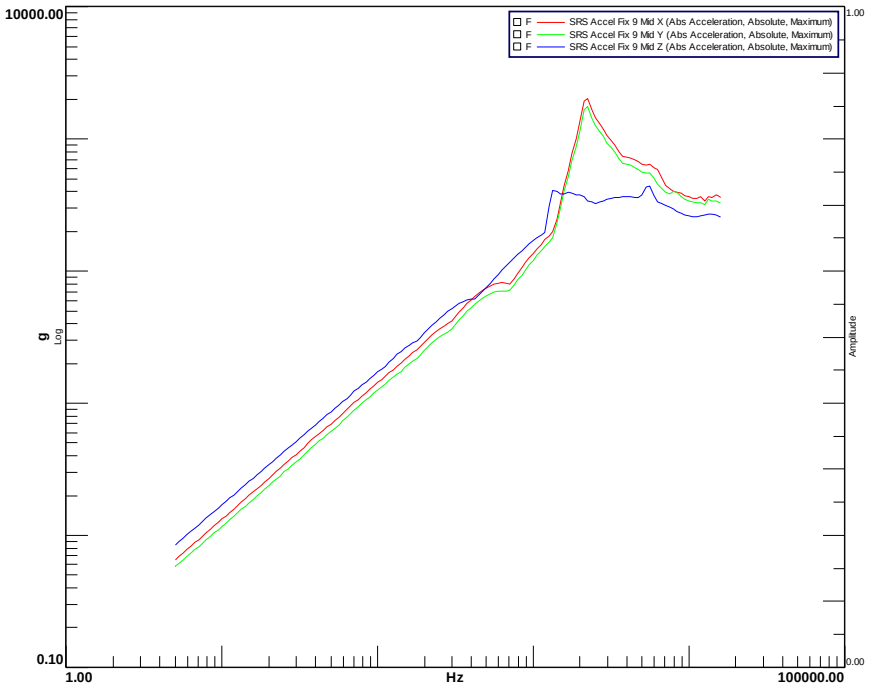

Figure 3.12: SRS of the center node of the fixture in all directions with impact offset in the middle of the plate

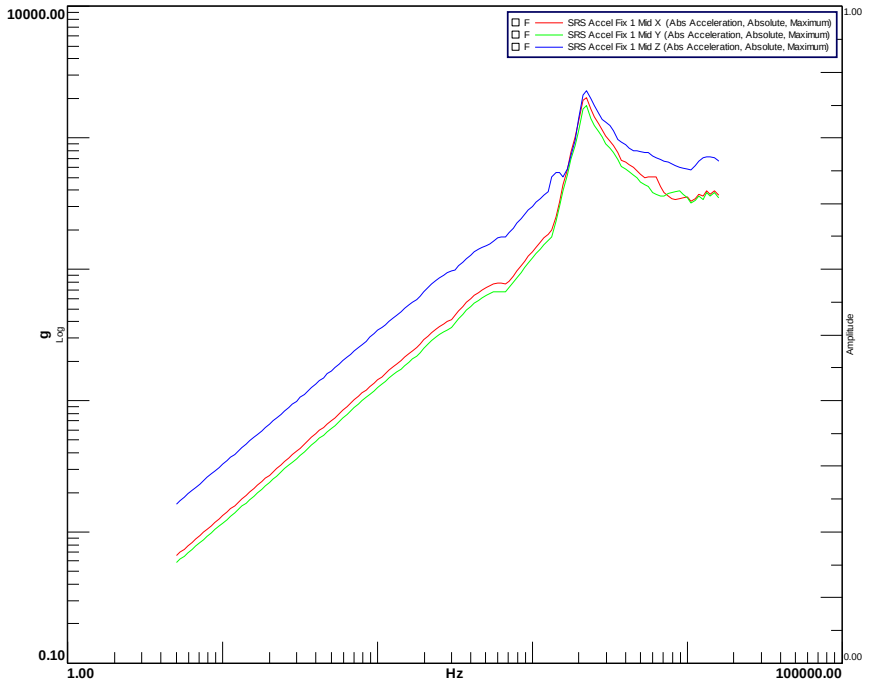

Figure 3.13: SRS of the corner node of the fixture in all directions with impact offset in the middle of the plate

The last part of the experiment involved moving the input location again closer to the edge of the plate shown in Figure 3.14. The time history of the input from experimental data is shown in Figures 3.15 and 3.16 along with the time histories of the acceleration and velocities in both the center and corner node of the fixture respectively. Once again, the effect of moving the input has changed the magnitudes of both the velocity and acceleration and it can be observed that the change in magnitude increases more when the input location is offset more in the off-axis directions.

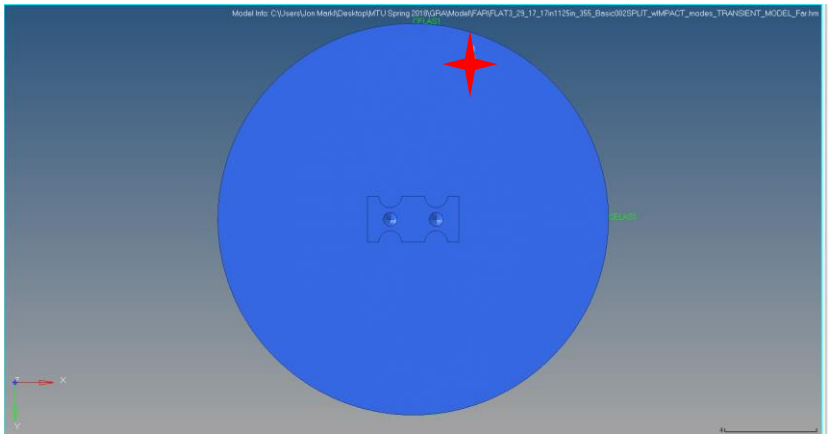

Figure 3.14: Impact location offset in the edge of the resonant plate

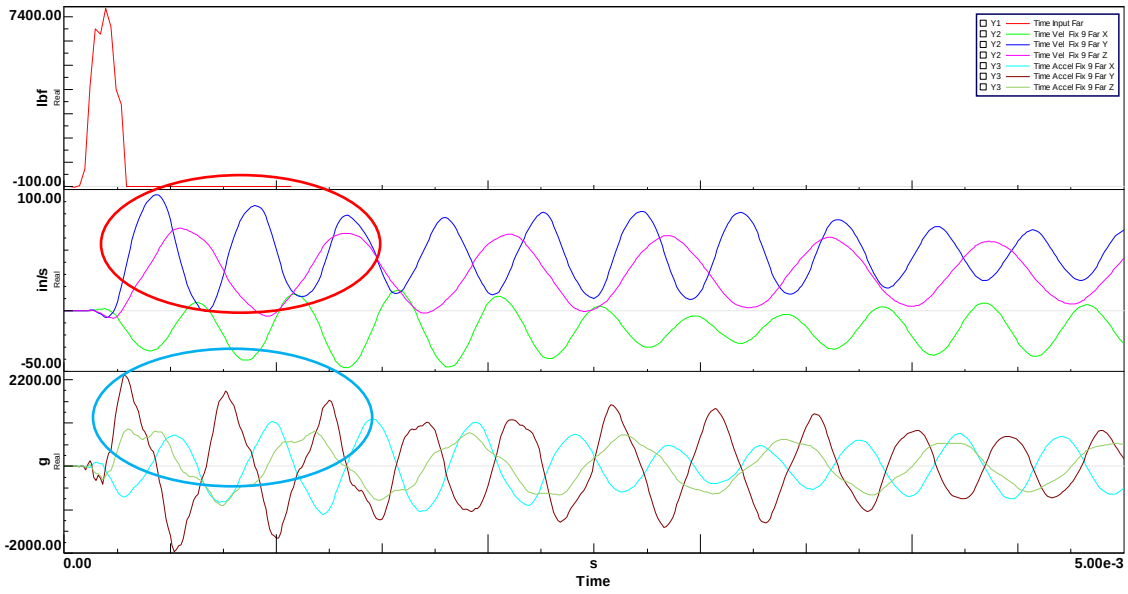

Figure 3.15: Time histories for the input, velocities, and accelerations in all directions with impact offset in the edge of the plate and output in the center of the fixture

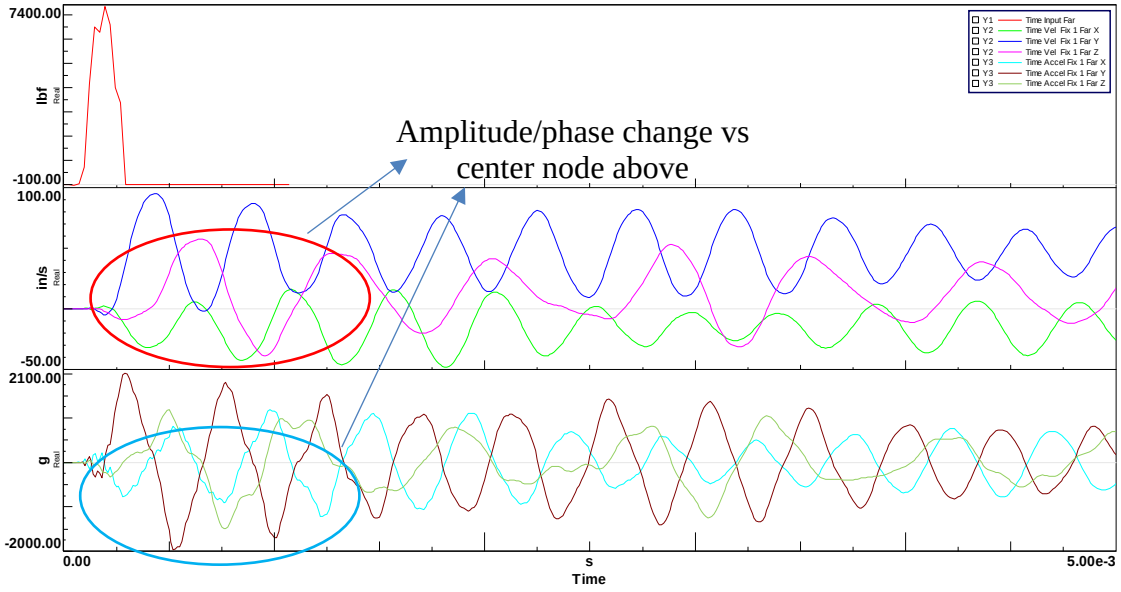

Figure 3.16: Time histories for the input, velocities, and accelerations in all directions with impact offset in the edge of the plate and output in the corner of the fixture

The SRS of the center and corner node of the fixture with the impact offset on the edge of the plate were estimated and are found in Figures 3.17 and 3.18 respectively. With the impact location offset on the edge of the plate, it can be observed that in both the center and corner nodes of the fixture the magnitudes of the off-axis responses are greater than the in-axis response around the knee frequency. It is also apparent that the in-axis knee frequency is not the same as the off-axis knee frequency in both the center and corner nodal locations and the shapes of the SRS is dependent upon the location of output and can affect test specifications as well.

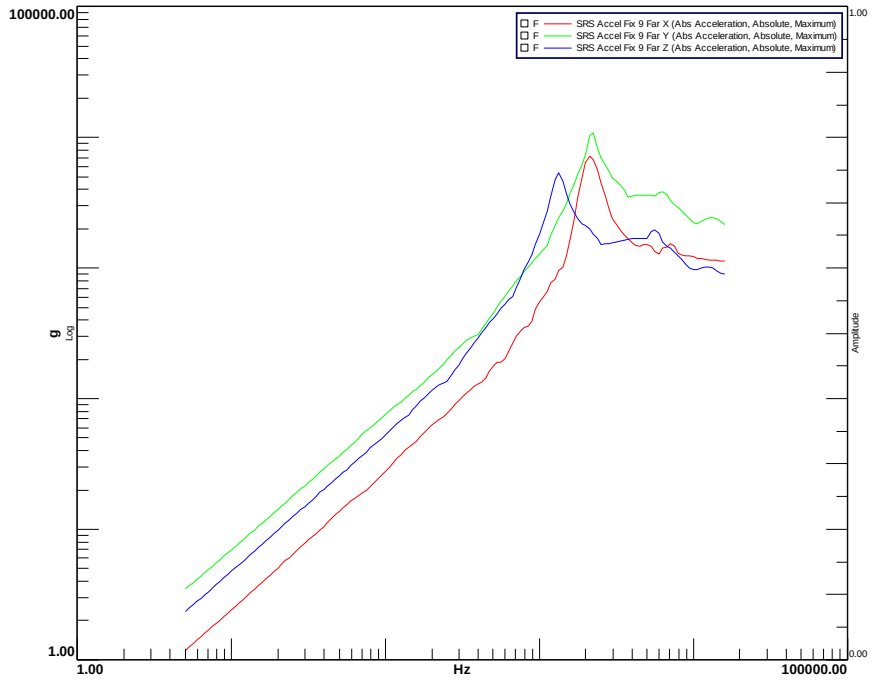

Figure 3.17: SRS of the center node of the fixture in all directions with impact offset on the edge of the plate

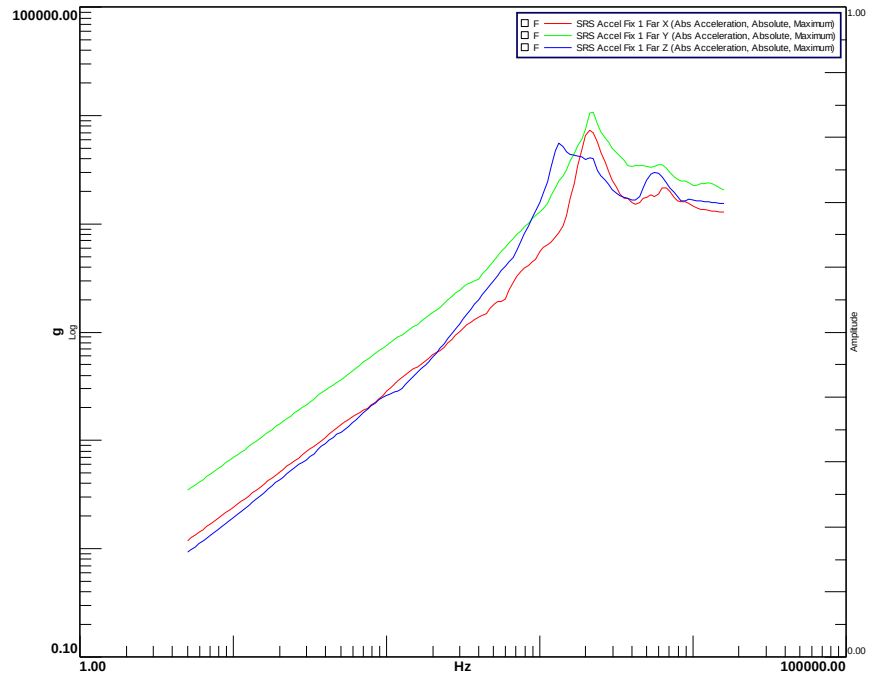

Figure 3.17: SRS of the corner node of the fixture in all directions with impact offset on the edge of the plate

4 Correlated Model Assembled with Contact Surfaces

This model was made in collaboration with Charles Van Karsen and improved on the previous design that was developed by William Larsen. The new model was no longer constructed as one solid piece but consisted of several sub-assemblies that were connected with contact surfaces that more accurately reflected the physical plate and the subsequent dynamics of the system. The fixture and impact pad of the model was made using higher order elements for more accuracy whereas the plate was made with shell elements thus decreasing the computation time. The boundary conditions were also changed to accurately depict the physical configuration in the laboratory.

4.1 Methods Correlated Model Assembled with Contact Surfaces

An updated FEA model was created in Hypermesh using the material properties shown below with changes from the previous model that include separate assemblies of the plate, the impact pad, and the fixture. The assemblies were connected via surface contacts in Hypermesh to more accurately depict the physical mounting configurations and the subsequent dynamics. It also allowed for useful testing used later in the thesis for moving the fixture and impact pad in different configurations which was not possible for the previous model. Other changes include the mesh pattern of the fixture and impact pad being changed to 2^{nd} order tetrahedral and the plate mesh pattern to shell elements. The advantage of using 2^{nd} order elements versus 1^{st} order elements is there is strain and slope continuity at the nodes leading to more accurate results and shell elements for the plate are more advantageous because of the reduced computation time and are less prone to negative Jacobean errors. These changes were used in conjunction with a modal test of the physical plate to ensure the model depicts a more suitable representation of the dynamics of the physical plate and the comparison of the modal frequencies are shown in Table 4.1. The natural frequencies from the solid model used previous were found to have the percent error of the FEA to the experimental frequencies increase as the modes increased.

Material Properties:

- $\nu = 0.33$ (Poisson's ratio)
- $\rho = 0.000254$ lbf-sec^2/in^4 (density)
- E = 9900000 psi (modulus of elasticity)
- G = 80769 psi (shear modulus)
- Uniform structural damping coefficient: 0.001

Table 4.1: Modal frequencies of experimental and FEA used for correlation

Mode Number	Experimental Frequency (Hz)	FEA Frequency (Hz)	Percent Difference (%)
1	887	915	3.2
2	974	950	-2.4
3	1249	1190	-4.8
4	1750	1791	2.3
5	1766	1795	1.7
6	2017	1938	-3.9
7	2081	1964	-5.6
8	2972	3035	2.1
9	2975	3036	2.1

4.1.1 Center and Edge Impact

The effects on the SRS due to changing input locations on the plate using the updated model was completed and compared with an experimental test. The locations of the inputs are shown by the blue triangles in Figures 4.1-4.2 and the output nodes of interest are shown in Figure 4.3. The input used on the model was again taken from the experimental test data and the time histories for the center impact on the pad and the edge of the plate are shown in Figures 4.4-4.5 respectively. The purpose of using different input time histories was to replicate what the physical device was undergoing during an experimental test and compare the responses of the physical response versus the modeled response.

Comparing the input at the center versus the input on the edge of the plate shows the impulse duration of the center impact is 0.42 ms and the impulse duration of the edge impact is 0.73 ms which means that the most amount of energy put into the system would be found up to 2381 Hz and 1370 Hz respectively. Shorter pulse durations were important to use considering the frequency range of interest are from 0 – 5000 Hz, so ideally the pulse duration should be 0.2 ms. The force of the center impact is 1120 lbf versus 890 lbf for the edge impact and the difference is due to the edge impact was not protected by an impact pad so caution was used for fear of damaging the plate.

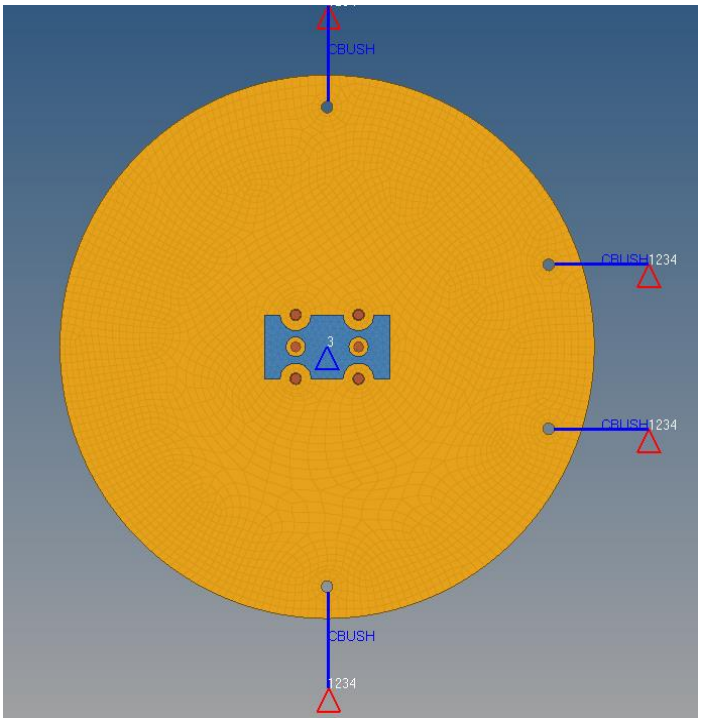

Figure 4.1: Input location at the center of the impact pad

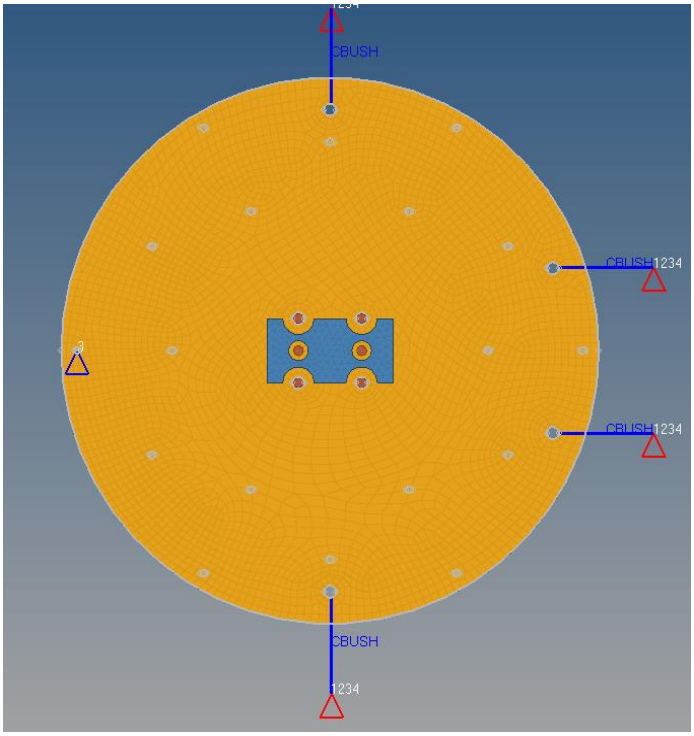

Figure 4.2: Input location at the far edge of the resonant plate

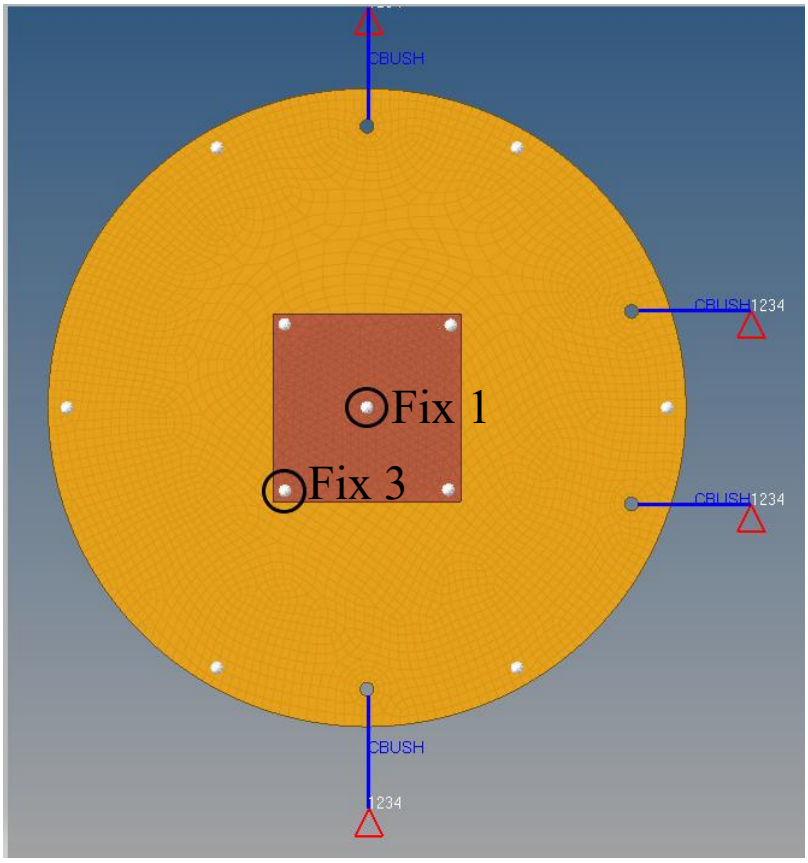

Figure 4.3: Output nodes on the center of the fixture (Fix 1) and the corner of the fixture (Fix 3)

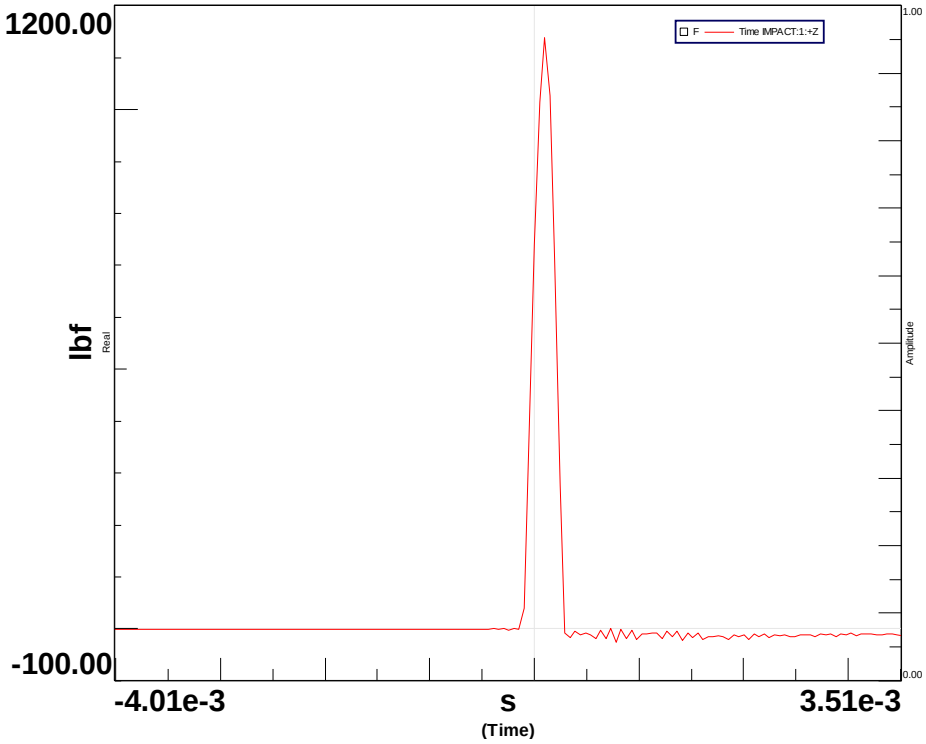

Figure 4.4: Time history for center impact

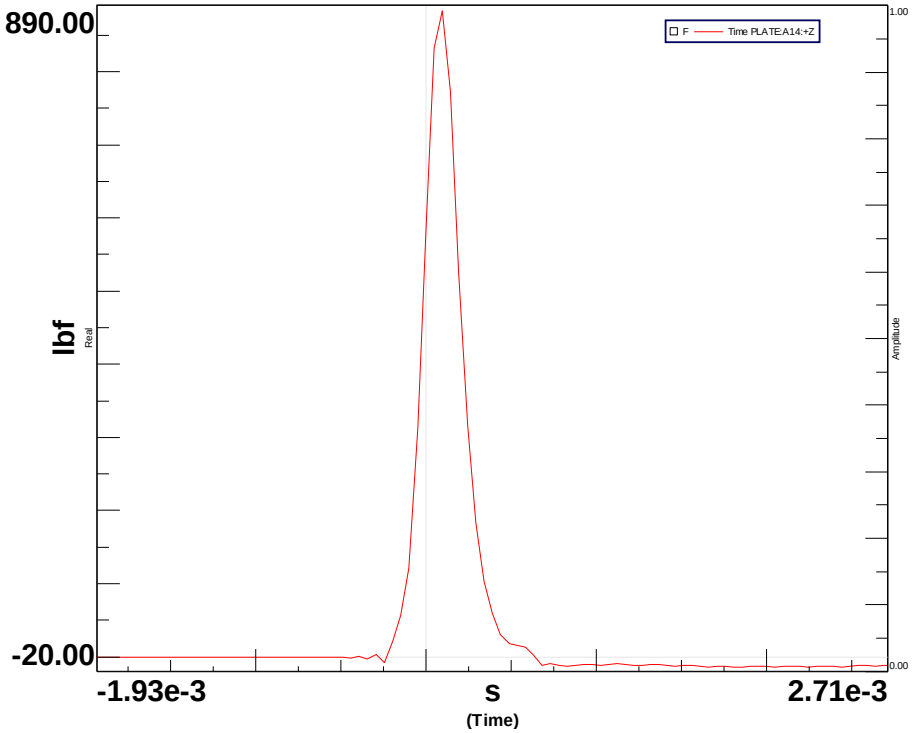

Figure 4.5: Time history for edge impact

4.1.2 Input at angle

Using the same model configurations as the previous experiment, the effects on the SRS by changing the input angle was explored. In Hypermesh, the load collector for input was edited and changed from having only 1 DOF to 2 DOFs in the +Z and +X directions. The effects of implementing a 20˚ angle in the +X direction was chosen and can be visualized in Figure 4.6. The input used was the same as the center impact used in the previous experiment with a force of 1120 lbf and an impulse duration of 0.42 ms, and once again an ideal pulse would be 0.2 ms, but for comparison purposes the experimental input was used for this study.

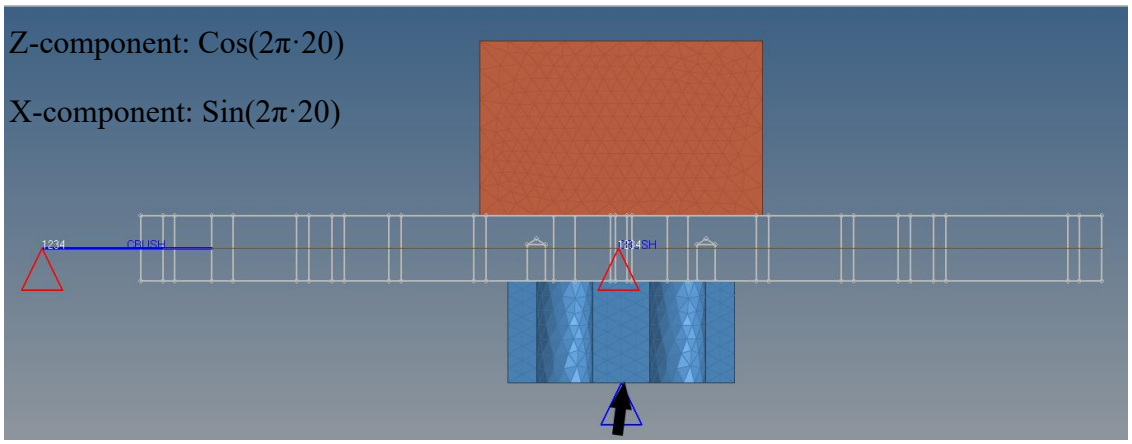

Figure 4.6: Model with input at 20˚ in the +X direction

4.2 Results Correlated Model Assembled with Contact Surfaces

4.2.1 Center and Edge Impact

The changes made to the FEM described in section 3.2 were explored and the effects the new configuration would have on the SRS were investigated. Similar to the previous experiment in the previous section, a study of the response at nodal locations in the center and the corner of the fixture were conducted with impact locations in the center of the impact pad and an offset impact location towards the edge of the resonant plate with the new model that employs subassemblies attached with contact surfaces. Figures 4.7 and 4.8 show the SRS of the center and corner node respectively with the impact location at the center of the impact plate. Like the previous experiment, the magnitude of the in-axis SRS is greater than the off-axis responses, but there are differences in the shapes of the SRS which involve the change in the constant velocity slopes no longer being straight lines. The boundary conditions used in this experiment affected the shape of the SRS before the knee frequency and caused the slope of the constant velocity line to be nonlinear, and those observations can also be observed in experimental data with similar boundary conditions used [16].

The only changes observed from the SRS of the center node versus the corner nodes are changes to the general shape of the SRS after the knee frequency of 1190 Hz which results from the effects of the higher mode shapes at those locations.

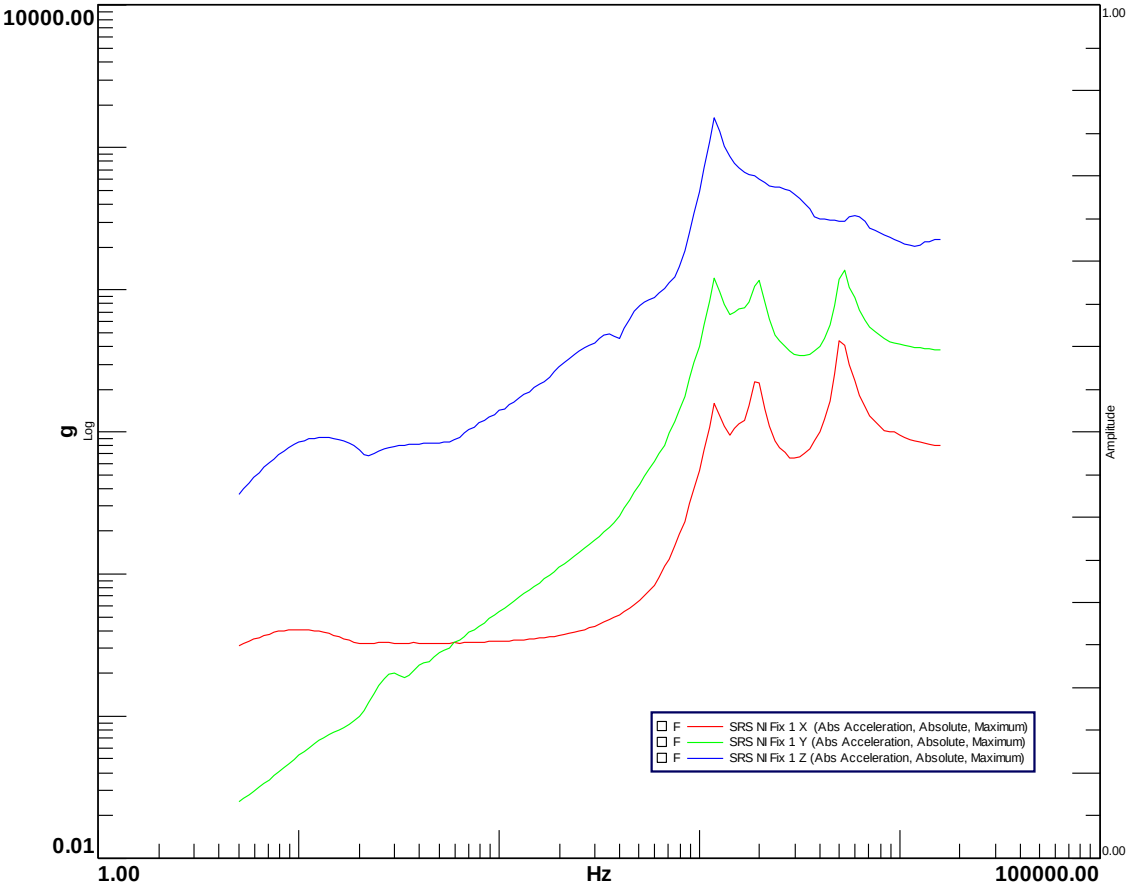

Figure 4.7: SRS of the center node of the fixture in all three directions with the input location in the center of the impact pad

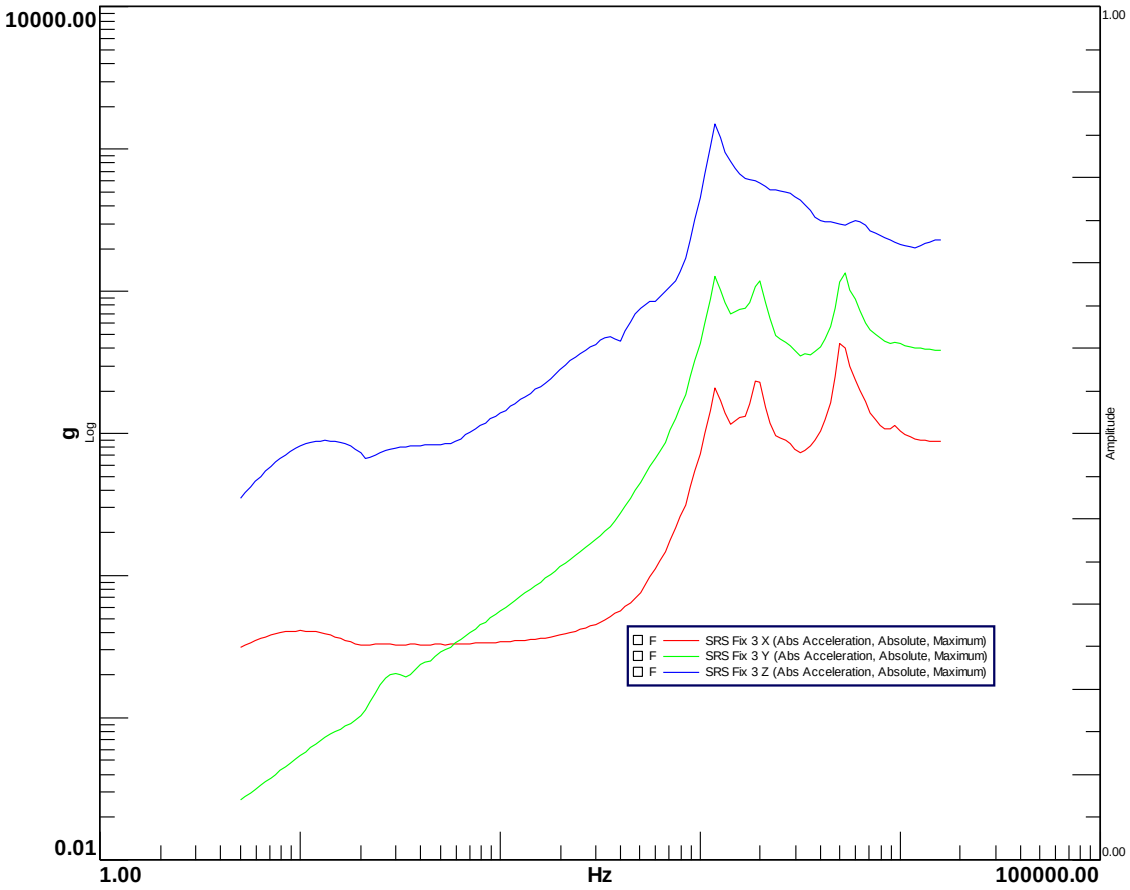

Figure 4.8: SRS of the corner node of the fixture in all three directions with the input location in the center of the impact pad

The impact location was then changed to the edge of the plate shown in Figure 4.2 and again SRSs were made for the center and corner node of the fixture shown in Figures 4.9 and 4.10 respectively. Once again it can be noted that the magnitudes of the off-axis responses increase when changing the impact location from the center of the plate to the edge of the plate, however, the +Y response did not increase as greatly in this experiment compared to the solid resonant plate edge impact performed in section 4.2.1. The change of boundary conditions from symmetrical to asymmetrical change the dynamics of the plate depending on the location of impact and have attributed to the change of magnitude for a given direction. Comparing the center node SRS from Figure 4.9 to the corner node SRS in Figure 4.10 it can be determined that the knee frequencies for the in-axis response (shown in blue) change depending on the location of the output on the fixture and the off-axis responses have no significant change from the center node to the corner node.

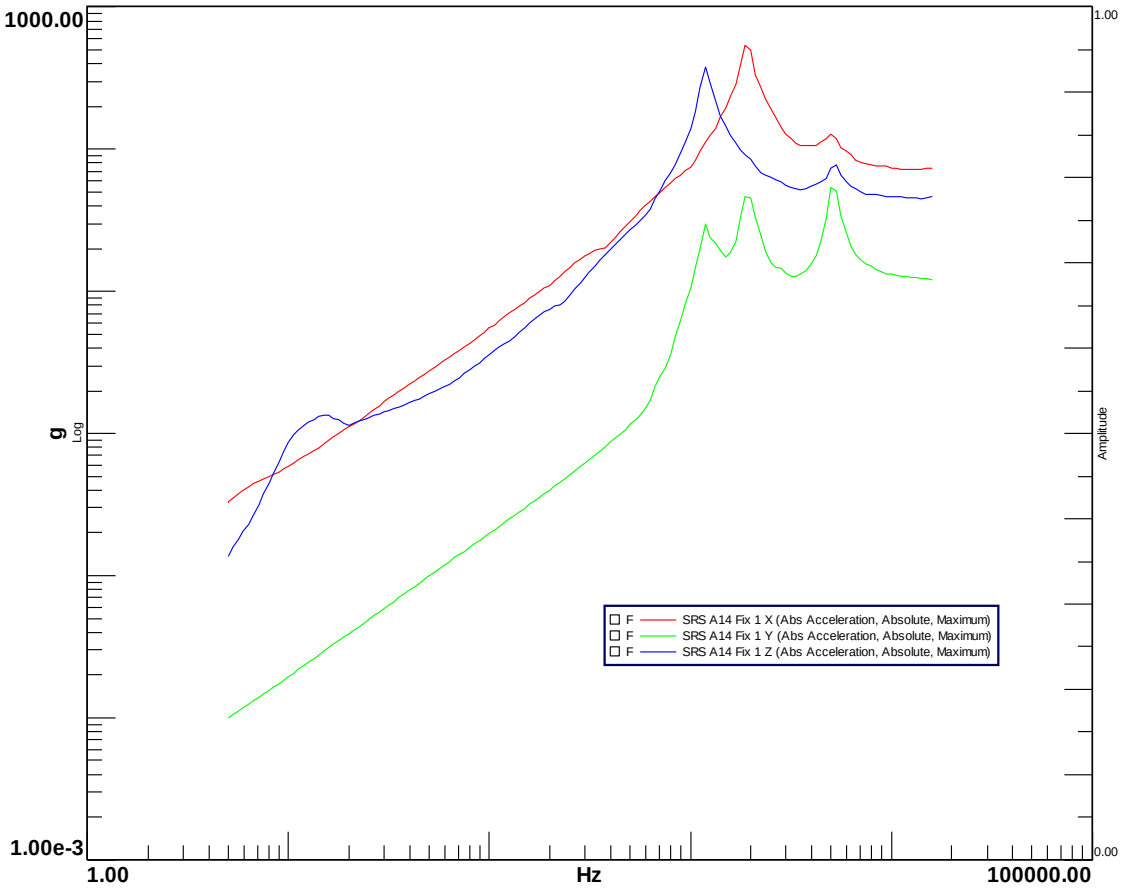

Figure 4.9: SRS of the center node of the fixture in all three directions with the input location on the edge of the resonant plate

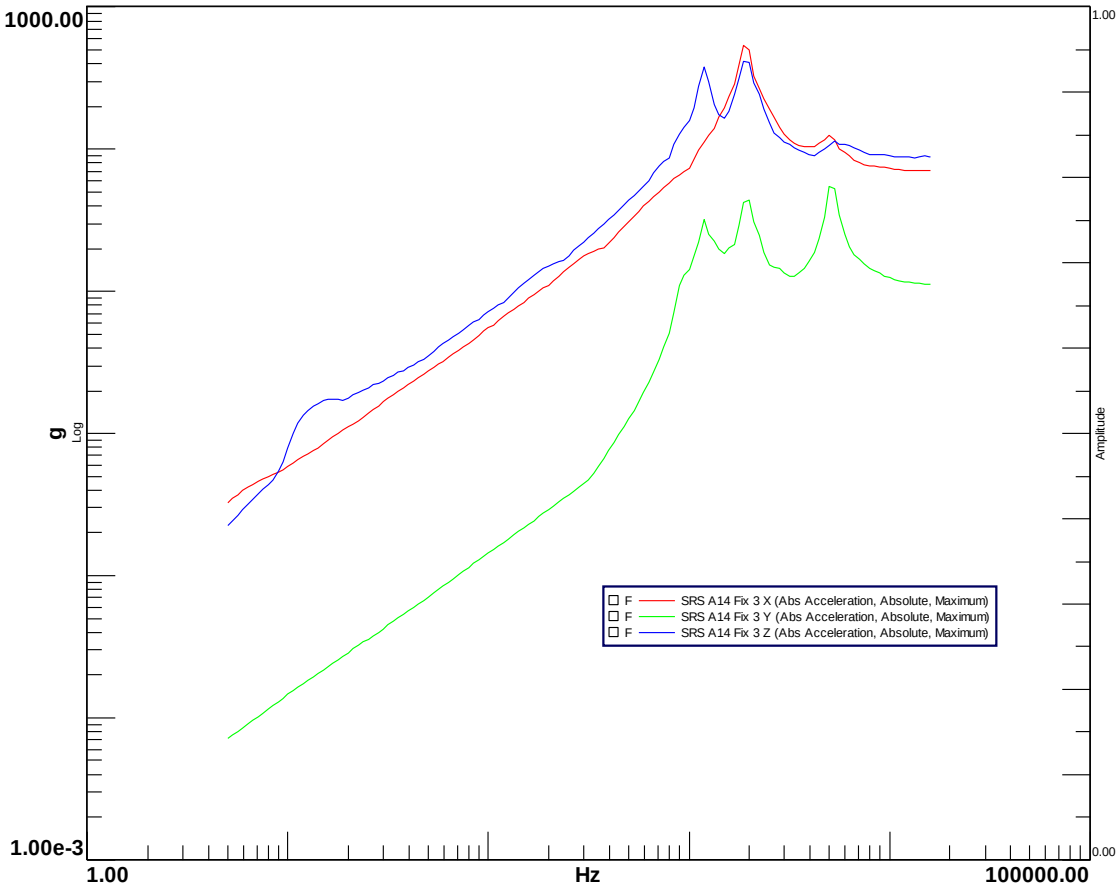

Figure 4.10: SRS of the center node of the fixture in all three directions with the input location on the edge of the resonant plate

4.2.2 Input at angle

The angle of impact for experimental testing is rarely perfectly in-plane to the test plate, and some methods such as pneumatic projectiles offer more accuracy than others e.g. using a hammer. Figure 4.11 shows the acceleration time history of the center node with the impact in-plane (left) and the impact angle changed 20˚ in the +X axis (right). Examining the effects of changing the angle of impact on the model showed the acceleration time histories of the +X direction (shown in red on Figure 4.11) increase with an increased angle of impact. The in-axis and other off-axis response did not have any other significant changes.

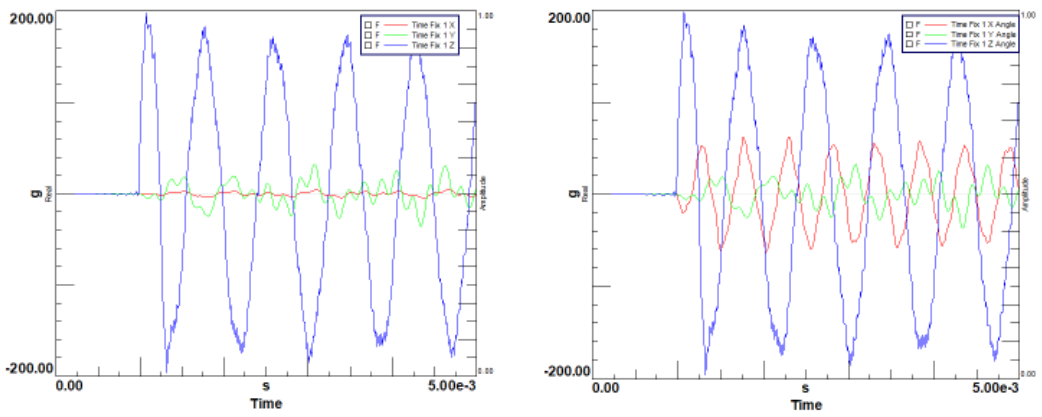

Figure 4.11: Acceleration time histories for the center node of the plate with the impact in the center of the impact pad in the in-plane (left) and at 20˚ in the +X direction (right)

An SRS of the center and corner nodes of the fixture were made for all directions with the angle of impact changed 20˚in the +X axis and compared with the SRS with the angle of impact only in the +Z direction shown in Figures 4.12 and 4.13 respectively. The +X response shown in red for both cases represent the impact angle of 20˚in the +X axis and comparing those responses to the impact only in the +Z axis, it was shown that the magnitude increases when there is an offset impact angle. The +Z and +Y for the center node in Figure 4.12 show no significant changes, but the +Z response on the corner node in Figure 4.13 shows variation in the response after the knee frequency of 1190 Hz.

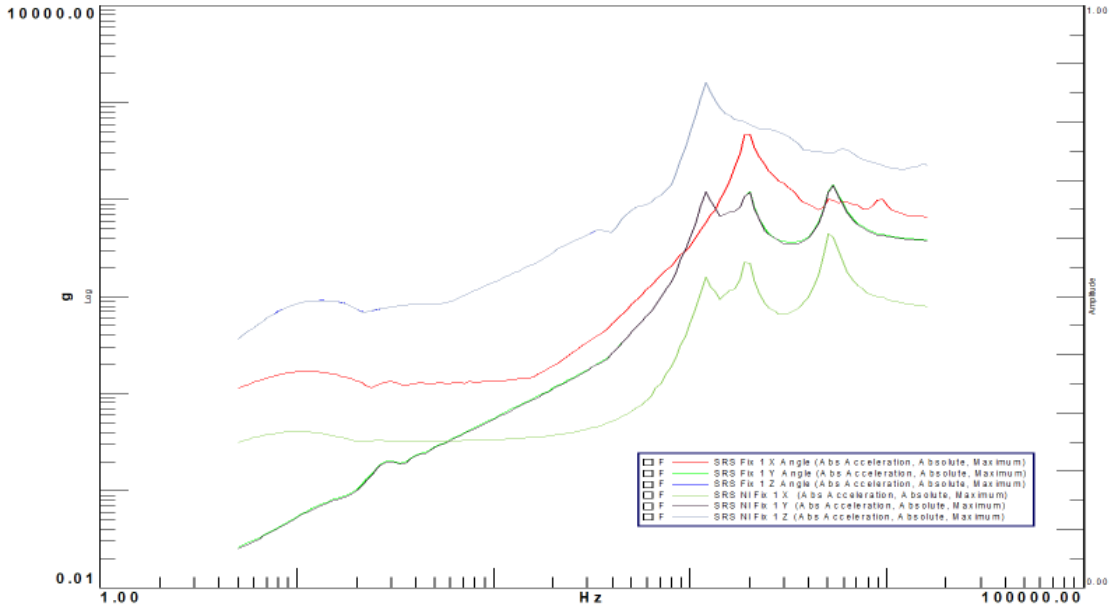

Figure 4.12: SRS of the center node on the fixture with the impact in the center of the impact pad in the in-plane and at 20˚ in the +X direction

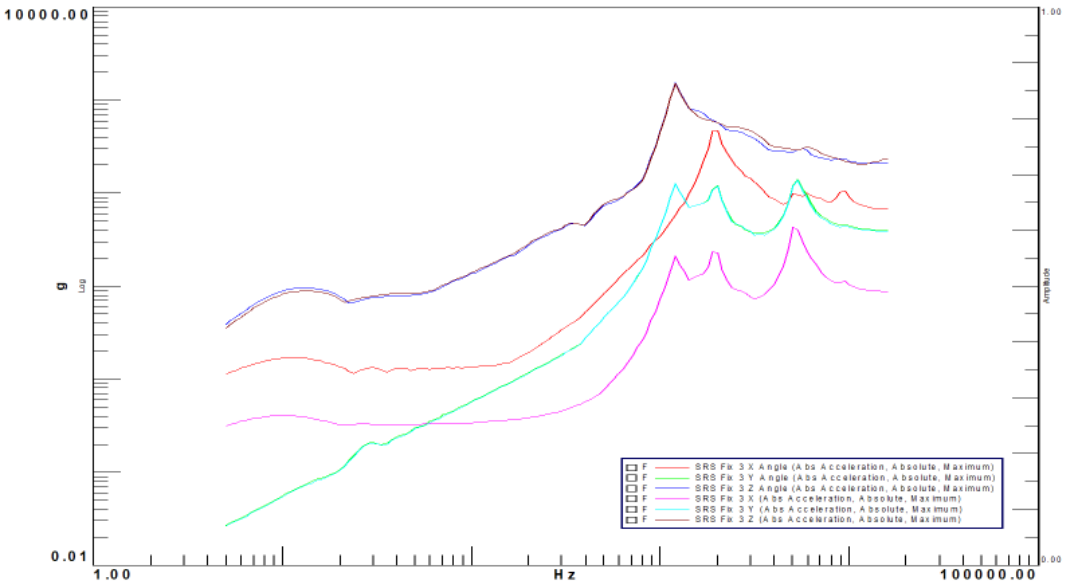

Figure 4.13: SRS of the corner node on the fixture with the impact in the center of the impact pad in the in-plane and at 20˚ in the +X direction

5 Movable Fixture

This chapter covers the study performed on the model that involved different configurations of the testing structure that included location and rotation about the in-plane axis to the impact. The intent was to explore the response of different locations across the test unit and compare how the location of test measurement differs for each axis. The impact was kept at the center of the plate opposite the test structure, and the same input was used for each test. The test structure was configured for seven different tests, and the study showed the off-axis response can affectively be manipulated by changing the location. It was also found that the placement of the test structure influenced the variation of response across the nine points on the test structure.

5.1 Methods of movable fixture

The circular resonant plate was machined to include 7 different configurations of the fixture under test shown in Figure 5.1. The goal of this experiment was to examine the effects of the different configurations on the SRS at several points on the test fixture. Hypermesh models were created for each configuration to match the physical test plate. This was done using the translation and rotation of components in the tools section in Hypermesh. The seven different configuration models are displayed in Figure 5.2. For each configuration, two load steps were created to get output files used for looking at the transient event and mode shapes.

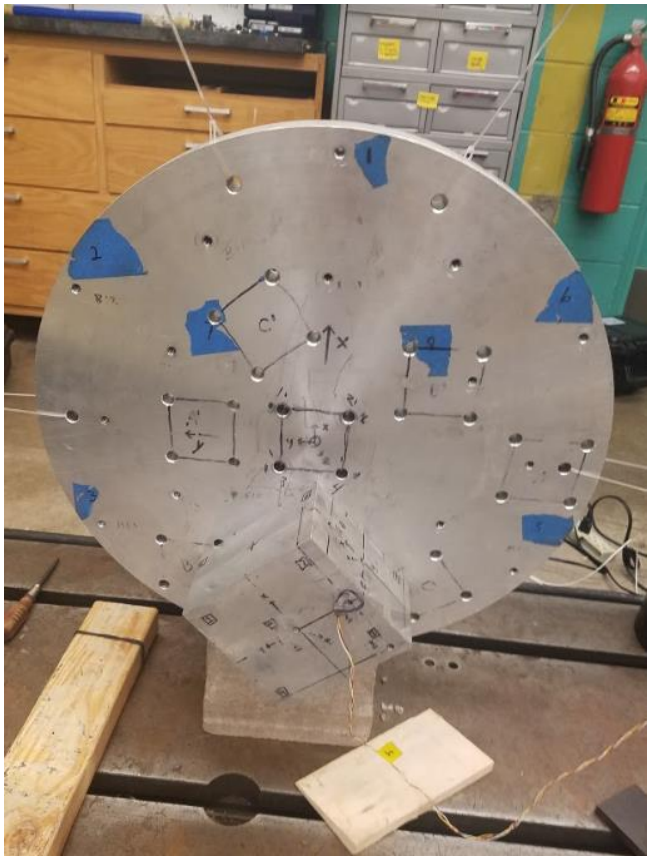

Figure 5.1: Machined plate for different configurations of the test fixture

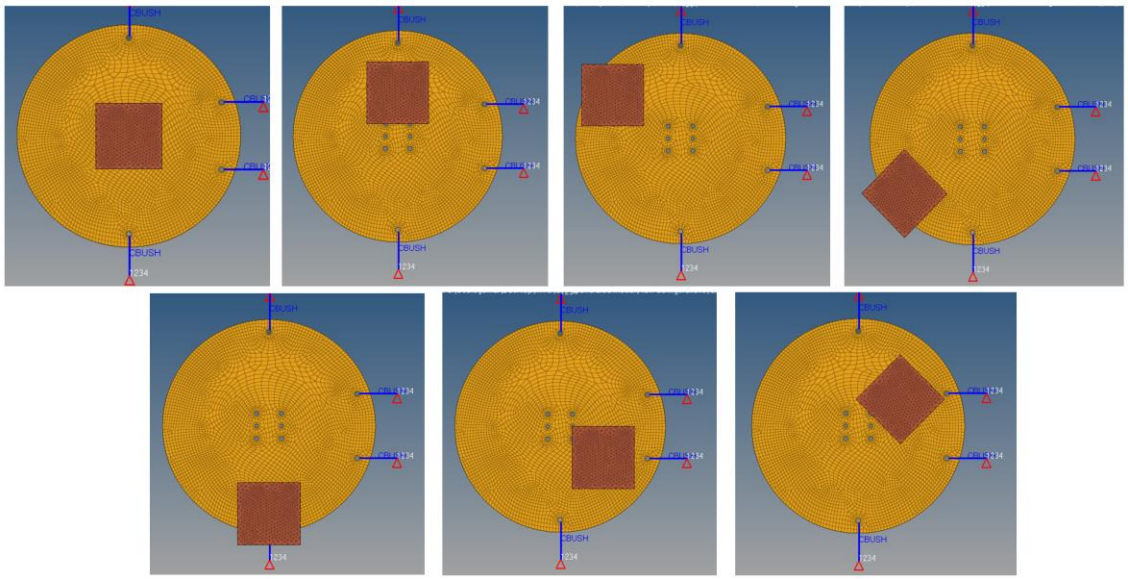

Figure 5.2: Hypermesh models for the seven different configurations of the test fixture

5.2 Results of movable fixture

Designing a resonant plate to meet SRS test requirements can be difficult and understanding the effects the placement of the test fixture has on the response to a given set of input/outputs can be useful to meet given criteria. Starting with the impact on the center of the impact pad and the fixture in the center of the plate, an SRS was made (Shown in Figure 5.3) and shows the in-axis response being greater in magnitude than the off-axis responses and having only one peak at the knee frequency of 1190 Hz. Both off-axis responses have a clear knee frequency at 1190 Hz, but also have peaks at 5132 Hz.

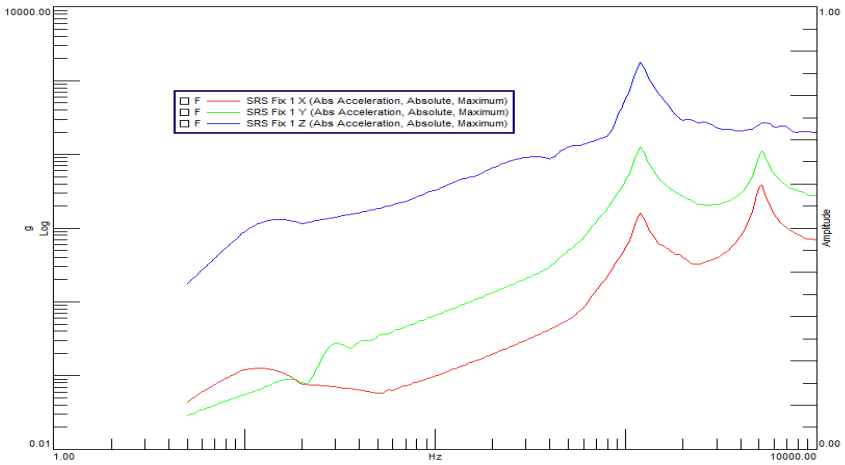

Figure 5.3: SRS of the center node in all three directions with the fixture in the center of the resonant plate

The nodes of interest on the fixture shown in Figure 5.1 were designated 2-5 for the corner nodes and 6-9 for the nodes on the edge of the fixture. The SRSs of the corner nodes were made and plotted against each other for the +X, +Y, and +Z directions shown in Figures 5.4 - 5.6 respectively to examine the variation of responses at different nodal locations. Figure 5.4 shows the SRS of the corner nodes in the +X direction and shows there is variation in magnitude from 40-3000 Hz and variation in shape between 1000-2000 Hz. Figures 5.5 and 5.6 show little variation in both magnitude and shape for the +Y and +Z responses at those nodal locations.

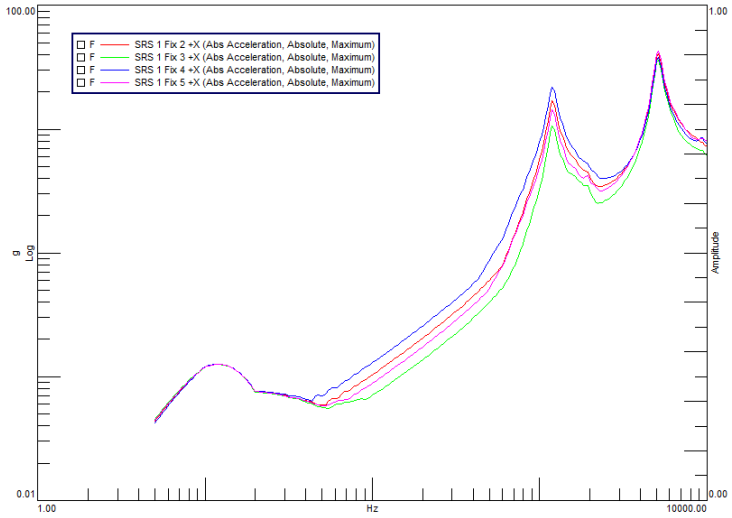

Figure 5.4: SRS of the corner nodes 2-5 in the +X direction with the fixture in the center of the resonant plate

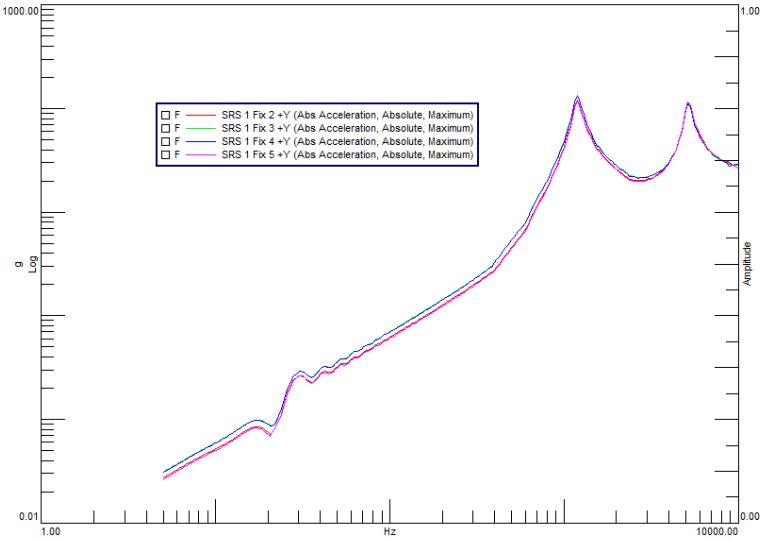

Figure 5.5: SRS of the corner nodes 2-5 in the +Y direction with the fixture in the center of the resonant plate

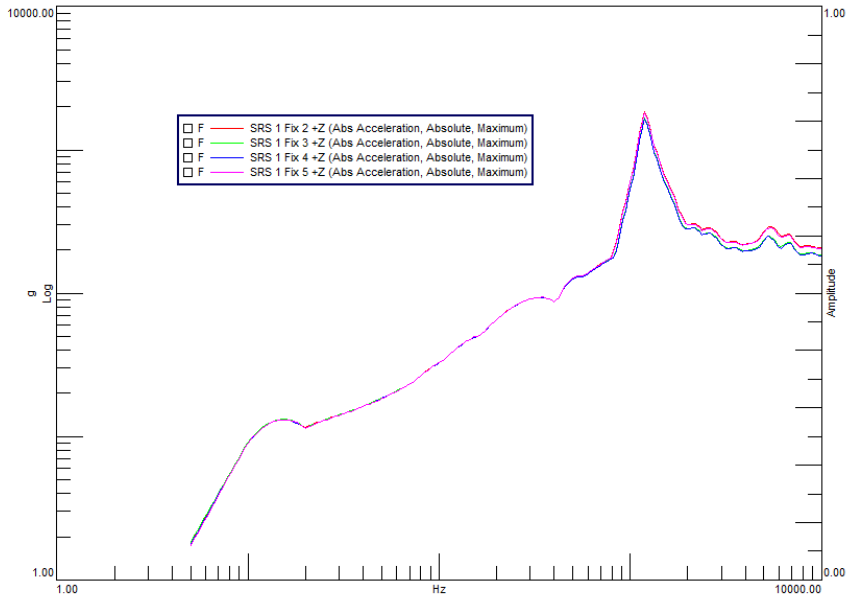

Figure 5.6: SRS of the corner nodes 2-5 in the +Z direction with the fixture in the center of the resonant plate

The SRSs of the edge nodes (6-9) were made and plotted against each other for the +X, +Y, and +Z directions shown in Figures 5.7 - 5.9 respectively and show only a slight variation in shape for the +X response in Figure 5.7, and no significant changes in magnitude for all three responses.

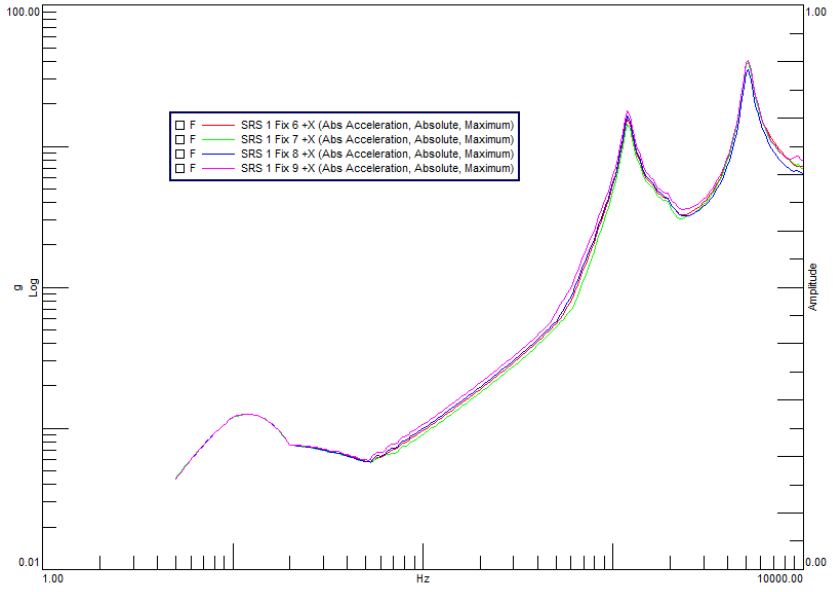

Figure 5.7: SRS of the edge nodes 6-9 in the +X direction with the fixture in the center of the resonant plate

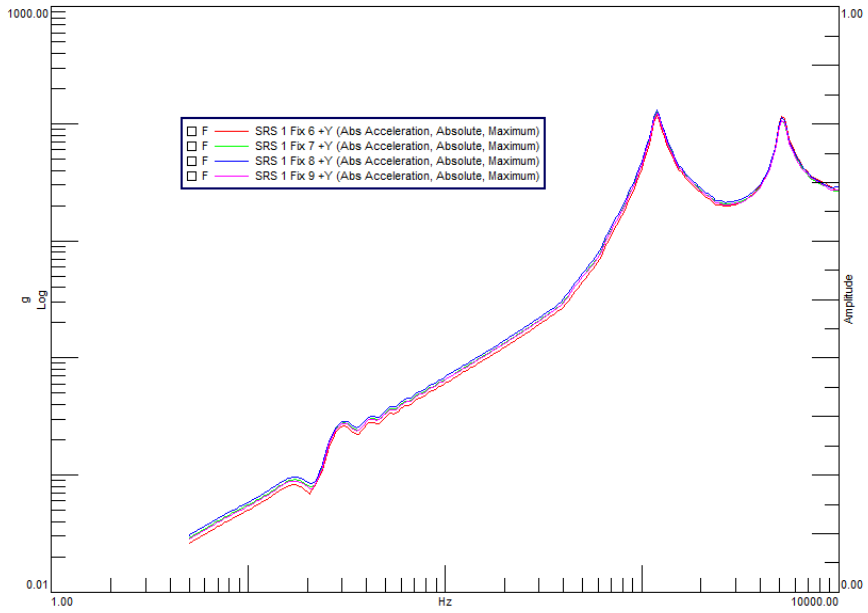

Figure 5.8: SRS of the edge nodes 6-9 in the +Y direction with the fixture in the center of the resonant plate

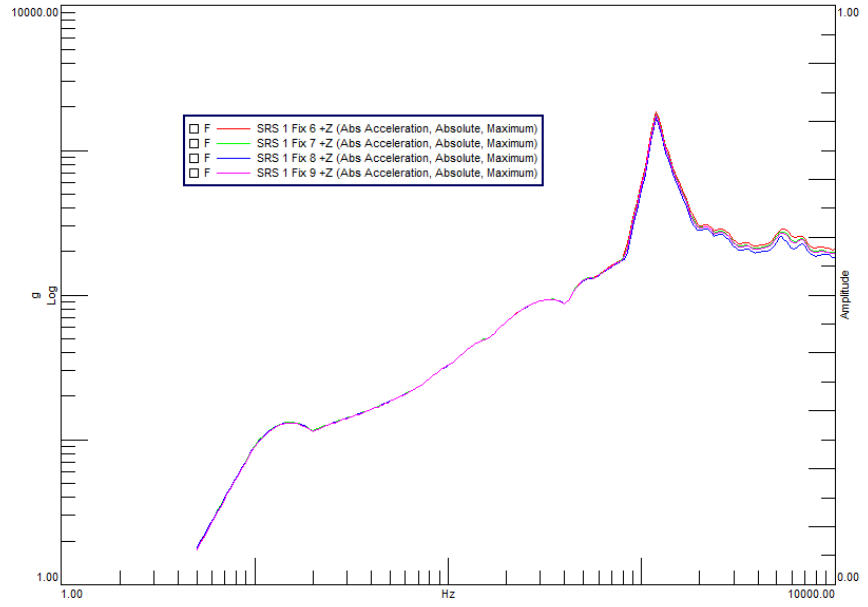

Figure 5.9: SRS of the edge nodes 6-9 in the +Z direction with the fixture in the center of the resonant plate

As mentioned in section 5.1, there were seven configurations of the fixture placement on the resonant plate that represent the physical mounting capabilities of the machined plate at Michigan Technological University. Configuration 6 consists (shown in Figure 5.10) of

the fixture moved from the center 3.5 inches in the +X direction and 2.5 inches in the -Y direction with the impact location at the center of the impact pad.

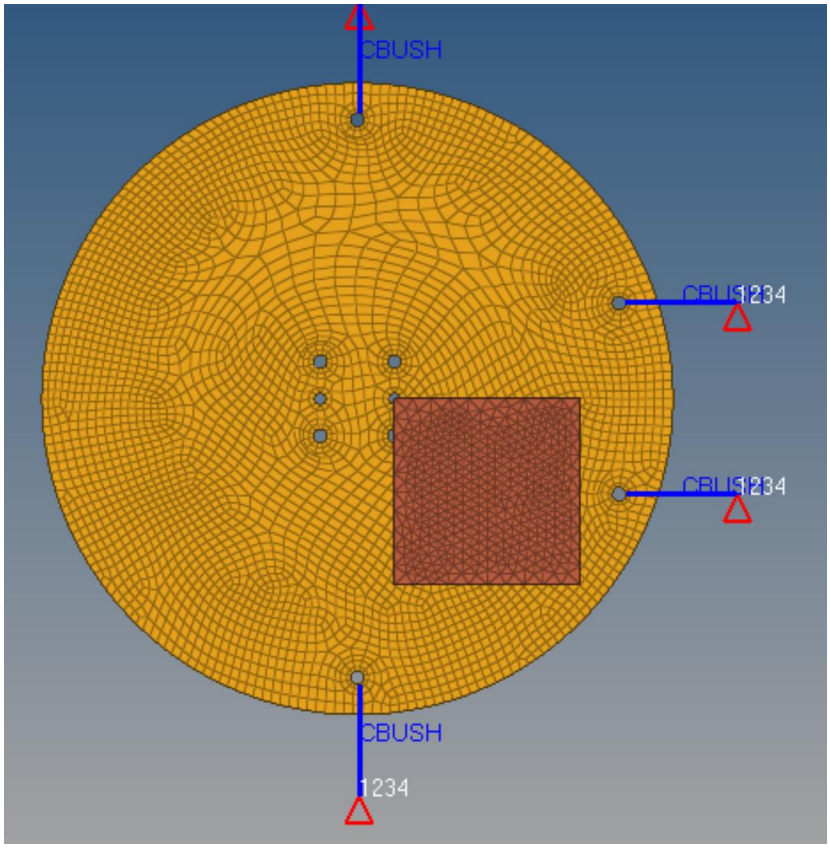

Figure 5.10: Configuration 6 with the fixture moved 3.5 inches in the +X direction and 2.5 inches in the -Y direction

The SRS of the center node of the fixture was made for all three directions with the fixture moved 3.5 inches in the +X direction and 2.5 inches in the -Y direction and plotted in Figure 5.11. Comparing the SRS with the fixture moved to the SRS with the fixture in the center from Figure 5.3, it can be noted that the off-axis responses (blue and green) have been effectively increased in magnitude and are greater than the in-axis response after 432 Hz. The large peaks in the off-axis responses at 5132 Hz with the fixture in the center have been substantially reduced and new peaks at 712 Hz are now noticeable. Changing the fixture location 3.5 inches in the +X direction and 2.5 inches in the -Y direction has introduced modal participation from the mode 712 Hz and reduced the effect of the higher mode at 5132 Hz for the overall SRS at the center node location which can be useful for designing SRS test specifications. SRS targets bands of ± 6 dB were placed on the responses and despite not meeting the criteria, reducing the peaks by adding damping could essentially help meet SRS test specifications.

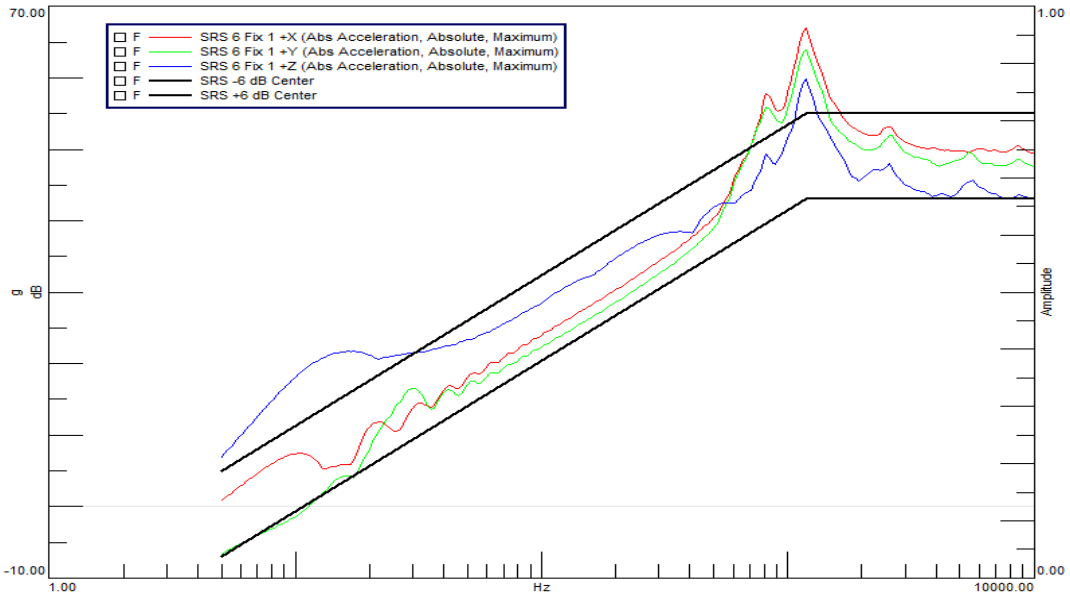

Figure 5.11: SRS of the center node in all three directions with the fixture offset 3.5 inches in the +X direction and 2.5 inches in the -Y direction with ± 6 dB bands

Analyzing the variations at the corner nodal points on the fixture was done for this configuration and the responses at nodes 2-5 were made in the +X (upper plot in Figure 5.12), +Y (lower left plot in Figure 5.12), and +Z (lower right plot in Figure 5.12). The off-axis responses in Figure 5.12 show little variation in the magnitude of the responses at the different nodal locations on the fixture, however, there is some slight variation in the shapes of the SRSs at frequencies in the "plateau" region of the SRS at frequencies after 2000 Hz. The +Z responses in the lower right plot of Figure 5.12 shows the magnitude of the responses varies as much as an order of magnitude from nodal location 9 which is closest to the center of the plate nearest the impact compared to nodal location 8 which is located nearest the edge of the plate on the fixture. There are also noticeable peaks in nodal locations 6 and 9 at 2300 Hz that are not visible at locations 7 and 8 on the fixture. This demonstrates the shape and magnitudes of the SRS depend greatly on the testing location of the fixture.

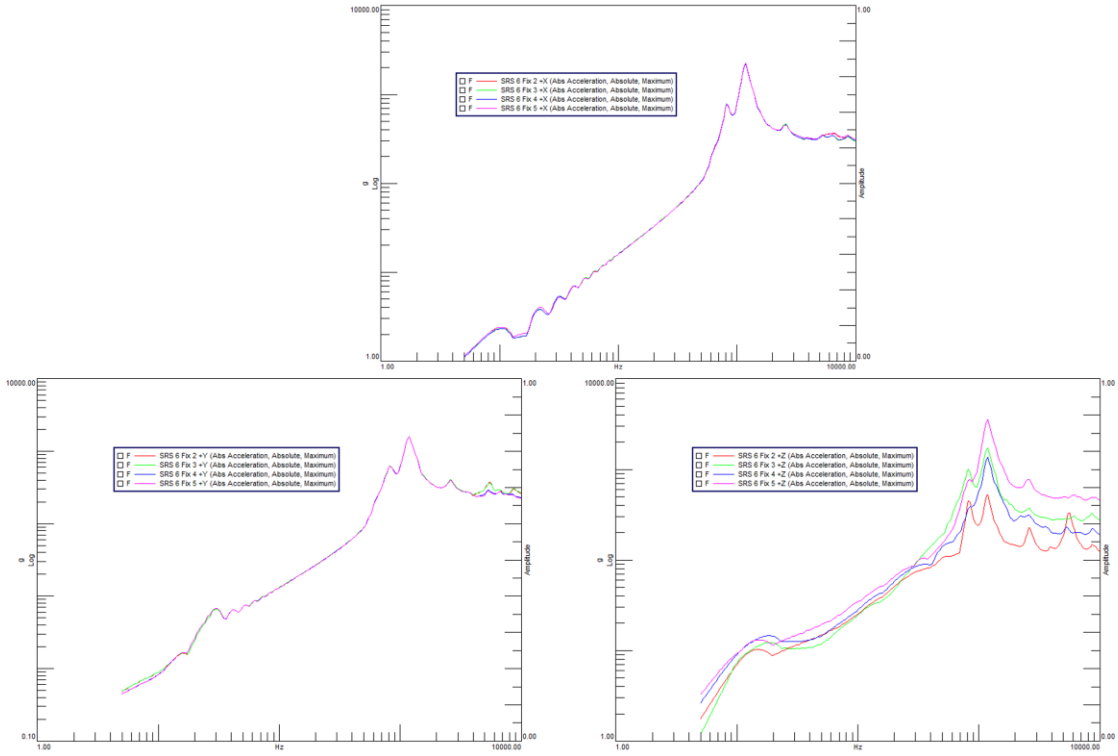

Figure 5.12: SRS of corner nodal points with +X (upper), +Y (lower left), +Z (lower right) with fixture offset 3.5 inches in the +X direction and 2.5 inches in the -Y direction

6 Modal Contribution to Shock Response

This chapter covers the modal contribution to the shock response analysis for a given point on a structure and a specified direction. It was initially developed by Charles Van Karsen and was improved upon by decreasing the computation time and automation of the analysis. The simulation of the SRS was deconstructed and examined by each individual mode to determine which of the modes contributed the most to the shape/magnitude of the overall response at a given point on the structure. This analysis was used to describe the variations that were observed in the last chapter.

6.1 Methods Modal Contribution to Shock Response

The modal contribution to the shock response at a given point/direction on the test fixture was initially developed by Charles Van Karsen [16]. His MATLAB code worked in conjunction with Amesim and a Hypermesh punch output file. The code was manipulated to operate only in MATLAB for time efficiency and for automation purposes.

The process begins in Hypermesh where the models used for the different configurations were used. A load step was created to extract the mode shapes and natural frequencies for each node of interest (shown in Figure 6.1).

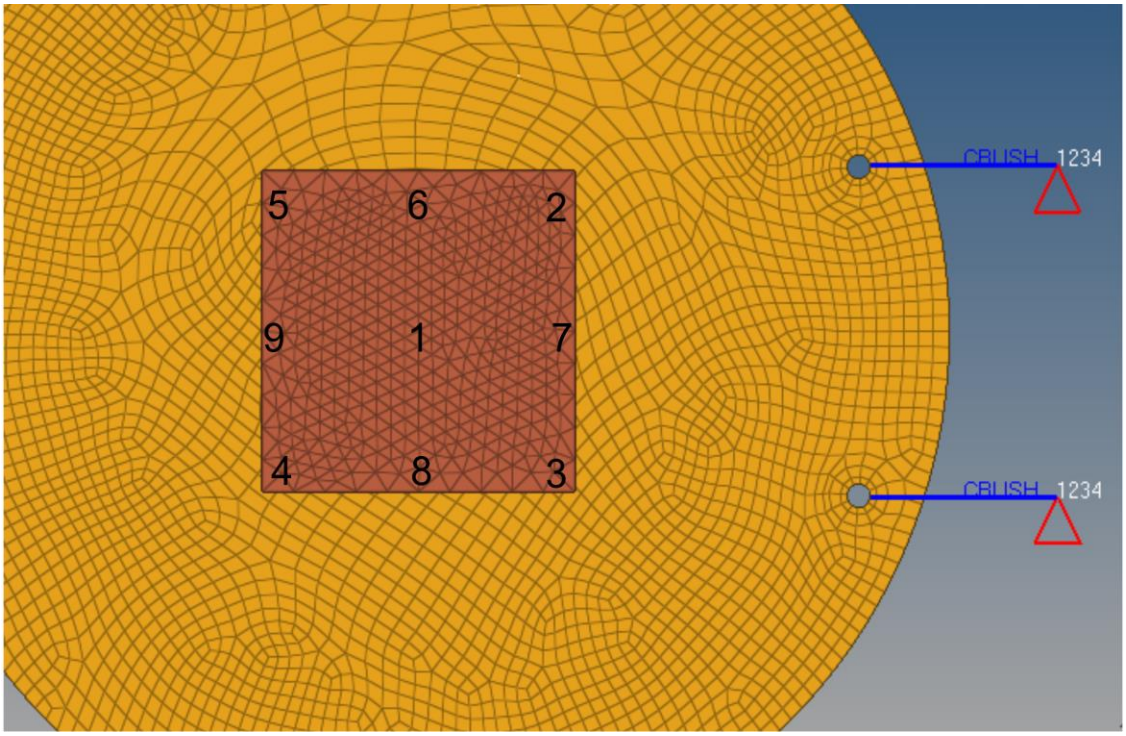

Figure 6.1: Nodal points of interest on the fixture

The output file specified by Hypermesh was chosen to be a punch file that contains the eigenvalues (modal natural frequency) and eigenvectors (mode shapes) for each mode contained in the range of 0 – 10000 Hz which was specified in Hypermesh. The data contained in the output file was then imported into Matlab as a matrix versus the default table option in the output type in Matlab and modal matrices were created. From the modal matrices, the residues were calculated using the equation

$$A_{pkq} = \frac{U_{pk}U_{qk}}{2j\sqrt{\omega}} \tag{6.1}$$

where A_{pkq} = residue matrix

ω = natural frequency

U = modal matrix

p = output degree of freedom

q = input degree of freedom

k = number of modes

and the output and input degree of freedom were chosen from the nodal points of interest in the output file. The residues are then calculated using the *residue* function in Matlab and the A and B coefficients of the transfer function are created from the displacement residues. The input excitation was also imported into Matlab as a matrix and a transfer function was created using the *tf* function along with the A and B coefficients of the transfer function in the LaPlace domain (6.2) from the displacement residues. The dynamic time response for each mode is calculated using the *lsim* function in Matlab with the transfer function and input to the system. The response was then used to create the SRS for each mode using Smallwood's Matlab code and Figure 6.2 shows an example plot of the individual modal SRSs plotted against the overall SRS [DS].

$$\frac{output}{input} = \frac{B(s)}{A(s)} = \frac{B_0+B_1s+B_2s^2+\cdots+B_Ns^N}{A_0+A_1s+A_2s^2+\cdots+A_Ms^M} \tag{6.2}$$

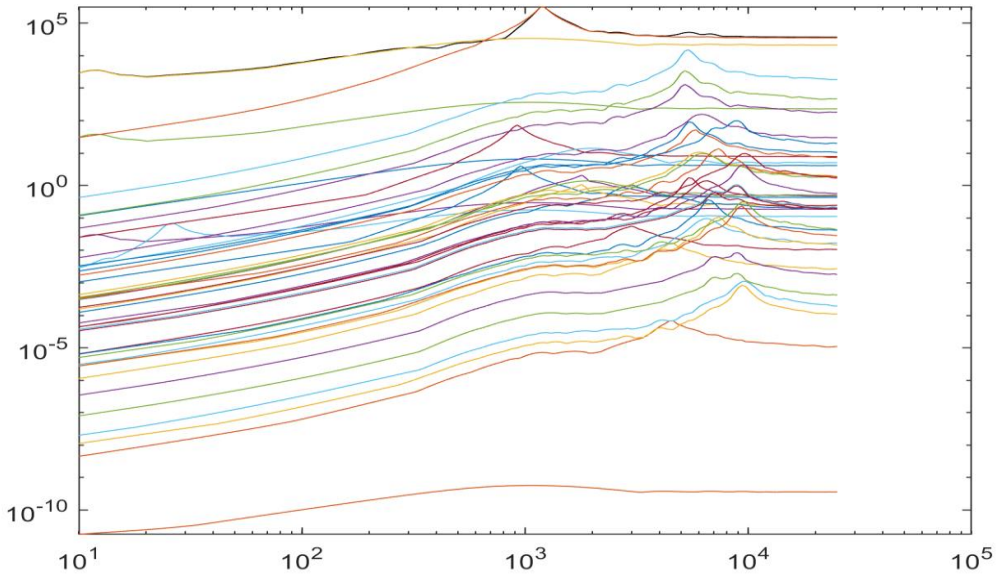

Figure 6.2: Individual SRSs for each mode and the overall SRS

The process of finding a significant contribution to the overall SRS was done by examining the individual SRSs for each mode and the code will iterate through each frequency and find the magnitudes that are within a specified range. The code will then take the SRS of the individual mode which has the magnitude closest to the overall SRS and checks to see if the percent difference was less than the specified percentage given (chosen to be 1% for this experiment). If it was not within the specified percent difference to the overall SRS, the next individual SRS was found, and the time histories of the two individual SRSs are summed. A new SRS was then estimated using Smallwood's Matlab code on the combined time histories. The process was repeated until the percent difference of the summed SRSs was within a specified percent difference to the overall SRS. This evolution of the SRS by building each modal SRS that contributes to the overall SRS is shown in Figure 6.3 where it can be observed that only 4 modes out of approximately 40 modes to accurately synthesize the SRS to within 1% difference which is useful when determining which modes to exploit when designing SRS test targets. The entire process of the Matlab code is modelled in the flowchart shown in Figure 6.4.

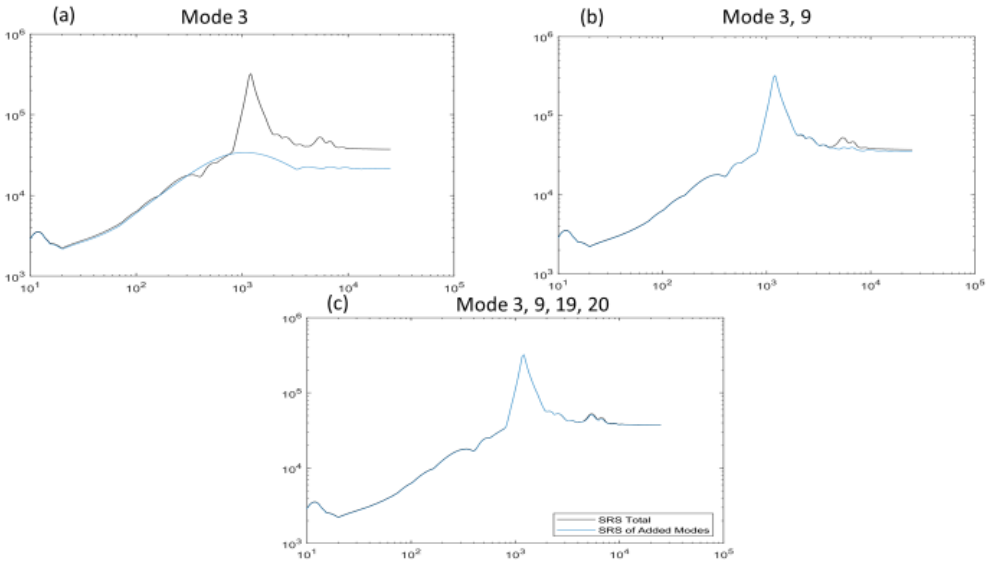

Figure 6.3: Iteration process to determine the contributing modes to the overall SRS

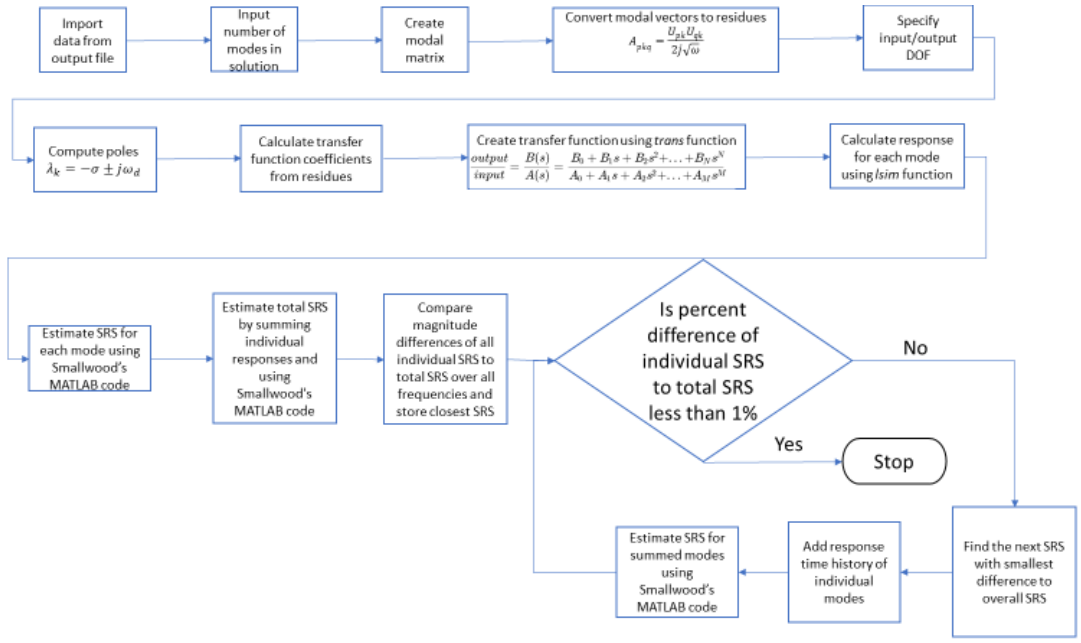

Figure 6.4: Flowchart of Matlab code for modal participation to overall SRS

6.2 Results Modal Contribution to Shock Response

Exploring the possible causes of the variations shown in the SRS of the different nodal points on the test fixture that was shown in Section 5.2 was done using the modal contribution code explained in Section 6.1. The configuration used for this experiment was configuration 4 from Figure 5.2 with the fixture moved 5 inches in the -X direction and 4.5 inches in the -Y direction. The code was used to determine the modal participation for each of the corner nodes labeled 2-5 from Figure 6.1 and documented in Table 4.1. For the 40 modes found from 0-10 kHz the table clearly shows that all nodes are equally affected by the rigid body modes 3-6 as well as the bending modes 7-11, which includes the knee mode. One of the higher-order modes, mode 16 at 3662 Hz, contributes to a peak shown in the plateau region in the X and Y SRS shown in Figure 6.5, and as well as the corner nodes of 2 and 3 in the Z direction. Table 4.1 shows the frequency at which each of the 40 modes occur found between 0-10 kHz and highlights which modes contribute to the overall SRS for each corner node found in Figure 6.5. The slight variations in the modal contribution can be noticed in the table after 3 kHz, but the areas that most affect the SRS are within the 0-3000 Hz range.

The table highlights which subset of modes contribute to the overall response on the structure. The subset of modes that contribute to the overall response in the x-direction for nodal point 2 in shown in Figure 6.5 can be found in the first column in Table 4.1. Here it can be found that modes 1, 3-12, 16, 18, 23, 27, 29, and 30 are the major contributors to the overall response. The table can also be useful in determining the contribution of a mode for all responses in all directions by examining the rows. Here it can be shown that modes 13-15, 17, 19, 21, 24-25, 32-36, and 38-40 do not contribute to any of the responses on the structure in any direction.

Table 4.1: Modal participation of each mode in total SRS for configuration 4 from 0-10 kHz

Mode	*freq* (Hz)	X				Y				Z			
		2	3	4	5	2	3	4	5	2	3	4	5
1	0.007	■											■
2	4.44							■					
3	10.8	■	■	■	■	■	■	■	■	■	■	■	■
4	11.2	■	■	■	■	■	■	■	■	■	■	■	■
5	11.3	■	■	■	■	■	■	■	■	■	■	■	■
6	24.1	■	■	■	■	■	■	■	■	■	■	■	■
7	642	■	■	■	■	■	■	■	■	■	■	■	■
8	738	■	■	■	■	■	■	■	■	■	■	■	■
9	1079	■	■	■	■	■	■	■	■	■	■	■	■
10	1531	■	■	■	■	■	■	■	■	■	■	■	■
11	1693	■	■	■	■	■	■	■	■	■	■	■	■
12	2034	■	■	■	■	■	■	■	■				■
13	2618												
14	2880												
15	3161												
16	3662	■	■	■	■	■	■	■	■				
17	4018												
18	4455	■											
19	4716												
20	4834												■
21	5004												
22	5060								■		■		■
23	5376	■			■						■		■
24	5786												
25	5942												
26	6215			■									
27	6262	■		■					■				
28	6646												
29	6761	■		■		■			■				■
30	7059	■											
31	7254												■
32	7543												
33	7733												
34	8156												
35	8203												
36	8593												
37	9042												■
38	9307												
39	9725												
40	9777												

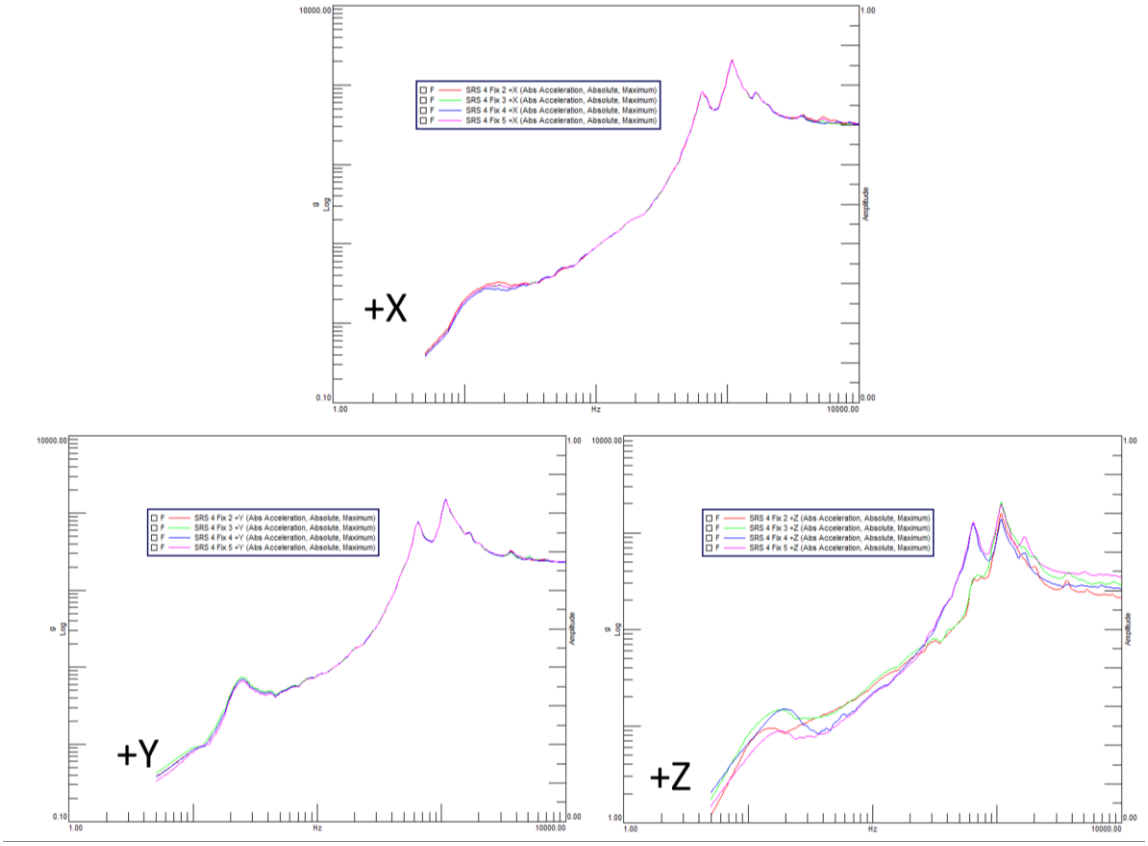

Figure 6.5: SRS of corner nodal points on the test fixture in all 3 directions

Another way to look at modal participation is by looking at the individual SRS for each mode that contributes to the overall SRS at a given point. Figure 6.6 shows the rigid body modes 3 - 5 dominate the shape of the SRS at frequencies below the "knee frequency." Mode 9 at 1097 Hz controls the knee range, and the higher-order modes 11 and 16 control the response in the frequencies above 1100 Hz where small peaks can be observed in the "plateau" region of the SRS displayed in Figure 6.7.

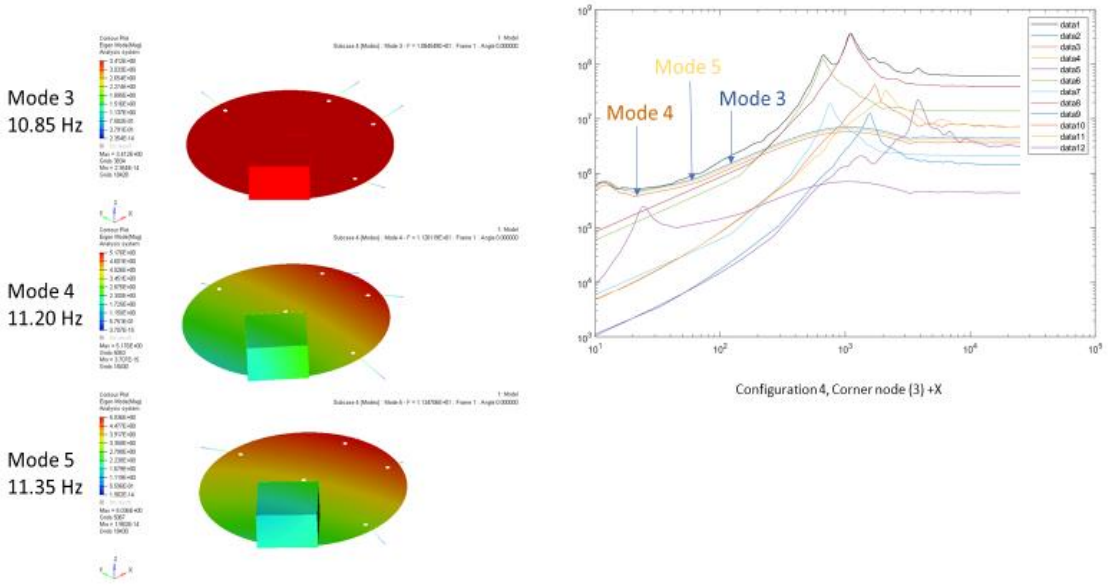

Figure 6.6: SRS of individual participating rigid body modes

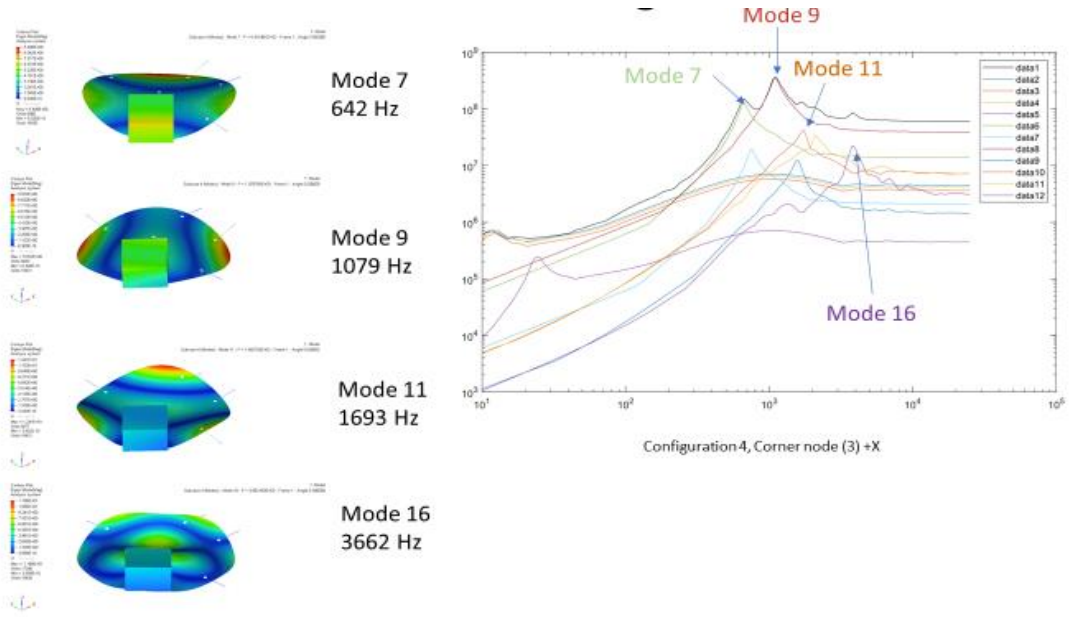

Figure 6.7: SRS of individual participating modes for the bending modes

Describing the variation in magnitude in the +Z direction that was observed in Figure 6.5 was accomplished by examining the participating modes for nodal points 2 and 4 in the +Z direction. Figure 6.8 shows corner nodal points 2 and 4's respective SRSs in the +Z direction. Both have the rigid body mode 6 and the bending mode 7 that contribute to the

overall shape of the SRS, however, it can be observed that the rigid body mode 6 has a higher magnitude for node 4 in the frequency range from 10-100 Hz, and thus changes the shape of the overall SRS in that range. The same phenomena can be observed for the bending mode 7 at 642 Hz where the higher magnitude of the mode created a larger peak for nodal point 4. This demonstrates that two points on the test fixture may have the same modes that contribute to the shape of the total SRS, but the magnitude of the contributing mode affects the overall shape of the SRS.

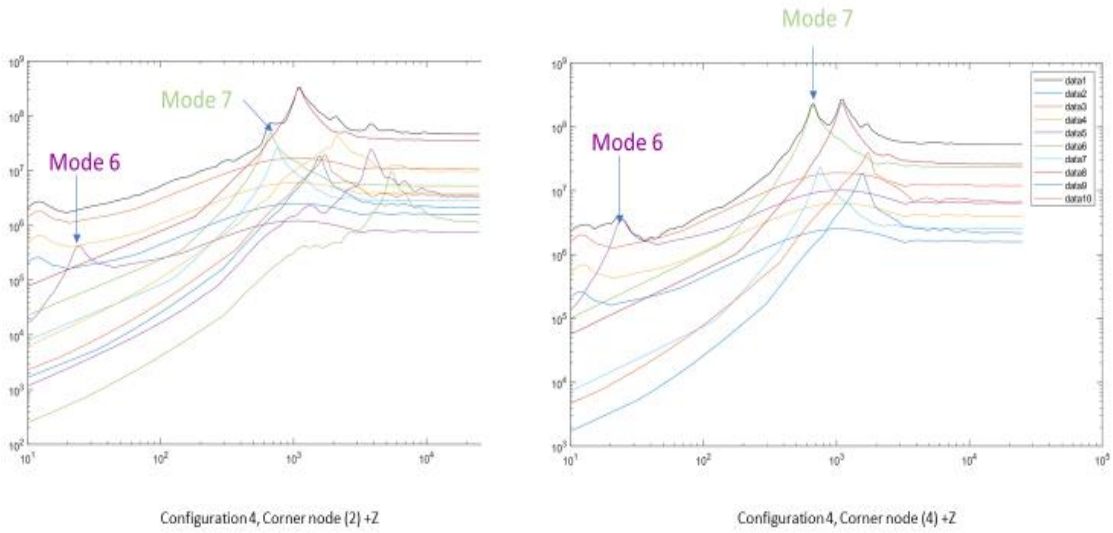

Figure 6.8: Participating modes in the overall SRS for nodal points 2 (left) and 4 (right) in the +Z direction

7 Movable Impact Pad

This chapter included an exploration into the effects of moving the impact pad on the test structure. It was found from Chapter 5 that the off-axis response can be manipulated and affectively be increased by moving the test structure, and this chapter expands on that research by introducing the change in location of the impact pad to study those effects on the response. The study utilizes the modal contribution analysis that was introduced in the last chapter and explains some of the phenomena that was observed when the impact pad was moved across a modal nodal line. Mode shapes were also examined to determine the most suitable location for impact based on which modes are desired to exploit. This chapter also describes the effects of changing boundary conditions on the constant velocity line of the SRS.

7.1 Methods Movable Impact Pad

Similar to the movable fixture experiment, the effects on the response of the resonant plate due to a movable impact pad were conducted. The same model in Hypermesh used for the movable fixture was used for this experiment. The translation option was used in Hypermesh to move the impact pad on the resonant plate in several locations on the plate to examine the effects on the SRS in the in axis and off-axis directions (shown in Figure 7.1).

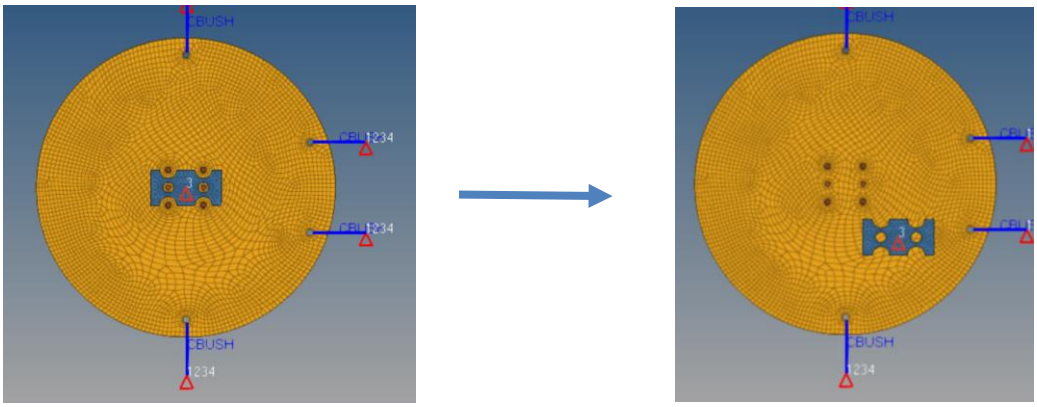

Figure 7.1: Impact pad moved from center to 3 inches in the +x and +y directions

This study examines the effects of the SRS in specified points on the fixture by moving the impact pad across modal nodal lines with the fixture placed in the center as well as the fixture offset. The modal nodal lines were determined by examining the mode shapes in Hyperview using the output file from the FEM.

An examination of the effects on the SRS due to the support springs was also performed to analyze the effects on the rigid body controlled region of SRS where the constant velocity line would be linear if the support springs were made to be less stiff by decreasing the value

by two orders of magnitude. The support springs were created using the card image PBUSH in the properties section and each of the springs had the following properties:

Table: 7.1: Support Spring Properties

Spring Name	Direction	Original Value (in-lb)	Experimental Value (in-lb)
K1 Rigid	X translation	200	2
K2 Rigid	Y translation	200	2
K3 Rigid	Z translation	200	2
K4 Rigid	X rotation	100	1
K5 Rigid	Y rotation	0	0
K6 Rigid	Z rotation	0	0

7.2 Results Movable Impact Pad

Investigating other techniques to better understand the response of a structure with a given set of inputs/outputs was done using a movable impact pad and the effects were studied using the SRS. To explore how to sufficiently increase one of the off-axis responses the study started with configuration 2 from Figure 5.2 where the fixture was placed 3.5 inches in the +Y direction and the impact pad placed in the center of the plate opposite the fixture shown in Figure 7.2.

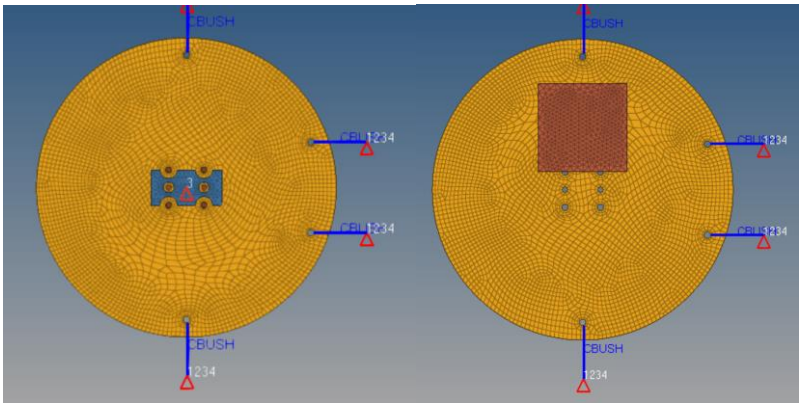

Figure 7.2: Configuration 2 with fixture moved 3.5 inches in +Y direction and impact pad in the center of the resonant plate

The SRS was made for the center node of the fixture in all three directions (shown in Figure 7.3) and it shows that moving the fixture in the +Y produced the response in that direction increase in magnitude and become larger than the +Z response which is in-plane to the impact at 432 Hz and beyond. The other off-axis response in the +X direction is several orders of magnitude below the other responses.

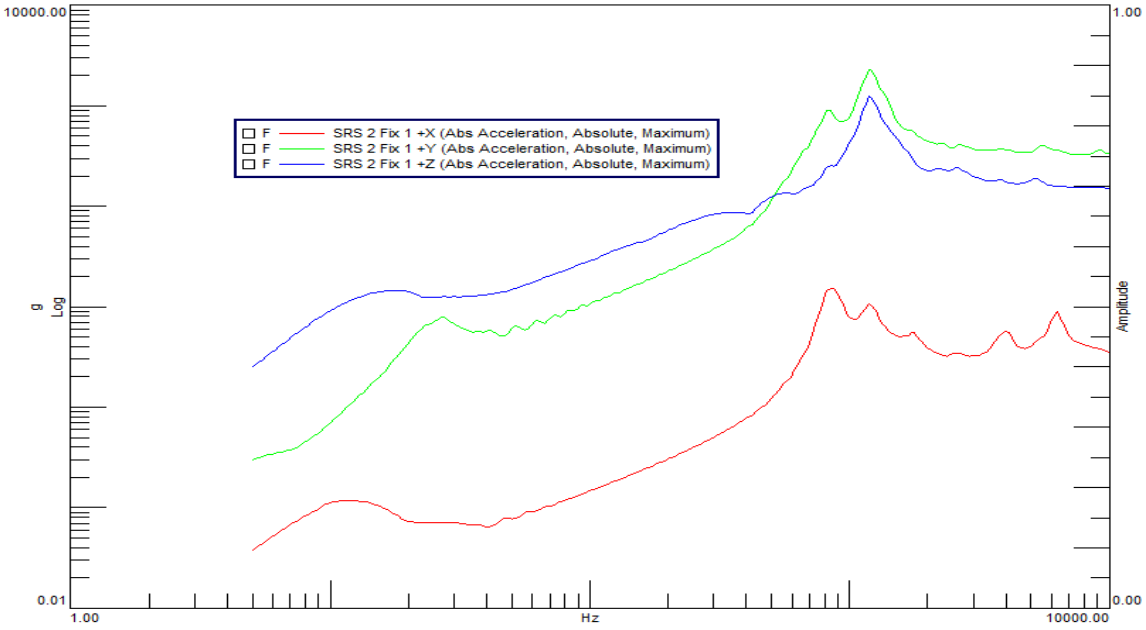

Figure 7.3: SRS of the center node of the fixture with fixture moved 3.5 inches in +Y direction and impact pad in the center of the resonant plate

Examining whether the change of the impact pad placement in the direction of the response with the lowest magnitude from the plot above, the impact pad was placed 2.5 inches in the +X direction shown in Figure 7.4.

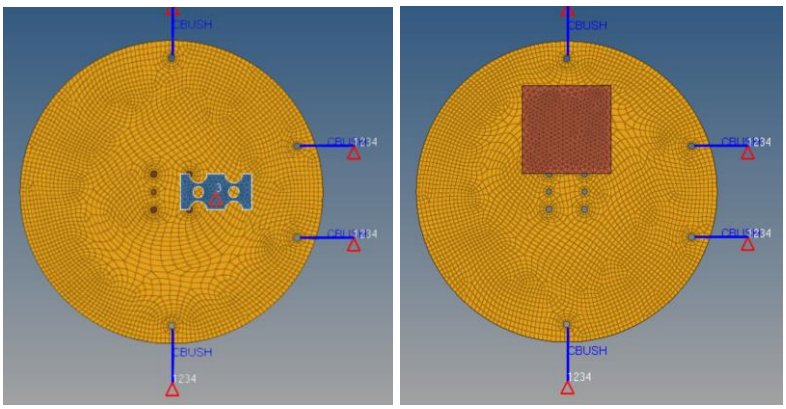

Figure 7.4: Fixture moved 3.5 inches in +Y direction and impact pad moved 2.5 inches in the +X direction

The SRS of the center node of the fixture with the impact pad moved 2.5 inches in the +X was made and plotted in Figure 7.5 and it shows that the +X response was effectively increased when compared to the +X response in Figure 7.5. The responses in the +Y and +Z remain unchanged.

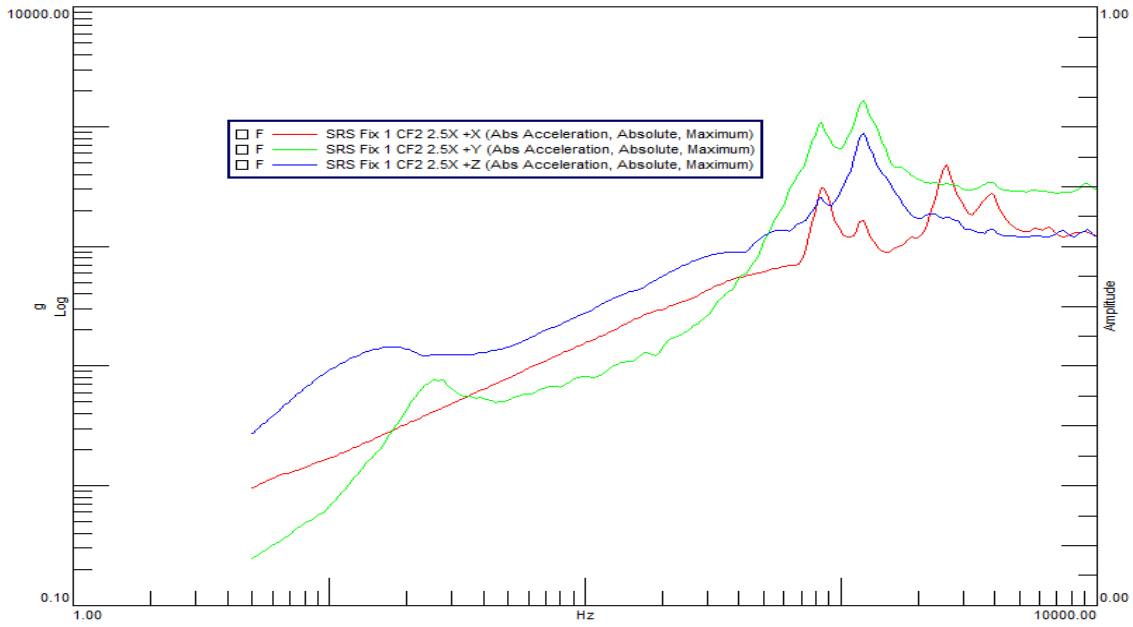

Figure 7.5: SRS of the center node of the fixture with fixture moved 3.5 inches in +Y direction and impact pad moved 2.5 inches in the +X direction

Studying the effects of only moving the impact pad and placing the fixture in the center of the plate was then done. The impact pad was moved 3 inches in the -X and -Y directions displayed in Figure 7.6.

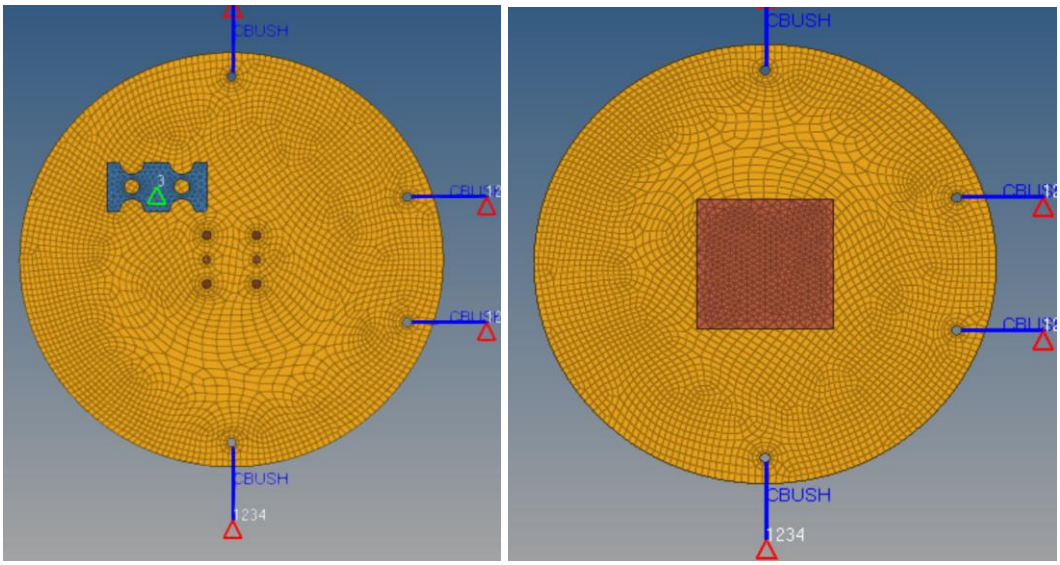

Figure 7.6: Fixture in the center and impact pad moved 3 inches in the -X and -Y directions

The responses in all three directions were made for the center node of the fixture and plotted in Figure 7.7. Examining the SRS shows that the responses are dominated by the rigid body modes and the in-axis response does not have the same knee frequency as the off-axis responses.

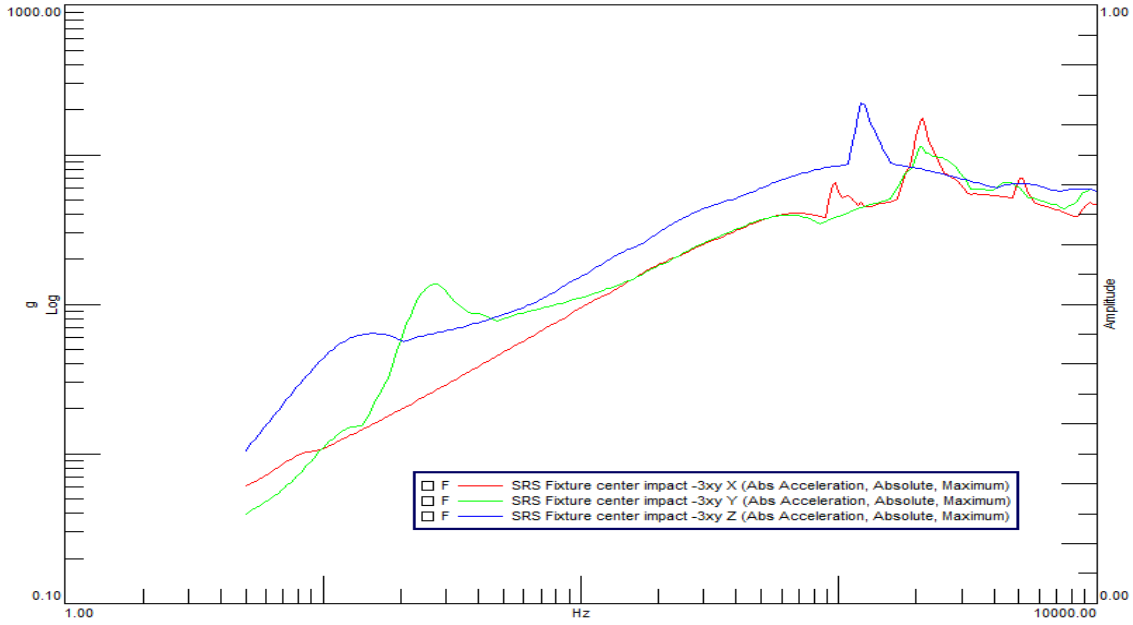

Figure 7.7: SRS of the center node with the fixture in the center and impact pad moved 3 inches in the -X and -Y directions

With the fixture remaining in the center the impact pad was then placed 1.5 inches in the -X and -Y, shown in Figure 7.8, to examine if the same phenomena occur.

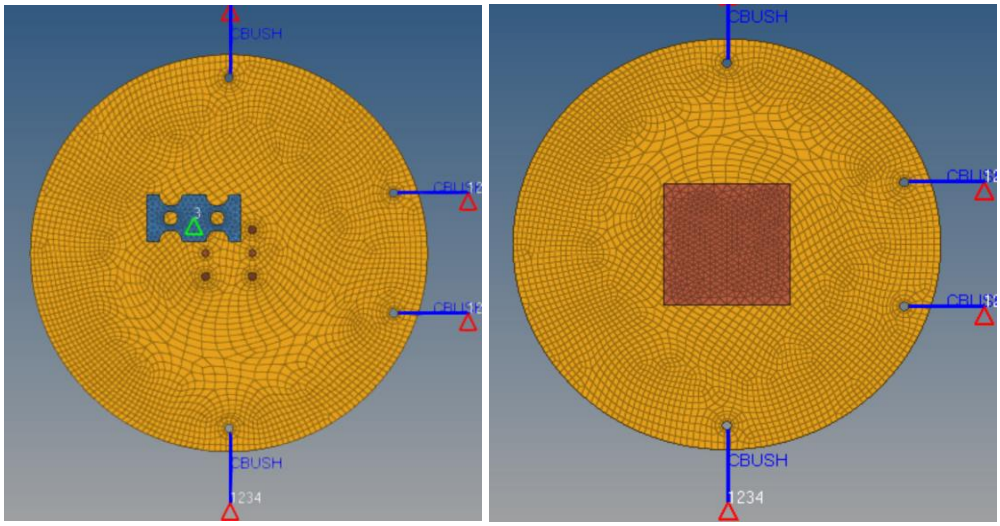

Figure 7.8: Fixture in the center and impact pad moved 1.5 inches in the -X and -Y directions

The SRS of all three directions were made for the center node of the fixture and plotted in Figure 7.9. The phenomenon of rigid body mode domination was not observed in this case and it can be noted that all responses have the same knee frequency of 1138 Hz.

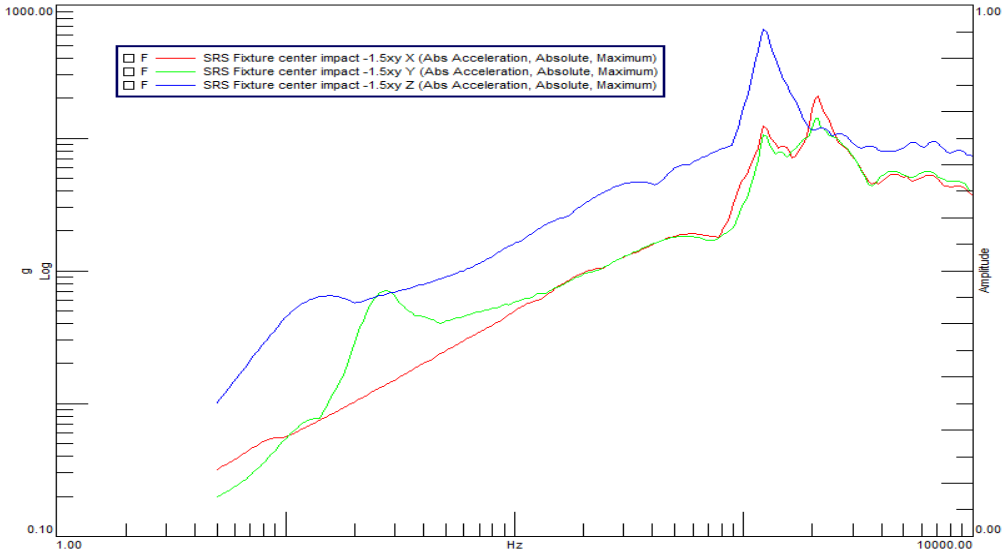

Figure 7.9: SRS of the center node with the fixture in the center and impact pad moved 1.5 inches in the -X and -Y directions

The next part of the study involved moving the impact pad and center to the same location and being offset from the center of the plate to examine the effects on the response at the center node of the fixture. The impact pad and fixture were moved 3.5 inches in the +X direction and 2.5 inches in the -Y direction displayed in Figure 7.10.

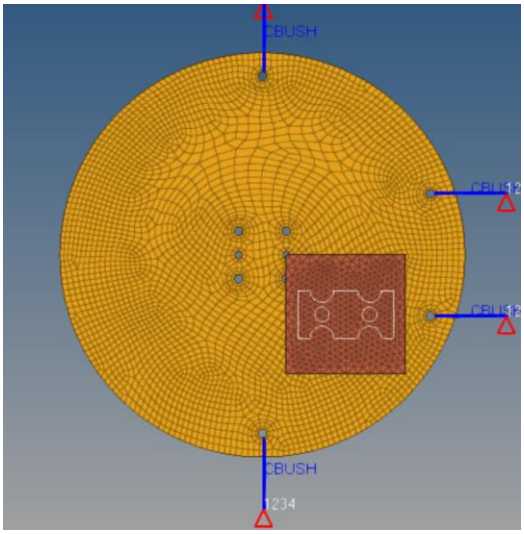

Figure: 7.10: Fixture and impact pad moved 3.5 inches in the +X and 2.5 inches in the -Y directions

The SRS of the center node was plotted in Figure 7.11 and shows only the in-axis response is dominated by rigid body modes and the off-axis responses are dominated by the bending modes. All the responses have the same knee frequency and the off-axis responses have a peak in between 2000-3000 Hz which demonstrates that mode is controlling in that region.

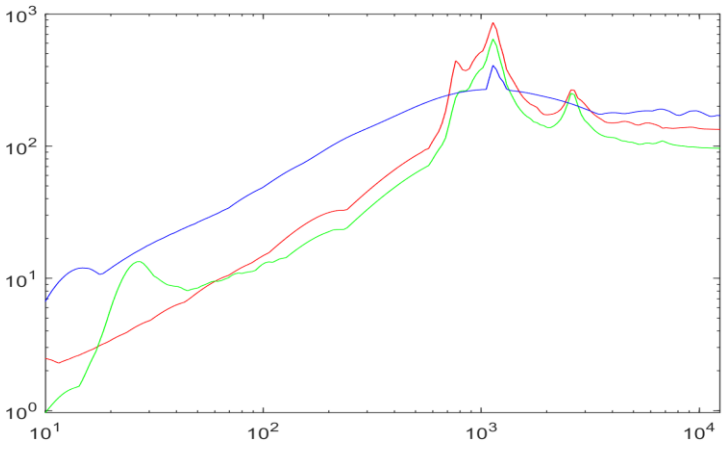

Figure 7.11: SRS of the center node with fixture and impact pad moved 3.5 inches in the +X and 2.5 inches in the -Y directions

Using the modal contribution code described in section 6.1, the individual modal SRSs for the center node in the +Z were plotted in Figure 7.12 using Matlab. The study revealed that all the rigid body modes excluding the second mode contributed to the overall SRS and the only peak visible comes from the knee mode.

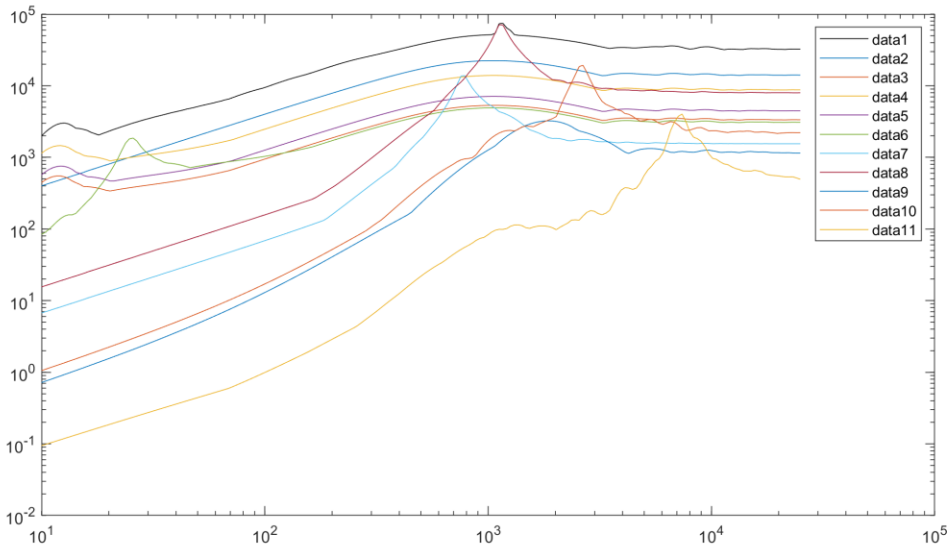

Figure 7.12: Modal contribution to the overall SRS of the center node in the Z direction with fixture and impact pad moved 3.5 inches in the +X and 2.5 inches in the -Y directions

The code was then used for the same node in the +X direction, and the individual modal SRSs were made shown in Figure 7.12. It was found that all the rigid body modes contributed to the overall SRS, however, they do not dominate the shape of the overall SRS for this direction. It can be observed that the first rigid body mode is greater than the overall SRS which shows that the acceleration time history of that mode was out of phase and instead of adding to the overall SRS, it was subtracted. The study also showed that mode 7 at 785 Hz and mode 12 at 3124 Hz contributed to the peaks seen in Figure 7.13 which were not as seen in the +Z response.

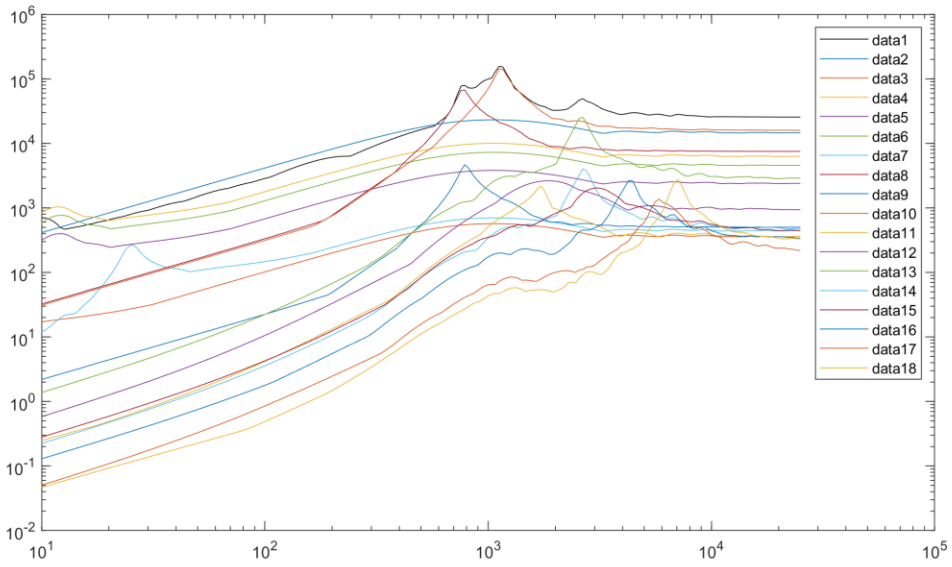

Figure 7.13: Modal contribution to the overall SRS of the center node in the X direction with fixture and impact pad moved 3.5 inches in the +X and 2.5 inches in the -Y directions

The next part of the study involved moving the impact pad to the position opposite of the fixture and changing the placement to investigate the effects on the SRS to see if the modal contribution can be manipulated. The first model tested began with the fixture moved 3.5 inches in the +X and 2.5 inches in the -Y directions and impact pad moved 3.5 inches in the -X and 2.5 inches in the +Y directions demonstrated in Figure 7.14.

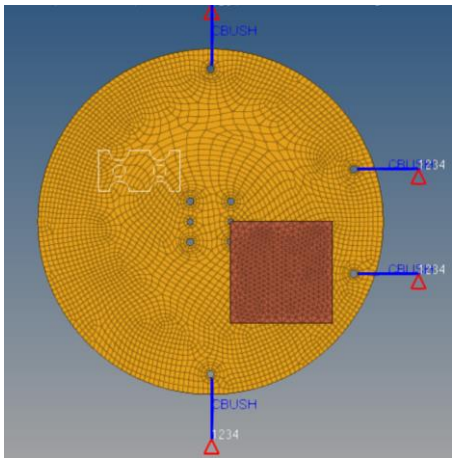

Figure 7.14: Fixture moved 3.5 inches in the +X and 2.5 inches in the -Y directions and impact pad moved 3.5 inches in the -X and 2.5 inches in the +Y directions

The SRS was again made for the center node in all directions and plotted in Figure 7.15. Rigid body controlled responses were not observed for this case, and peaks at 770 Hz were noticed for all of the responses.

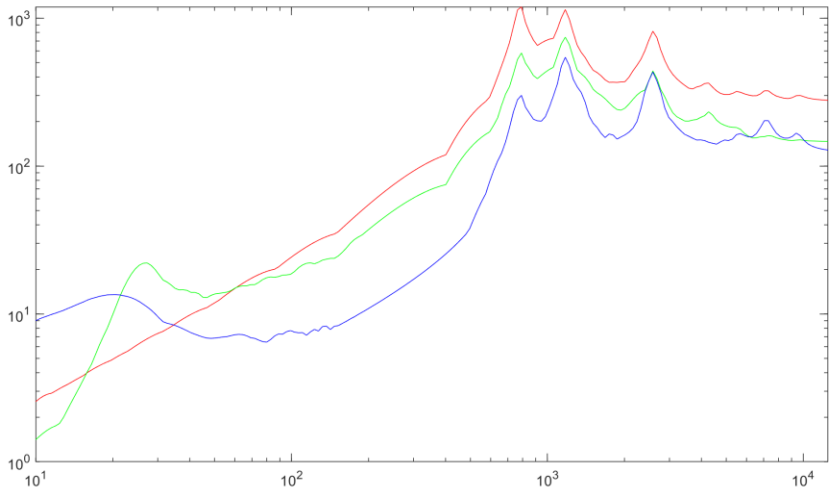

Figure 7.15: SRS of the center node with fixture moved 3.5 inches in the +X and 2.5 inches in the -Y directions and impact pad moved 3.5 inches in the -X and 2.5 inches in the +Y directions

The impact pad was then moved to 3 inches in the -X and left at 2.5 inches in the +Y shown in Figure 7.16. The response of the center node was completed and plotted in Figure 7.17. Moving the impact pad only 0.5 inches from the previous run has shown that the peak at 770 Hz has been reduced for the SRS in all three directions and there were no other obvious changes.

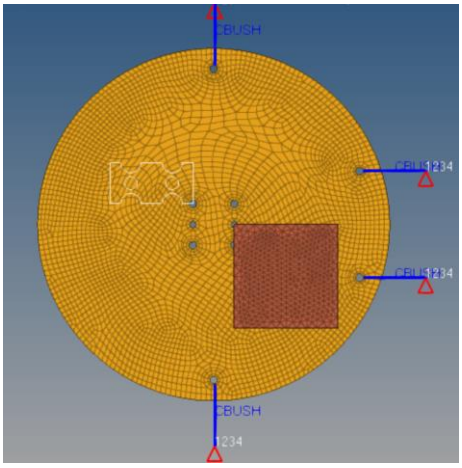

Figure 7.16: Fixture moved 3.5 inches in the +X and 2.5 inches in the -Y directions and impact pad moved 3 inches in the -X and 2 inches in the +Y directions

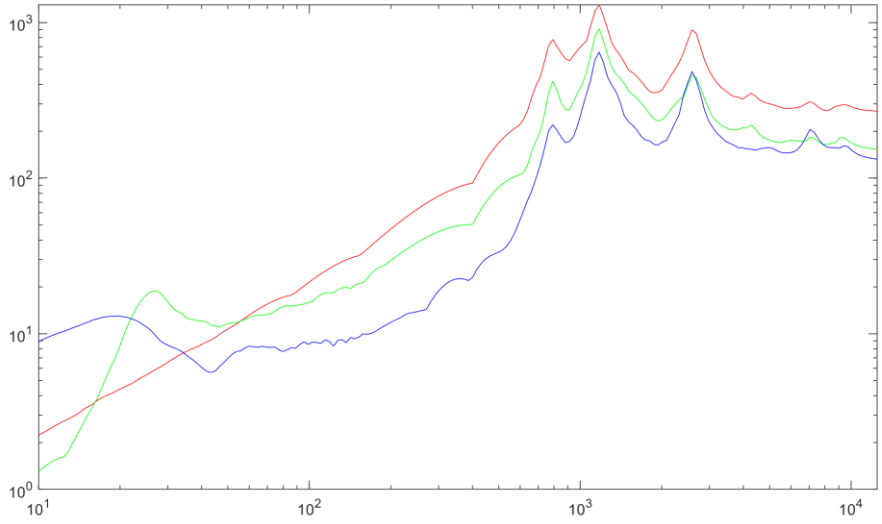

Figure 7.17: SRS of the center node with fixture moved 3.5 inches in the +X and 2.5 inches in the -Y directions and impact pad moved 3 inches in the -X and 2 inches in the +Y directions

Again, the impact pad was moved slightly from 3 inches in the -X and 2 inches in the +Y directions to 2 inches in the -X and 2 inches in the +Y directions depicted in Figure 7.18. The SRS of the center node was plotted in Figure 7.19 for all three directions, and the peak at 770 Hz has been significantly reduced for all three responses. Changing the placement location of the impact pad has found to be an effective way to minimize the effect of particular modes of interest, however examining where the impact pad should be placed needs to be explored.

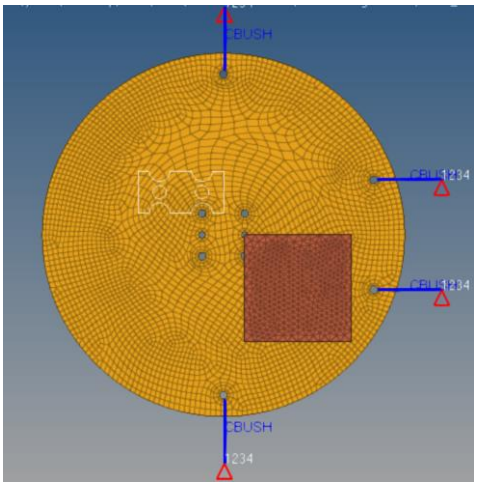

Figure 7.18: Fixture moved 3.5 inches in the +X and 2.5 inches in the -Y directions and impact pad moved 2 inches in the -X and 2 inches in the +Y directions

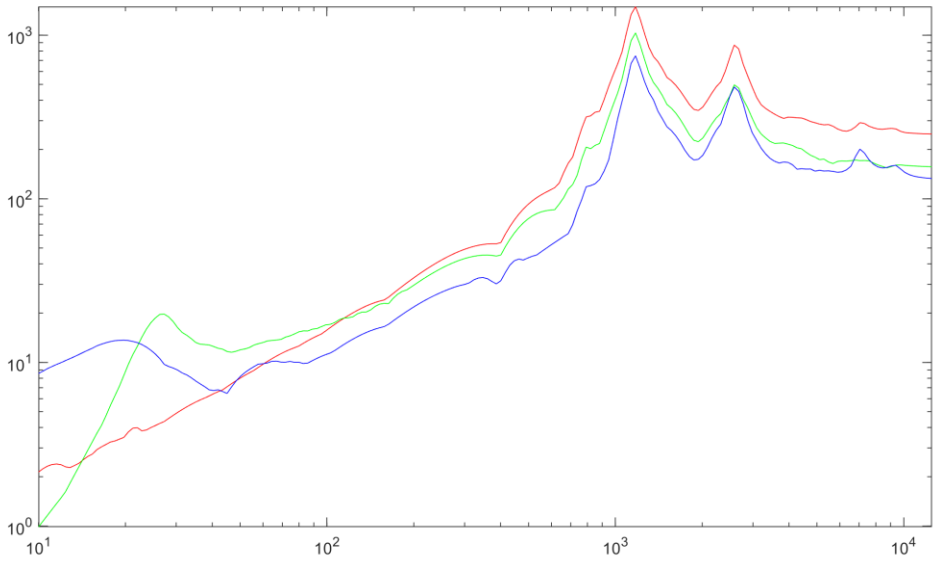

Figure 7.19: SRS of the center node with fixture moved 3.5 inches in the +X and 2.5 inches in the -Y directions and impact pad moved 2 inches in the -X and 2 inches in the +Y directions

The impact at the edge of the plate was explored in previous studies and was motivation for the next part of the study. Moving the Fixture 3.5 inches in the +X and 2.5 inches in the -Y directions and impact pad moved 8 inches in the +Y direction was done and is illustrated in Figure 7.20.

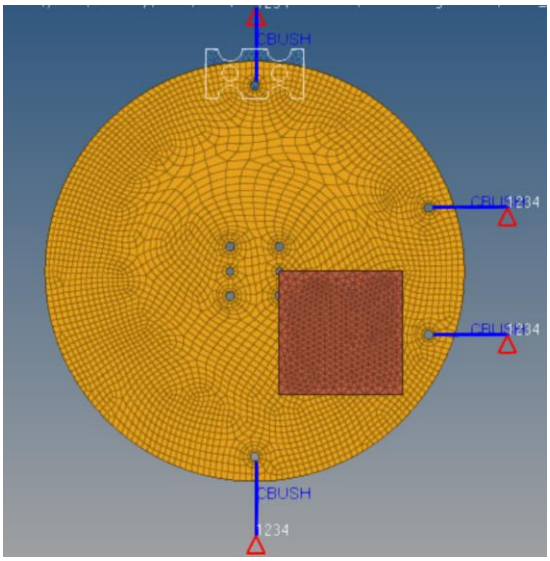

Figure 7.20: Fixture moved 3.5 inches in the +X and 2.5 inches in the -Y directions and impact pad moved 8 inches in the +Y directions

The SRS of the center node was made and plotted in Figure 7.21. This configuration of impact pad and fixture placement changed the knee frequency of all responses to 1109 Hz and the off-axis responses are greater than the in-axis response above 38 Hz.

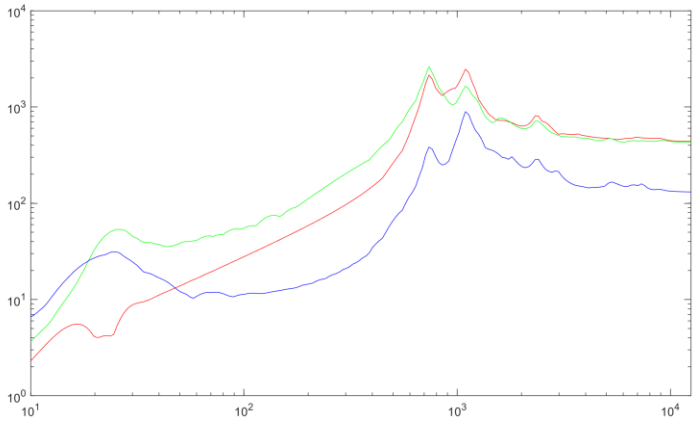

Figure 7.21: SRS of the center node with fixture moved 3.5 inches in the +X and 2.5 inches in the -Y directions and impact pad moved 8 inches in the +Y directions

Looking at the mode shapes in Hyperview of this configuration show where the modal nodal lines exist and where we can observe the most amount of acceleration at different locations on the plate. Figure 7.22 contains the mode shapes and illustrates the most acceleration for the impact pad lie at modes 7, 9, and 12. Modes 8, 10, and 11 are either on a modal nodal line or are close in proximity.

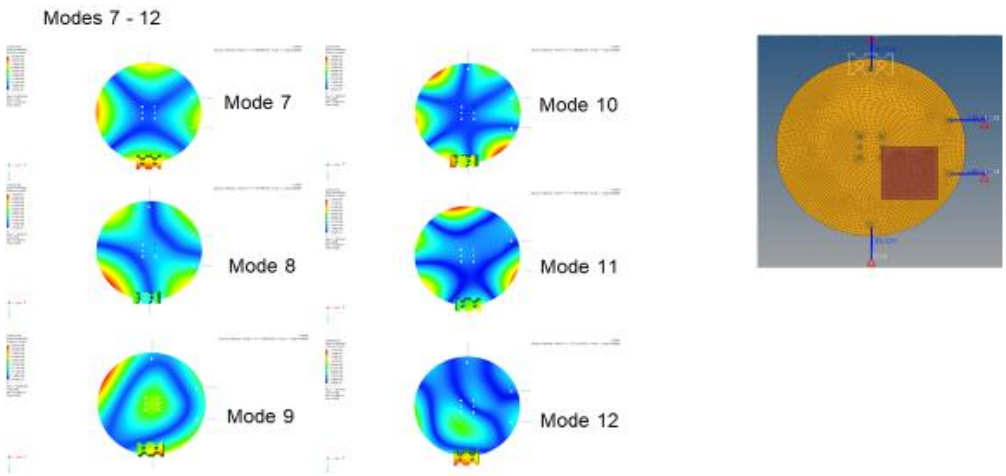

Figure 7.22: First 6 bending modes of the plate with the fixture moved 3.5 inches in the +X and 2.5 inches in the -Y directions and impact pad moved 8 inches in the +Y directions

Looking at the modal participation to the overall SRS of the center node in the +Z direction in Figure 7.23 shows that modes 7 at 735 Hz, 9 at 1109 Hz, and 12 at 2372 Hz are the largest contributors to the shape of this particular SRS. Mode 10 at 1686 Hz does contribute, but the magnitude of the individual modal SRS does not create peaks that are significant.

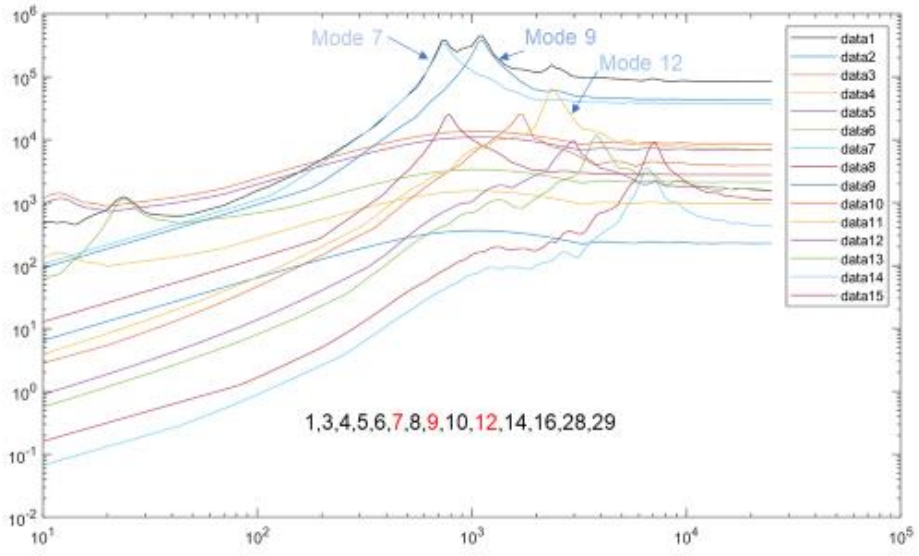

Figure 7.23: Modal contribution to the overall SRS of the center node in the Z direction with fixture moved 3.5 inches in the +X and 2.5 inches in the -Y directions and the impact pad moved 8 inches in the +Y direction

The placement of the impact pad was changed to be on the edge of the plate but offset in both the X and Y directions. Figure 7.24 shows the impact pad moved 5.5 inches in the -Y and -X directions.

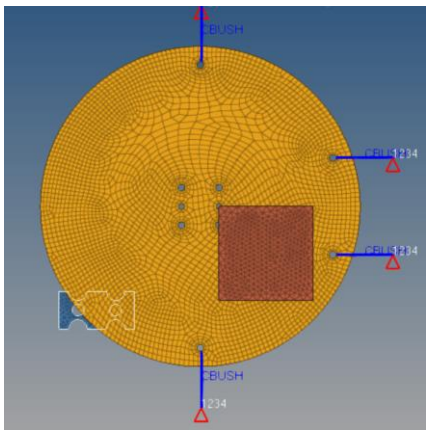

Figure 7.24: Fixture moved 3.5 inches in the +X and 2.5 inches in the -Y directions and impact pad moved 5.5 inches in the -Y and -X directions

The SRS of the center node of the fixture for all three directions was plotted and shown in Figure 7.25. The off-axis responses are shown to be greater in magnitude than the in-plane response except between 600-700 Hz where the +Z response (shown in blue) is larger than the +X response (in red).

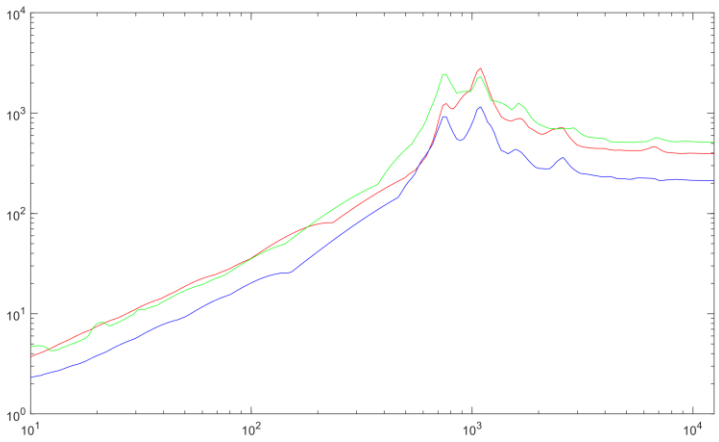

Figure 7.25: SRS of the center node with the fixture moved 3.5 inches in the +X and 2.5 inches in the -Y directions and impact pad moved 8 inches in the +Y directions

Analyzing the mode shapes for this configuration reveals the impact pad is on modal nodal line on mode 8 and mode 11 which shows the acceleration at those modes will be insignificant compared to the other modes. Modes 7,9,10,12 are shown to be in locations where the acceleration was more substantial, and an assessment of the modal contribution is needed for confirmation.

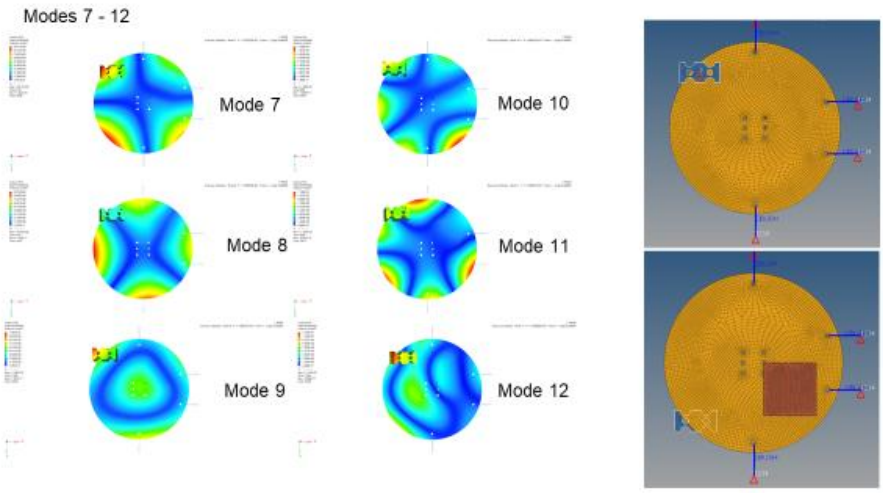

Figure 7.26: First six bending modes with the fixture moved 3.5 inches in the +X and 2.5 inches in the -Y directions and impact pad moved 5.5 inches in the -Y and -X directions

The individual modal SRSs of the center node in the +Z direction were made and plotted in Figure 7.27. Mode 7 at 748 Hz, mode 9 at 1080 Hz, mode 10 at 1649 Hz, and mode 12 at 2558 Hz was found to be the largest contributors to the overall SRS at this location/direction. This helps support the notion that examining the mode shapes can be useful when trying to reduce the participation from a particular mode when designing SRS specifications.

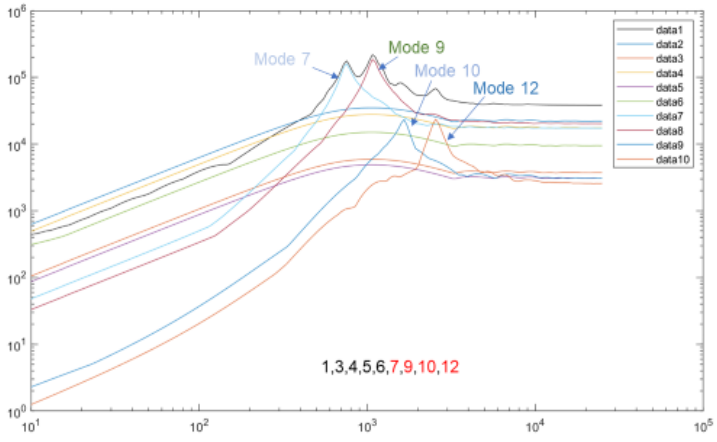

Figure 7.27: Modal contribution to the overall SRS of the center node in the Z direction with fixture moved 3.5 inches in the +X and 2.5 inches in the -Y directions and the impact pad moved 5 inches in the -Y and -X directions

The same configuration of the impact pad at 5.5 in the -X and -Y directions but change the placement of the fixture back to the center was done and the schematic is shown in Figure 7.28.

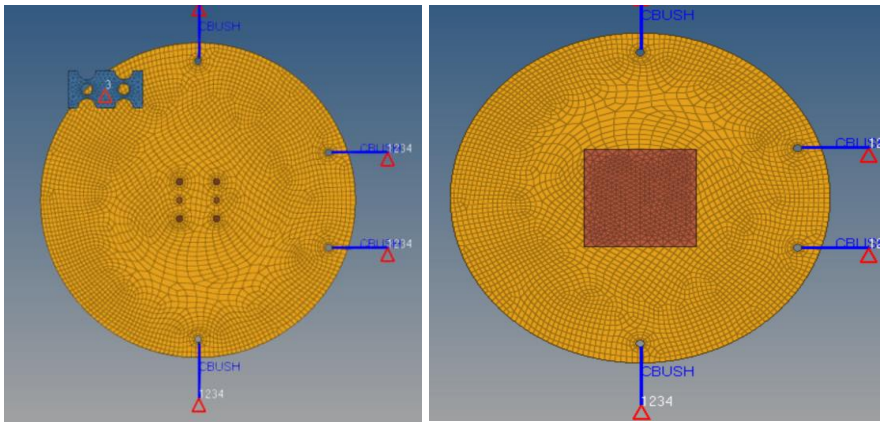

Figure 7.28: Fixture in the center and impact pad moved 5.5 inches in the -Y and -X directions

The SRS of the center node was made for all three directions and was plotted in Figure 7.29. The rigid body phenomenon occurs and there is no clear knee frequency for both off-axis responses. However, the proximity of all responses makes this a case that could prove to be beneficial for designing SRS testing specifications. With damping added, the peaks of the +Z response could be reduced and should be examined further.

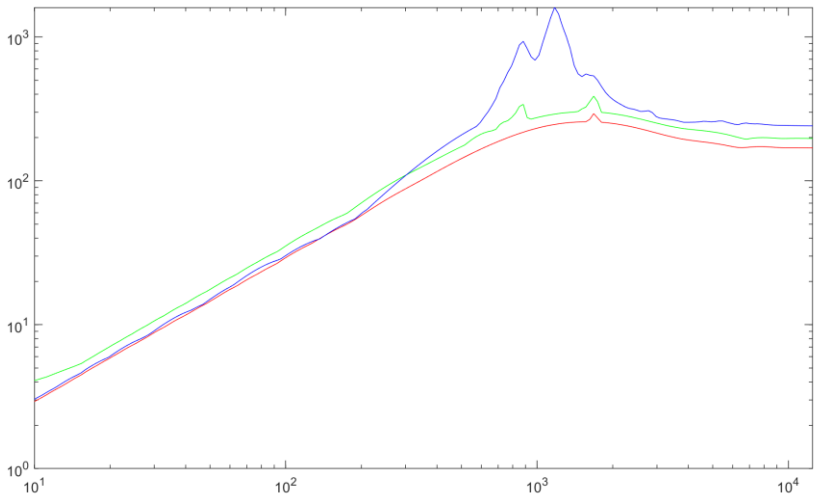

Figure 7.29: SRS of the center node with Fixture in the center and impact pad moved 5.5 inches in the -Y and -X directions

One way to effectively eliminate the contribution of the rigid body modes would be to make the boundary conditions rigid. The effects of making the support springs "softer" and reduced by two orders of magnitude were explored and explained in Section 7.1. Figure 7.30 shows the SRS with the original configuration of the support springs (left) and the reduced springs (right). The rigid body controlled response in the +Z direction still occurs, but the abnormality seen in the constant velocity region before the knee frequency is greatly reduced.

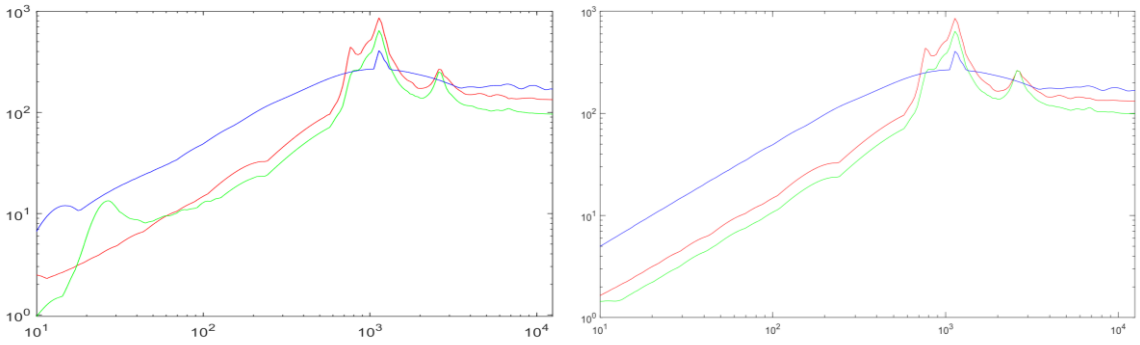

Figure 7.30: SRS comparison on the effects of spring support change

8 Conclusions

The analysis of a circular resonant plate for shock testing evolved from a single system to a sub-assembled system that includes movable fixtures. The solid resonant plate FEM yielded SRSs with different knee frequencies between the on-axis and off-axis responses and the shape of the SRS was dependent upon the location of the output on the fixture. The shape was primarily affected by the higher modes beyond the knee frequency in the plateau region. It was also found that the off-axis responses could be increased and manipulated depending on the location of impact.

The sub-assembled FEM with contact surfaces was made to more accurately depict the dynamics of the system and the frequencies were found to have less error than the single modeled system when compared to experimental data. Boundary condition locations were also changed from symmetric to asymmetric. A similar test was conducted to the solid FEM and it was found that the change in the off-axis response did not change as significantly and it was evident that there were more modes present in the off-axis responses with the updated model that utilized sub-assemblies and contact surfaces.

The impact angle was changed using the updated model and it shows the off-axis responses change depending on the angle of impact which can help explain inconsistencies in real-world testing. It could also be useful in manipulating the off-axis responses to ensure the test meets design targets.

A method to synthesize an SRS function from poles and mode shapes from a previous study was improved by decreasing the computation time and automating the modal contribution to SRS for a given point and direction. The process uses an Eigen solution from an FEA model in Matlab to create a time-domain response for each mode is created. SRSs are made for each individual mode and the code iterates through to find the contributing modes that when added are within a specified percent error of 1% of the total SRS.

The effects of moving the test fixture on the resonant plate showed that different points on the same fixture have variations in magnitude and shape of the SRS in the same directions which can give insight when designing SRS test targets. The variations were shown to be more significant based on the location of the test fixture due to changing the symmetry of the original configuration. The variations were examined for the configuration where the test fixture was moved in the -X and -Y direction and rotated 45˚ and a table was created to show the modal participation for the nodal points on the corners of the fixture. It was shown that the modes from 10-3000 Hz have the most effect on the behavior of the SRS for each nodal point. Another method of looking at the modal contribution showed that despite having the same modes that participate in the overall SRS, the magnitude of the mode changes the shape of the SRS which can explain some of the variations that were observed in the different nodes on the fixture in the same direction.

Moving the impact pad on the resonant plate showed the magnitude of the off-axis responses can be effectively changed, but it also demonstrated the shape of the response can change and more modes can be introduced. It was also found that the location of the impact pad can have rigid body modes dominate the response depending on whether modal nodal lines were crossed. The modal contribution was examined for a given configuration where the +Z response was dominated by the rigid body modes where the modes were added to the overall response versus the +X response at the same location showed the rigid body modes were subtracted from the overall response. It is known that eliminating the rigid body mode contribution to the response can be done by making the boundary conditions rigid, and it was shown that making the boundary conditions softer by two orders of magnitude the constant velocity line on the SRS was less affected by the rigid body modes. Another finding from this study revealed the mode shapes can be an efficient tool to use when deciding where to place the impact pad on the resonant plate and can be valuable in deciding which modes to exploit to help ensure the response meets test specifications.

All these insights can be used together to determine a suitable location of the test structure and impact pad based on the type of response that is desired. By changing the location of the test fixture in both of the off-axis directions, the consequent responses in those directions can be increased, and changing the location of the input pad based on mode shapes can be useful in employing the modes that are desired or not desired.

9 Future Work

For a more accurate representation of how the system will perform in experimental testing, the model should be fully correlated with experimental test data using modal assurance criteria (MAC). The damping estimation and boundary conditions should be verified with experimental testing as well.

A more inclusive study on the angle of impact should be useful in studying experimental testing. A test should be made that includes more than one angle of impact and a series of angles could be tested to fully understand the effects on the dynamics of the resonant plate.

Designing a process that determines the most suitable configuration of the resonant test plate that includes fixture design/location, impact location, etc. that lead to responses for the in-axis and off-axis that pass SRS test specifications should be explored and expanded.

10 Reference List

[1] Maurice A.Biot, "*Transient Oscillations in Elastic Systems*," Ph.D. Thesis No. 259, Calif. Inst. of Technology 1932.

[2] Pusey, "*An Historic View of Shock and Vibration,"* DYNAMIC TESTING REFERENCE ISSUE 2008.

[3] Irvine, "*An Introduction to the Shock Response Spectrum,"* 2012.

[4] A. Piersol, T. Paez and C. Harris, "*Harris' shock and vibration handbook,*" New York: McGraw-Hill, 2010.

[5] Brooks, R.O. "Shock Testing Methods" SC-TM-172-62, 1962.

[6] Dwyer, T. and Moul, D. (1988). Pyro shock simulation: Experience with the MIPS simulator. NASA, Goddard Space Flight Center, 15th Space Simulation Conference: Support the Highway to Space Through Testing, pp.125-138.

[7] J.L. Smith, "Effects of Variables Upon Pyrotechnically Induced Shock Response Spectra". NASA Technical Paper 2603, 1986.

[8] Davie, Neil T., "Pyroshock Simulation for Satellite Components Using a Tunable Resonant Fixture – Phase 2," Sandia National Laboratories Technical Library, Albuquerque, New Mexico, 1997.

[9] Newell, James M, "Mechanical Impulse Pyro Shock (MIPS) Simulation," IEEE, Workshop on Accelerated Stress Testing; Boston, MA; United States. Jet Propulsion Lab., California Inst. of Tech.; Pasadena, CA, United States. Oct 26, 1999.

[10] Filippi, Enrico, "Development of the Alcatel ETCA Pyroshock Test Facility," European Conference on Spacecraft Structures, Braunschweig, Germany, 1999.

[11] Filippi, Enrico, "Pyroshock Simulation using the Alcatel ETCA Test Facility," Launch Vehicle Vibrations. First European Conference. 1 CNES Toulouse, Dec. 14-16, 99.

[12] D. M. Cox, "Design of a multi-DOF tuned mounting fixture for the Navy's mediumweight shock machine," thesis, U.S. Navy, Monterey, California, 1993.

[13] Lee, Jung-Ryul et. al. "Review of pyroshock wave measurement and simulation for space systems," Measurement Volume 45, Issue 4, 2012. Pgs 631-642.

[14] Hsieh R., Moore R.M., Sroka S., Lake J., Stull C., Avitabile P. (2013) Analysis and Dynamic Characterization of a Resonant Plate for Shock Testing. In: Allemang R., De Clerck J., Niezrecki C., Wicks A. (eds) Special Topics in Structural Dynamics, Volume 6. Conference Proceedings of the Society for Experimental Mechanics Series. Springer, New York, NY

[15] Jayaraman S., Trikha M., Somashekar, Kamesh D., Ravindra M. (2016). Response Spectrum Analysis of Printed Circuit Boards Subjected to Shock Loads. Procedia Engineering. 144. 1469-1476. 10.1016/j.proeng.2016.06.710.

[16] Larsen W., Blough J.R., DeClerck J., VanKarsen C., Soine D., Jones R.J. (2020) "*Understanding Multi-Axis SRS Testing Results*". In: Walber C., Walter P., Seidlitz S. (eds) Sensors and Instrumentation, Aircraft/Aerospace, Energy Harvesting & Dynamic Environments Testing, Volume 7. Conference Proceedings of the Society for Experimental Mechanics Series.

[17] Mulville, Daniel R. "*Pyroshock test criteria."* NASA Technical Standard NASA-STD-7003, National Aeronautics and Space Administration NASA, May, http://standards. nasa. gov (1999).

[18] DOD, Pyroshock. "*MIL-STD-810G Method 517.1*." Department of Defense, New York, NY, USA (2008).

[19] Jacobson E. "*USING FREQUENCY BASED SUBSTRUCTURING TO OPTIMIZE MULTI-AXIS RESONANT PLATE SHOCK TESTS*" Master of Science, Mechanical Engineering, Michigan Technological University, 2018.

[20] Irvine T., "Derivation of the Filter Coefficients for the Ramp Invariant Method as Applied to Base Excitation of a Single-degree-of-Freedom System," May 17, 2018.

[21] Smallwood D., "AN IMPROVED RECURSIVE FORMULA FOR CALCULATING SHOCK RESPONSE SPECTRA," in VibrationData.com vol. August 2001, ed: Tom Irvine, 2001.

[22] Tůma J. and Kočí P., "*Calculation of a shock response spectrum*," 2011 12th International Carpathian Control Conference (ICCC), Velke Karlovice, 2011, pp. 404-409.

[HS] Hopkins R., Sisemore C., "*DESIGN OF A RESONANT PLATE SHOCK TEST FOR SIMULTANEOUS MULTI-AXIS EXCITATION"* 89th Shock & Vibration Symposium, 5 — 8 Nov 2018.

A MATLAB code for Modal Participation

```
% convert from optistruct.pch to modal matrix
% rows are DOFs from little to big, 2x,2y,2z,3x,3y,etc
% columns are modal vectors (increasing order)
% rotational DOFs are assumed to be zero.
%  ww = eigenvalues,    U is the modal matrix
% JBM# name of variable containing the optistruct.pch data
clear U ww

k= 42;  % number of modes
kd=10;  % number of nodes
kline =7;
ndd=1;
for nm=1:k
     ww(nm)=JBM65(kline,3);
    for nd=1:kd;
        U(ndd,nm)=JBM65(kline+1,3);
        U(ndd+1,nm)=JBM65(kline+1,4);
        U(ndd+2,nm)=JBM65(kline+1,5);
        ndd=ndd+3;
        kline=kline+2;
    end
     ndd=1;
     kline=kline+7;
end

%  convert optistruct modal vectors to residues
%  uses U (modal matrix) and ww (eigenvalues) from 'punch2matlab.m'
clear A
nm=42;  % number of modes
nd = kd*3;  % number of DOFs
for k=1:nm;
    for p=1:nd
        for q=1:nd
            A(p,q,k)=1/(2*j*sqrt(ww(k)))*U(p,k)*U(q,k);
        end
    end
end
save
% initialize required data
clear
load('matlab.mat')

% Set simulation end time  and the print interval
sim_opt.finalTime = 0.2;
sim_opt.printInterval = 1/100000;

% determine sample rate and frequency values for SRS output
sr=1/sim_opt.printInterval;
fn=logspace(log10(sr/1e4),log10(sr/4),200);

%  p= output DOF, q=input DOF,  index position in residue matrix
p=21;
```

```
q=30;
%  z = damping ratio is freq dependent
% z = .02;
% nm = number of modes
nm=42;
% compute poles
kk=1;
for k=1:nm
    if ww(k)<100*pi % 50Hz
        z=.015;
    else
        z=.001;
    end
    pole(kk)=-z*sqrt(ww(k))+i*(sqrt(1-z^2)*sqrt(ww(k)));
    pole(kk+1)=conj(pole(kk));
    kk=kk+2;
end
%% compute response one mode at a time
kk=1;
load('INPUT2.mat')
for k=1:nm
    res(1)=A(p,q,k); % residues from displacement
    res(2)=conj(res(1));
   [b1,a1]=residue(res(1:2),pole(kk:kk+1),0);  % coefficients from
displacement residues
   kk=kk+2;

b2=[b1(2),0,0];
time=INPUT(:,1);
resp=INPUT(:,2);

trans=tf(b2,a1);
bode(trans)
hold on
resp_to_excite(k,:)=lsim(trans,resp,time);
dt=time(2)-time(1);
accel1(k,:) = resp_to_excite(k,:);

% compute SRS per mode
 [srs(k,:),fn]=SHSPEC(accel1(k,:),fn,0.05,sr);  % mode
end
% compute total response and SRS, then plot
accel_tot =sum(accel1);
%   disp_tot=sum(disp1);
[srs_tot,fn]=SHSPEC(accel_tot,fn,0.05,sr);

%% Calculates Modes that contribute with less than 1 percent error from
total

x=1;
dist=x*srs_tot; % parameter used to find the closest SRS to the SRS
total
ix=any(srs>=dist,2); % logical matrix showing a 1 if it contributes 0
if it does not
```

```
xsave=srs(ix,:);
ixF=find(ix == 1); % The ixf matrix shows the modes that contribute to
the overall SRS
accel_addI=sum(accel1(ixF,:),1);
[srs_addI,fn]=SHSPEC(accel_addI,fn,0.05,sr); % Creates SRS for
iteration
PD=mean(100.*abs((srs_addI-srs_tot)./srs_tot)); % Percent difference of
SRS added vs SRS total
while PD > 1
   x=x-0.01;
    dist=x*srs_tot;
    ix=any(srs>=dist,2);
    xsave=srs(ix,:);

    ixF=find(ix == 1);

    accel_addI=sum(accel1(ixF,:),1);
    [srs_addI,fn]=SHSPEC(accel_addI,fn,0.05,sr);
    PD=mean(100.*abs((srs_addI-srs_tot)./srs_tot));
    if PD <= 1
        break
    end
end
 figure
 loglog(fn,srs_tot,'k')
 hold on
 loglog(fn,xsave)
 legend()
accel_addI=sum(accel1(ixF,:),1);
[srs_addI,fn]=SHSPEC(accel_addI,fn,0.05,sr);
figure
loglog(fn,srs_tot,'k')
hold on
loglog(fn,srs_addI)
legend('SRS Total','SRS of Added Modes','Location','Southeast')

ixF=ixF';
num2str(ixF,'%d') % Prints the ixF matrix to see contributing modes
```